Density Functional Theory Study of Graphene

Huang Lin

School of Chemical and Biomedical Engineering

A thesis submitted to the Nanyang Technological University

in partial fulfilment of the requirement for the degree of

Doctor of Philosophy

2015

Abstract

In this thesis we mainly focus on : (a) band gap manipulation of monolayer graphene by phenyl radical adsorption; (b) controlling armchair and zigzag edges in oxidative cutting of graphene with strain; (c) understanding of their photoluminescence (PL) mechanisms of graphene quantum dots (GQDs) using density functional theory (DFT) and time-dependent DFT (TDDFT) calculations. We observe that (a) the adsorption of single phenyl radical breaks the aromatic π-bond of graphene and generates an unpaired electron which is delocalized on ortho or para positions, (b) the adsorption of the second phenyl radical at ortho or para position saturates the generated unpair electron by electron pairing and results in semiconducting graphene, (c) adsorption of more even numbers of phenyl radicals on graphene by ortho-ortho and ortho-para pairings increases the band gap of graphene. We have also investigated the oxidation of graphene considering the adsorption at both sides of graphene sheet. We show that (1) the formation of armchair epoxy chain on graphene sheet is energetically favorable when the oxidation is occurred on both sides of graphene sheet, (2) whereas formation of zigzag epoxy chain is favorable when oxidation occurred on the same side of graphene, (3) when external strain is applied on graphene the zigzag epoxy chain formation on graphene sheet becomes energetically more favorable. We have also studied the PL properties of GQDs using both DFT TDDFT calculations to reveal the PL mechanism and also investigated the effect of size, edge configurations, shapes, attached chemical functionalities, heteroatom dopings and defects on PL properties of GQDs.

Acknowledgements

I am highly indebted and like to express my gratitude to my supervisor Associate Professer Chen Peng, School of Chemical and Biomedical Engineering, Nanyang Technological University, and Associate Professor Lim Kok Hwa, Singapore Institute of Technology for their constant active guidance, stimulating suggestions and endless encouragement throughout the course of my research.

I gratefully thank Dr. SK Mahasin Alam for his kind and encouraging interactive scientific discussions. I thank the past and present research group members: Dr. Xi Hongwei, Tan Shiow Jin, Li Xiang, Sultana Bedoura, Liu Chao, Wahyu Perdana Yudistiawan and Lim Rern Jern for their support. I also thank my friends for their moral support and encouragements.

I am grateful to School of Chemical and Biomedical Engineering, Nanyang Technological University. I am grateful too, to Nanyang Technological University for providing all the facilities and scholarship support.

At last, a heartfelt gratitude goes to my parents and relatives for their omnipresent love, trust and enthusiastic supports.

Table of Contents

List of abbreviations

Al_2O_3	Aluminum oxide
Ar	Argon
Atm	Atmosphere
Au	Gold
Å	Angstrom
BTE	Boltzman transport equation
BZ	Brillouin Zone
CB	Conduction-band
CBM	Conduction-band minimum
CCD	Coupled-cluster doubles
CCDS	Coupled-cluster singles and doubles
cm	Centimeter
CVD	Chemical Vapor deposition
DFT	Density functional theory
DFTB	Density Functional based Tight Binding
DOS	Density of state
eV	Electron Volt
Fe	Iron
FET	Field effect transistor
GGA	Generalized-gradient approximation
GNR	Graphene nano-ribbon
GQD	Graphene quantum dot

H_2	Hydrogen
HCl	Hydrogen chloride
HF	Hartree-Fock
HF	Hydrogen fluoride
HK	Hohenberg-Kohn
HOMO	Highest occupied molecular orbital
IBS	Ion beam synthesis
In	Indium
KS	Kohn-sham
LDA	Local-density approximation
LED	light-emitting diode
Li	Lithium
LUMO	Lowest unoccupied molecular orbital
mA.h/g	Milli ampere hour per gram
MD	Molecular dynamics
ml	Milliliter
Mpa	Mega Pascal
mTorr	Milli Torr
N_2	Nitrogen
nA	Nano ampere
Ni	Nickel
nm	Nano meter
PES	Potential energy surface

Pt	Platinum
RAM	Random access memory
ROM	Read-only memory
TS	Transition surface
T	Temperature
TD-DFT	Time-dependent density functional theory
VASP	Vienna *ab initio* Simulation Package
VB	Valence-band
VBM	Valence-band maximum
ZrO_2	Zirconium oxide

Chapter 1

Introduction

Modern semiconductor industry grows faster and faster, trying to achieve Moore's law which is the observation that "over the history of computing hardware, the number of transistors in a dense integrated circuit has doubled approximately every two years". To reach this target, new semiconducting materials such as graphene and related materials

attracted interests of many researchers. Graphene is an allotrope of carbon, which has a strictly two-dimensional structure of one-atom-thick planar sheet, made up of sp^2 hybridized carbon atoms that are densely packed in a honeycomb crystal lattice[1] (see Figure 1.1). All sp^2 hybridized carbon atoms, which forming graphene, have four bonds: three σ bonds connecting three neighboring carbon atoms and one π bond orienting perpendicular to the graphene plane. The lattice constant of graphene is 2.47 Å (See **Figure 1.1a**).[2] Graphene has interesting geometric, optical and electronic properties because of its sp^2 hybridized carbon atoms, honeycomb crystal lattice and one atom-thick layered structure,

Since the first successful synthesis of graphene by regular adhensive tape stripping method in 2004[3], a large number of methods have been reported for the synthesis of graphene including mechanical exfoliation[4], chemical vapor deposition (CVD)[5], arc discharge [6], epitaxial growth [7], chemical reduction of graphene oxide[8], substrate-free gas-phase synthesis [9], direct synthesis of graphene from graphite[10], electrochemical synthesis [11], unzipping carbon nanotube for graphene nano-ribbon[12], templated route to produce graphene[13], total organic synthesis [14], etc.

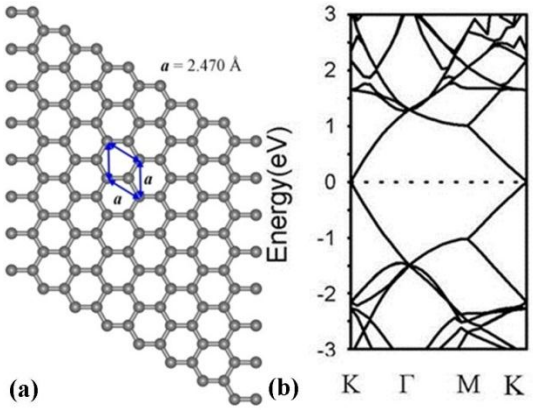

Figure 1.1 DFT optimized (a) geometric and (b) electronic structure of intrinsic graphene.

Theoretically, graphene is the thinnest structure human being can produce because of its one-atom-thick structure. Graphene has a large surface/volume ratio and experimental Young's modulus (elastic modulus) of graphene is 1.0 terapascals suggesting that graphene is one of the strongest material.[15]

Graphene has numerous attractive electronic properties. Intrinsic graphene is a zero band-gap semi-metal material with its valence and conductive bands degenerate at K point (See **Figure 1.1b**). The resistivity of graphene sheet would be $10^{-6}\Omega\cdot$cm, which is 10 times less than the lowest resistivity metal material known at room temperature – silver[16]. Graphene has remarkable ultra-high electron mobility (200,000 $cm^2V^{-1}s^{-1}$), demostrated by experiment[17]. In graphene, electrons and holes (Dirac fermions) have zero effective mass near the six corners of the two-dimensional hexagonal Brillouin zone, behaving like spin 1/2 relativistic particles described by the Dirac equation[18]. The Dirac fermions should have nearly the same mobility due to the high symmetry of the experimentally measured conductance[19]. Graphene also has low Johnson noise, which appeared due to thermal agitation of Dirac points.[20] Therefore, small modification in

carrier concentration (a surface molecular adsorption) leads to a sigficant variation of graphene conductivity.[20] The comparison of some common semiconducting and graphene are listed in **Table 1.1**.

Table 1.1 Electronic properties of commonly used semiconducting materials and graphene

Materials	Band gap (eV)	Effective mass(m_e)		Mobility (cm^2/V s)	
		Electron	Hole	Electron	Hole
Graphene	0	1/18[25]	1/18[25]	200,000[17]	200,000[17, 19]
Si	1.10[21]	1.080[21]	0.560[21]	1500[21]	450[21]
Ge	0.66[21]	0.550[21]	0.370[21]	3900[21]	1900[21]

[a] m_e indicates the mass of a free electron (9.11x10-31 kg).

Based on these amazing electronic and structural properties, graphene attracts wide applications in sensers[20, 22], transparent electrodes and battery[23], field emission (FE) displays[24], field effect transistors (FETs) [3]. Due to ultra-high surface/volume ratio and high conductive with low Johnson noise and low crystal defect, graphene is widely used in bio- and gas-sensor. Graphene has been proposed as an ideal material in photovoltaic applications such as transparent electrodes due to its high electron mobility, transparent[25] and lowest resistivity. FE displays emit electrons under a high electric field. The simplest method to achieve a high electric field is to enhance electric field at the tip of a sharp material. Because of the single-atom-layer thick, graphene is a perfect material to produce FE displays. Graphene is also a proposed material for use in FETs because of its high electron mobility and switching speed (on-off ratios of about 10^7) [12].

Graphene quantum dots (GQDs) and Graphene nanoribbons (GNRs) are nanometer-sized graphene, which can be produced by graphene oxidation cutting. GQDs are single-layer or multi-layer fragments of graphene with a size from 1 to 50 nm and GNRs are strips of graphene with width thinner than 50 nm. GQDs have interesting elec-optical properties such as photoluminescence (PL). Due to the PL properties, GQDs can be used in bioimaging[26] and detecting[27] (sensers). GNRs have interesting electronic properties related to their edge shape and GNR width. Density functional theory calculation results showed that GNRs are semiconductings with band-gaps inverse of the GNR widths and armchair edge dominated GNRs always have larger band-gap than zigzag edge dominated GNRs. Due to the semiconducting properties, GNRs can be used to fabricate FETs with on-off ratios of about 10^6.

Although graphene has a lot of potential applications, we still face some challenges in real application. (a) First challenge is the zero band-gap of intrinsic graphene. If we want to use graphene in semiconducting industry, its band-gap should be opened. (b) Second challenge is the graphene cutting. GQDs and GNRs are used in sensors and FETs. The edge shape of GQDs and GNRs affect their electronic and optical properties. GNRs with dominant armchair edges have larger band-gap as compared to similar sized GNRs with dominant zigzag edges.[28] Theoretical calculations also revealed that GQDs with armchair edges have different electronic and optical properties as compared to similar sized GQDs with zigzag edges.[29] Thus, controlling the edges of GNRs and GQDs is important for their wider applications. (c) Third challenge is understanding the tunable photoluminescence (PL) properties of GQDs. GQDs can be employed as the universal fluorescent tags to specifically label the molecular targets and enable real-time imaging

of their trafficking dynamics in live cells.[30] Better understanding of PL properties of GQDs can widen the applications of GQDs. My research projects are mainly focused on solving the above challenges.

The goals of the present work are –

(a) to study the structural and electronic properties of graphene.

(b) to study the band-gap opening of graphene by radicals adsorption.

(c) to understand the edge shapes controlling of GQDs and GNRs by oxidative cutting of graphene.

(d) to reveal the mechanism of photoluminescence (PL) properties of GQDs and to investigate the effect of size, edge configuration, shape, attached chemical functionalities, heteroatom doping and defects on PL properties of GQDs.

Chapter 2

Literature Review

In this chapter we briefly discsuss the repoted works on synthesis of graphene, properties, applications and challenges of graphene and theoretical calculations performed on graphene.

2.1. Synthesis of graphene

In 2004, Geim and Novoselov used micromechanical exfoliation of bulk graphite to produce graphene[3]. It is the first successful method in which a one-atom-thin carbon flake was stripped using regular adhesive tape followed by deposition onto silicon substrates. After that a large number of graphene synthesis methods have been reported including mechanical exfoliation[4], chemical vapor deposition (CVD)[5], direct synthesis method from graphite[10], arc discharge method[6], epitaxial growth method[7], chemical reduction of graphene oxide[8], substrate-free gas-phase synthesis method[9], electrochemical synthesis method[11], unzipping carbon nanotube for graphene nano-ribbon[12], templated route to produce graphene[13], total organic synthesis method[14], etc. Some of the graphene synthesis methods are briefly described below.

2.1.1 Arc discharge method

Wu et al. reported a method using hydrogen arc discharge to reach an instantaneously increased high temperature (up to 2000 ℃) to produce graphene sheets from graphite oxide.[6] Because of the etching effect of hydrogen and in-situ defect-elimination effect at high plasma temperature on undesirable amorphous carbon, the arc discharge method has advantages in producing high thermal stability and crystallinity graphene sheets. In 2009, Rao et al. found a way to produce nitrogen and boron doped graphene using arc discharge method with pyridine and diborane, respectively.[31] The nitrogen and boron doped graphene sheets synthetized by arc discharge method exhibit high electrical conductivity and thermal stability.

2.1.2 Chemical vapor deposition (CVD)

In CVD method, hydrocarbon gases (mostly a mixture gas of hydrogen and methane) act as graphene precursors to deposit on surface of transition metal at a high temperature. Li et al. reported a CVD method to produce large-area graphene using a gas mixture of hydrogen and methane deposited on surface of copper substrates at temperature up to 1000 ℃.[5a] Most area of the synthesized graphene sheets was dominated by monolayer graphene sheets with less than five percent of multilayer graphene sheets. Vanhulsel et al. showed a plasma-enhanced CVD method without using any catalyst to get micrometer-wide multilayers graphene sheets by controlling a gas mixture of hydrogen and methane in microwave plasma at 700 ℃.[5f]

2.1.3 Epitaxial growth method

Epitaxial growth method is a way to synthesize wafer-size graphene film layers on silicon carbide (SiC) which is heated in vacuum to about 1400 ℃. Because the sublimation rate of carbon is higher than silicon, carbon atoms can be left from SiC substrates to form graphene sheets through rearranging. Shivaraman reported an epitaxial growth method to synthesize free-standing graphene in 2009, in which the 4H-SiC substrate was heated under vacuum condition to 1400 ℃ for 1 hr.[7a] Aristov et al. discovered a method to synthesize graphene sheets onto commercially available cubic SiC/Si substrates.[7b] More recently, Emtsev et al. reported a method to synthesize graphene sheet in 1 bar argon atmosphere using polycrystalline SiC as substrates instead of single-crystal SiC.[7c] But generally speaking, the epitaxial growth methods need strict conditions including high temperature (up to 1000 ℃), vacuum or argon atmosphere,

which may limit the commercialization of this method for large scale graphene production.

2.1.4 Chemical reduction of graphene oxide

There are two advantages to produce graphene using chemical reduction of graphene oxide. One is this method can be used to produce low-cost, large-scale graphene sheets. The other is that the synthesized monolayer graphene sheets can be easily deposited on any substrate, which is helpful to apply in biochemical and electrochemical devices. However, due to hydrophilicity of graphite oxide and the hydrophobicity of graphene sheets, the obtained graphene sheets easily agglomerate which makes the process and the application difficult. To improve graphene solubility and dispersibility in water, scientists try to control some experimental conditions. Li et al. reported that reduced graphene sheets obtained from graphite oxide can form stable aqueous colloid rapidly in a high pH condition.[8] This can help to produce large-scale aqueous graphene dispersions without any surfactant stabilizers or polymeric materials.

2.1.5 Substrate-free gas-phase synthesis

Dato et al. presented a method to produce graphene sheets in atmospheric pressure without substrate. Graphene can be obtained continuously from a microwave plasma reactor using a mixture of argon gas and liquid ethanol droplets.[9] When the input of ethanol was 164 mg min^{-1}, the rate of graphene sheet production can reach to 2 mg min^{-1}, which means this method may be a possible avenue to produce large-scale graphene.

2.2. Applications of graphene and its derived materials

Based on the amazing electronic and geometric properties mentioned in **Chapter 1**, graphene attracts wide applications in sensors[20, 22], transparent electrodes[23], field emission (FE) displays[24], field effect transistors (FETs)[24b, 32]. In this sub-section we will discuss the properties based potential applications of graphene and its derived materials.

Because of the extreme high surface/volumn ration and the sensitive of electronic properties (mainly conductivity) to surface modification, graphene is widely used in sensors. The first graphene based sensor has been reported by Novoselov's group[20] and used to detect single molecules e.g. NH_3, CO, H_2O and NO_2.. A Hall-type configuration(see **Figure 2.1**) shows that when an electron-donor molecule such as NH_3 and CO adsorbed on graphene, the increase of conduction of graphene induced due to the electron; when an electron-withdrawing molecule such as NH_3 and CO adsorbed on graphene, the decrease of conduction of graphene induced due to the holes.

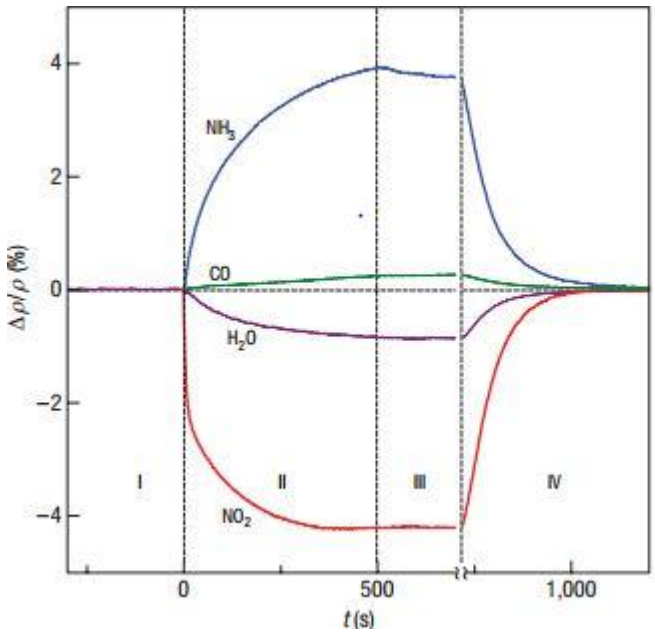

Figure 2.1 The adsorption of NH_3, CO, H_2O and NO_2, changes the resistivity of graphene. [Reprinted by permission from Nature Publishing Group: Nature Materials (ref [20]), copyright 2007]

Despite gas sensing, graphene has potential application in bio-sensing.[22a] Shan et al. demonstrated an electrochemical biosensor based on polyvinylpyrrolidone-protected graphene/polyethylenimine-functionalized ionic liquid/ glucose oxidase (GOD). Direct electron transfer and up to 14 mM linear glucose response has been reported, which shows the potential application of graphene in glucose detecting. Alwarappan et al. employed graphene for electro-chemical detection of dopamine and serotonin.[22b] Compare to carbon nanotube, graphene performs much better in areas such as sensitivity, stability and signal/noise ratio when used to detect dopamine and serotonin.[22b]

Graphene also has potential application in Field emission (FE) displays. In FE displays a high electric field is applied to emit electrons from a material. A sharp tip is used to enhance the electric field in FE displays. Graphene is an ideal material to produce the sharp tip for field enhancement due to its one-atom-layer thin geometric structure. Eda et al. reported a field effect enhancement structure fabricated by graphene thin film erecting on silicon substrate.[24a] This structure was synthesized by spin coating the silicon substrate using graphene oxide/polystyrene solution. The orientation of graphene thin film is controlled by the spin coating speed (see **Figure 2.2**). The low spin coating speed could erect graphene on substrates (see **Figure 2.2B**). The graphene based FE displays prepared by spin coating method showed a turn-on electric field of up to 4V/μm and a field enhancement factor of up to 1200. Wu et al. dispersed graphene sheet in isoprophyl alcohol and then deposited the solutions onto indium tin oxide coated glass substrate to

get erecting graphene on substrate.[24b] The preapared graphene based FE displays showed a field enhancement factor of up to 3700 and a turn-on electric field of 2.3V/μm.

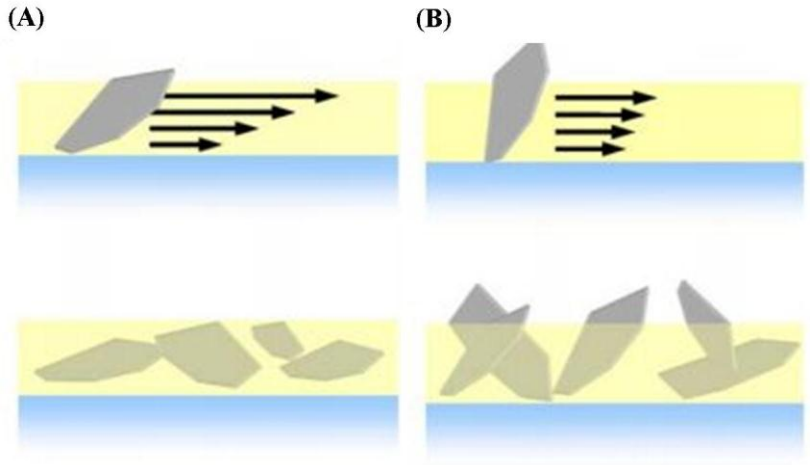

Figure 2.2 Spin coating process at (A) high and (B) low spin coating speeds. Low spin coating speed could erect graphene on substrates [Reprinted by permission from AIP Publishing LLC: Applied Physics Letters (ref[24a]), copyright 2008]

Due to the high electron mobility and switching speed, graphene can also be used to fabricate FETs. Novoselov et al. reported the field effect of graphene in 2004.[3] In thier work, they found that graphene based FETs have extremely high electrons and holes concentration (10^{13} /cm^2) with a mobility of up to 10000 cm^2/V-s. The first graphene based FETs (graphene frake size around 1μm^2) fabricated by e-beam lithography (See **Figure 2.3**) has been reported by Gilje et al, which demonstrated a response to gate voltage range between ±15 V.[24b] Tung et al. have synthesized much larger (up to 20x40 μm) graphene flakes.[32] Based on the larger graphene flakes, multi-arrays of field effect transistors can be fabricated by conventional photolithography method.

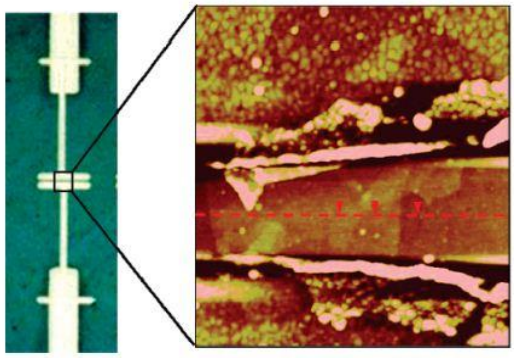

Figure 2.3 FETs fabricated by graphene sheet with Au electrodes. [Reprinted with permission from ref [24b]. Copyright (2007) American Chemical Society.]

Currently the transparent electrodes in touch panels, solar cells, liquid crystal displays and flat panel displays are mainly made by indium tin oxide (ITO). However, ITO is limited supply and high cost, restricting its industrial applications. Graphene is an ideal alternative transparent electrode because of its high transparency, one-atom-layer thickness and extraordinary thermal and chemical stability. Wang et al. have synthesized novel dye-sensitized solar cells (DSSC) with graphene based transparent electrodes (See **Figure 2.4**).[23a] The graphene films are synthesized from thermally reduced exfoliated graphite oxide, which shows a transparency of not less than seventy percent between wavelength range 1000−3000 nm and an excellent conductivity of 550 S/cm. Graphene electrodes based DSSC has a low energy conversion efficiency of 0.26% due to the low-quality graphene sheet. Hong et al. reported a DSSC with graphene and polystyreneslufonate doped poly(3,4-ethylenedioxythiophene) composite films deposited on ITO substrates as transparent electrodes.[23b] The energy conversion efficiency reaches to 4.5%.

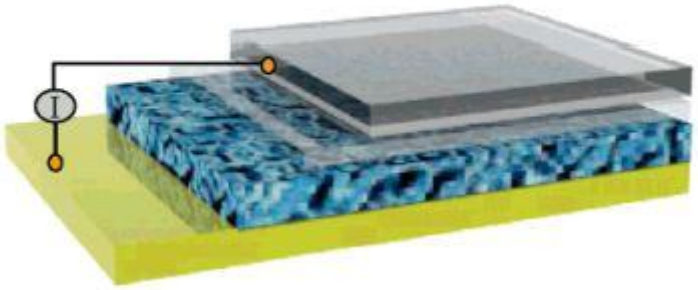

Figure 2.4 Graphene as transparent electrode used in solar cell, 4 layers are graphene film, compact TiO_2, dye-sensitized heterojunction and gold from top to bottom. [Reprinted with permission from (Ref [23a]). Copyright (2007) American Chemical Society.]

2.3. Graphene band-gap manipulation

One of the major challenge of graphene is the opening of its band gap as mentioned in Chapter 1. Intrinsic graphene is a zero band gap material. The band gap opening of graphene is neccessary to widen its applications in semiconductor industries. The technique used to open band-gap of graphene include strain-induced band-gap opening[33], electron field induced band-gap opening on bilayer graphene[34], cutting graphene into graphene nanoribbons and graphene quantum dots to open the band-gap[12] and chem-deposition on graphene surface to open band-gap[35, 41, 42].

Gui et al. first studied the band-gap opening of graphene under external strain.[33] Electronic structures of graphene under external strain in different directions have been studied using density functional theory (DFT) method. No band gap opening is observed when the symmetric strain is applied on graphene sheet. However, the band-gap opening of graphene at Fermi level is observed when the asymmetric strain is applied on graphene sheet. The band-gap opening of graphene is controlled by half diagonal lengths of

graphene primitive cells (L_x and L_y,see **Figure 2.5a**). The diagonal length, L_x can be controlled by applying the strain perpendicular to C-C bond (as shown in **Figure 2.5a**) while the diagonal length, L_y can be controlled by applying strain along C-C bond (as shown in **Figure 2.5a**). A maximum band-gap of 0.49 eV (0.17 eV) is obtained by inceasing the L_y (L_x) to 0.2396 nm (0.1323 nm) as shown in **Figure 2.5b** (**2.5c**).

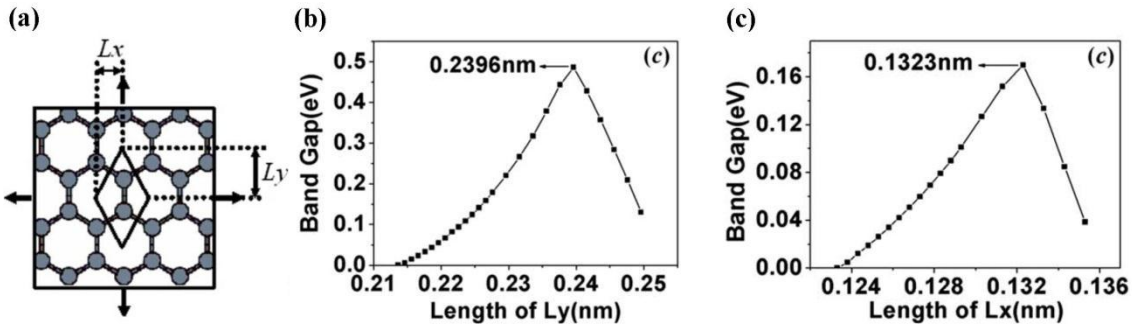

Figure 2.5 (a) Graphene sheet with two stress directions: paralled to the C-C bonds and perpendicular to the C-C bonds.(b) & (c) The graphene band-gap as a function of length of L_y and L_x. [Reprinted with permission from (Ref[33]). Copyright (2008) American Physical Society.]

Applying an external electric field on bilayer graphene is an another approach to open the band-gap of graphene material.[34] Both experimental (Hall conductivity) and theroretical results (using tight-binding method) showed that the band-gap of bilayer graphene can be turnably controlled from zero to mid-infrared energies by applying external electric field on bilayer graphene. Similar to monolayer graphene, the band-gap opening of bilayer graphene is observed near the K point in *k*-space (see **Figure 2.6**).

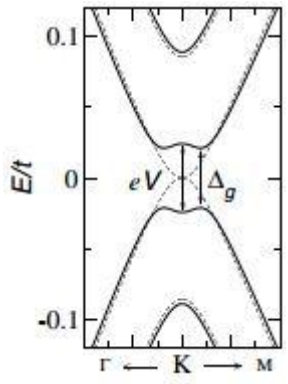

Figure 2.6 Band structure of bilayer graphene with no external electric field (dot line) and external electric field equals to 150 meV (solid line). The band-gap opening occurs at K point. [Reprinted with permission from (Ref[34]). Copyright (2007) American Physical Society.]

Graphene nanoribbon is a quasi-one dimensional structure of graphene with narrow widths. Transforming graphene into graphene nanoribbon (GNR) can open the band-gap of graphene. Graphene based FET fabricated using GNRs showed that the I_{on}/I_{off} ratio increases (see **Figure 2.7**) when the width of GNR decreases[12]. This indicates that the GNRs are semiconducting and their band-gaps can be tuned by tuning the width of GNRs. This is also supported by first principles theoretical calculations (see **Figure 2.7 B)**.[12]

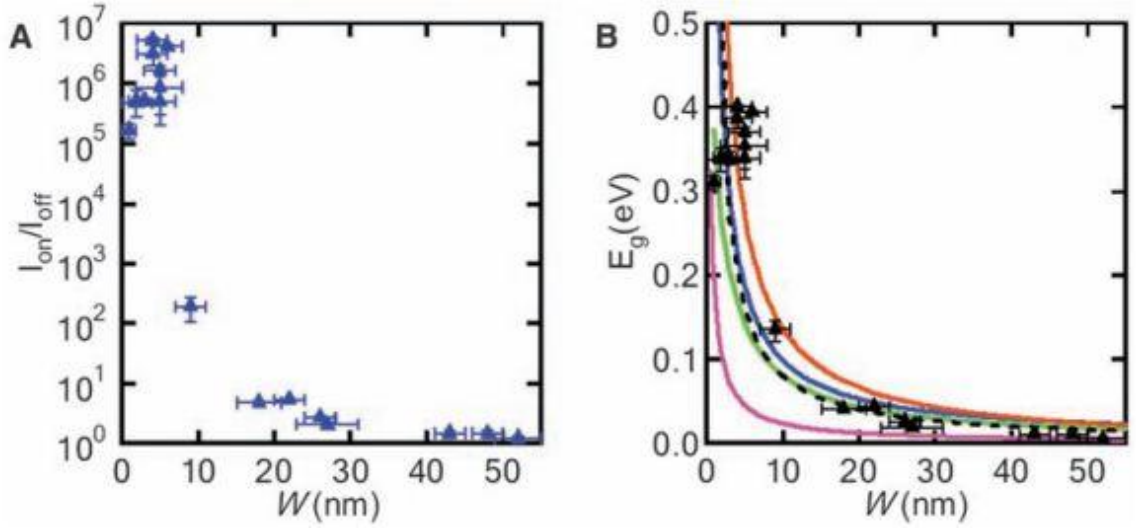

Figure 2.7 (A) On-off current switching ratio of GNRs vurses GNR width. (B) GNRs band-gap energy vurses GNR width. The black dashed line is a fit of empirical equation: $E_g(eV) = 0.8/[W(nm)]$. The purple, blue, orange and green solid lines are experiment data of three kinds of GNRs with armchair edges and one kind of GNR with zigzag edges vurses GNR width. [From (reference [12]). Reprinted with permission from AAAS]

Chemical deposition on graphene surface is one of the most common methods to open band-gap of graphene. Atoms[35b, 41, 42], radicals and noble-metal[35a] can be chemically deposited on graphene surface to open its band-gap. Band-gap opening of graphene by hydrogen atoms adsorption are studied both experimentally[35b] and theoretically[36] . First principles calculations show that when one hydrogen atom adsorbed on graphene sheet, the band-gap opens.[36b] Balog et al. experimentally have showed the band-gap opening of hydrogen adsorbed graphene.[35b] Angle-resolved photoemission spectroscopy (ARPES) was used to get the photoemission intensity. The photoemission intensity of graphene (see **Figure 2.8c**) shows a clear gap (about 0.3 eV), which theoretically should be larger than band-gap, can be observed with the top of π band below Fermi level (E_f). Varykhalov et al. found that some noble metal e.g. Ag and Cu doping on graphene can open band-gap of graphene, but Au doping can not open the band-gap.[35a]

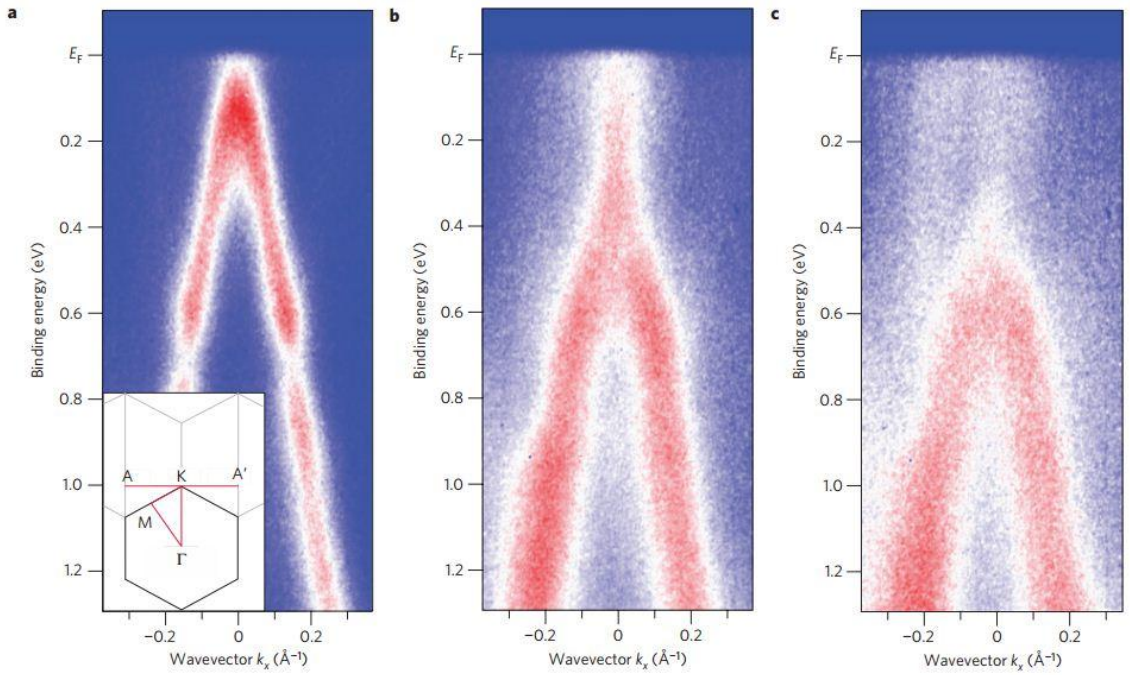

Figure 2.8 Gap (from Fermi level to maximum valence band) opening in hydrogen atom adsorbed graphene. Photoemission intensity along the A–K–A' direction of the Brillouin zone (see inset) for (a) pure graphene, (b) graphene with 30 percentage surface coverage of hydrogen atoms (c) graphene with 50 percentage surface coverage of hydrogen atoms. [Reprinted by permission from Nature Publishing Group: Nature Materials (ref [35b]), copyright 2010]

2.4. Graphene cutting

Band-gap opening of graphene by cutting the graphene sheet is challenging jobs as uncontrolled cutting will results in GNRs, GQDs, etc with different shapes and edges which will strongly affect the electronic properties. GQDs and GNRs are widely used in sensors and FETs. GQDs, GNRs are produced mainly by cutting graphene sheets which include electron-beam lithography and plasma etching[37], sonochemical and electrochemical etching[12, 38], metal catalyzed cutting[39], and reduction of exfoliated

graphene oxide (hydrothermal method)[40] and oxidation unzipping[41]. In this subchapter we briefly describe the methods used to cut graphene sheets.

Electron-beam lithography and plasma etching have been used to cut graphene into GNRs.[37] Chen et al. used electron-beam lithography to pattern graphene, followed by using hydrogen silsesquioxane (HSQ) as etching mask and applying an oxygen plasma etching to get GNRs with different width ranging from 20 to 200 nm.[37a] Here, electron-beam lithography is used to prepare small pieces of graphene which has similar size of the HSQ mask and the oxygen plasma etching is used to etching unprotected graphene away. The produced GNRs have been fabricated into field effect transistors to study their electronic properties.

Sonochemical and electrochemical etching is also widely used method to cut graphene.[12, 38] Li et al. dispersed graphene into a 1, 2-dichloroethane (DCE) solution of poly (m-phenylenevinylene-co-2, 5-dioctoxy-p-phenylenevinylene) (PmPV) by sonication for 30 minutes. [12] After removing the large pieces of materials by centrifugation, GNRs have been systhesised. The widths of produced GNRs range from 10 to 50 nm. Wu et al. produced GNRs with similar sonochemical method, but they dispersed graphene into 0.1 wt% sodium dodecyl sulphate and 0.1 wt% polyvinylpyrrolidone (PVP) mixed solution instead of DEC solution of PmPV.[51] The reaction time is 1 hour and 85% of produced GNRs have widths range from 5 to 50 nm.

Graphene can be cut into small pieces using metal nanoparticles as a knife.[39] Datta et al. demonstrated the cutting of few layers graphene at 900 ^{o}C by Fe nanoparticle catalyst.[39b] The proposed metal catalyzed graphene cutting mechanism is shown in **Figure 2.9 b**. Ci et al. further studied nickel catalyzed graphene cutting.[39a] The nickel

nanoparticles deposited on highly-ordered pyrolytic graphite (HOPG) was heated with Ar/H_2 mixed (volum ratio: 17:3) gas flow at high temperature at 1000 ^oC for 30 mins which produced 2 μm long nanotrenches. The angles between nanotrenches are 60^o and 120^o, which means that the nickel catalyzed graphene cutting follows similar orientations in the graphene honeycomb lattice (see **Figure 2.9 a**).

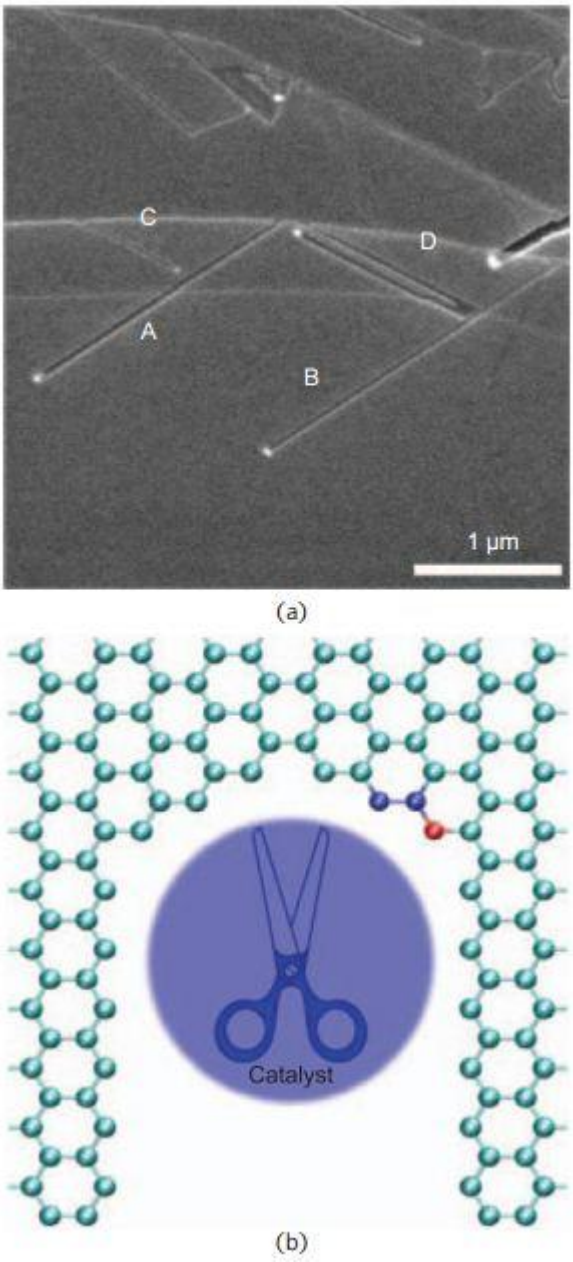

Figure 2.9 (a) SEM figure of nanotrenches etched on nickel deposited graphene by thermal cutting. (b) Metal catalyzed graphene cutting. (Reprinted from ref[39a] with kind permission from Springer Science and Business Media).

Hydrothermal method is also commonly used to synthesize both GNRs and GQDs from graphene. Deng et al. synthesized blue-luminescent GQDs using hydrothermal method.[40] Concentrated sulfuric acid and nitrate acid mixed solution was used to oxidize graphene sheet (GS). The hydrophilic groups such as hydroxyl, carbonyl/carboxyl and epoxy will appear both on the basal plane and at the edge of graphene. The oxidized GSs were then hydrothermally treated at 200 ^{o}C. The cutting mechanism has been proposed as the epoxy chain formation on graphene sheet. Then, the hydrothermal deoxidation leads to the unzipping of graphene sheet (see **Figure 2.10**).

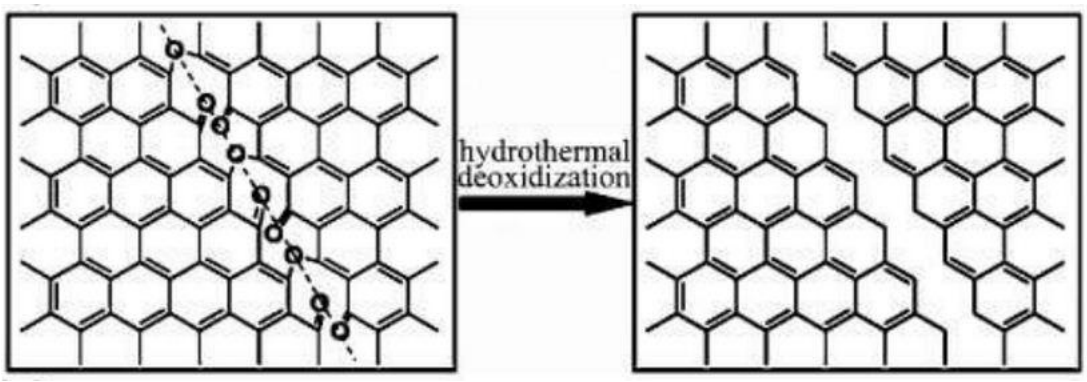

Figure 2.10 Mechanism for hydrothermal cutting of oxidized graphene sheet. [Reprinted with permission from ref[40]. Copyright 2009, John Wiley and Sons]

Fujii et al. unzipped graphene by a pure oxidation method.[41] Concentrated sulfuric acid and potassium permanganate mixed solution was used to oxidize the graphene. During the oxidation, stirring is applying for 1 hour to the solution to form thick paste. Water is added to the thick paste and stirred for another 30 mins. After that, more water is

added followed by slow addition of hydrogen peroxide. The oxidized samples has been filtered and washed and dried at 80 ^{o}C for 20 hours to get the purified nanosized graphene pieces.

2.5. Theoretical studies of graphene

In this subchapter we briefy describe the theoretical works on chemical modification of graphene to open graphene band-gap, oxidative unzipping of graphene and photoluminescence properties of GQDs.

2.5.1 Chemical modification on graphene surface

2.5.1.1 Interaction of graphene with molecules

Thierfelder et al. reported the interaction of graphene with methane, using DFT complemented with a semiempirical dispersion correction scheme (DFT-D).[42] The adsorption configuration is shown in **Figure 2.11**, the absorption energy of methane is 0.17 eV, which is close to experimental data.

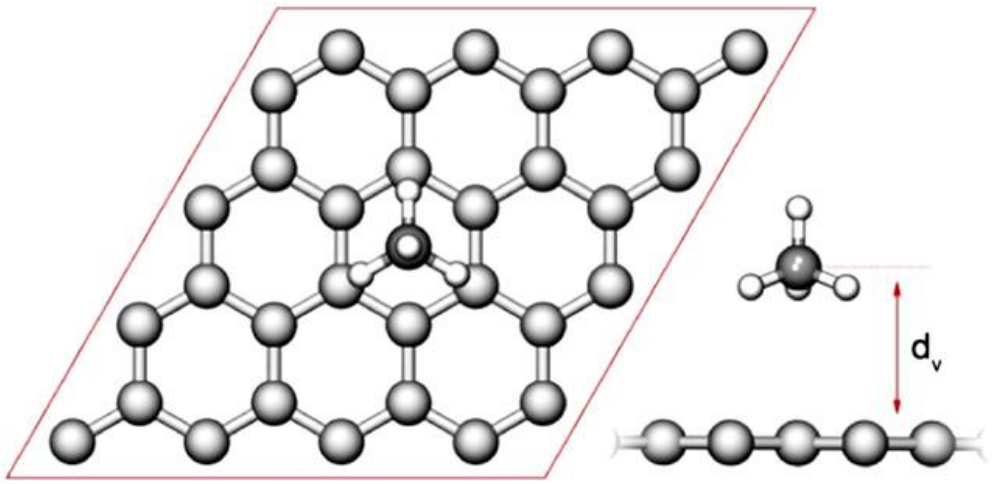

Figure 2.11 Top and side views of methane adsorbed on graphene. [Reprinted with permission from ref [42]. Copyright 2011, Elsevierr]

Shigeaki et al. presented interaction of graphene with ethylene carbonate (EC) by DFT calculations.[43] EC preferred to bindat the edge region of graphene which is 4.2 kcal/mol stronger than the binding at hexagonal position of graphene. The theretical study shows that the EC can move freely on graphene surface before down into edge region.

Liu et al. studied the interaction between graphene nanodot and CO, using first-principles DFT calculations.[44] It has been found that when CO comes close to the vacancy defect in graphene, CO and vacancy recombination remerge instantaneously. In addition, application of external electric field can enhance the CO adsorption on the defective graphene nanodot.

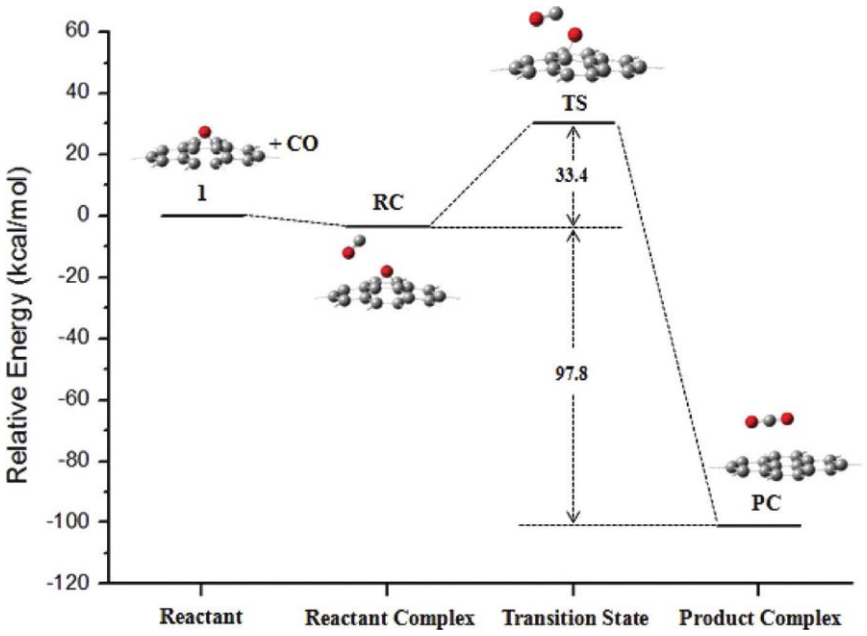

Figure 2.12 Energy profile of vacancy defect of graphene healed with CO adsorption and CO2 desorption. [Reprinted with permission from Ref[44]. Copyright (2012) American Chemical Society.]

2.5.1.2 Interaction of graphene with Atoms/ Radicals

Dzhurakhalov et al. studied the interaction of single layer graphene with hydrogen atoms, using atomistic simulations with the second generation of reactive empirical bond order Brenner inter-atomic potential.[45] When single H atom adsorbed, it prefers to attach on the top of carbon atom. However, when two or more atoms attaching, ortho hydrogen pair is formed. Theoretical binding energy calculation results also proved that H atoms prefer to form ortho pair, ortho-para pair configuration and para pair configuration at different of graphene sheet.

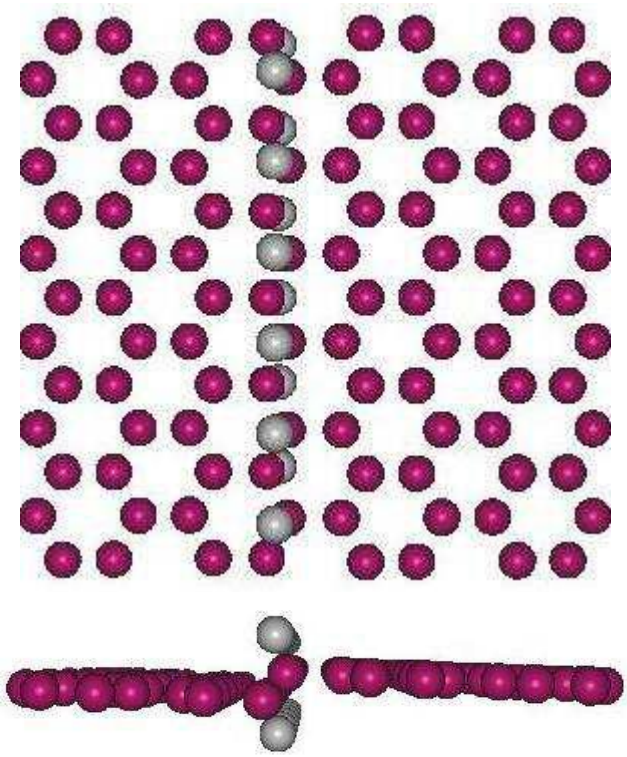

Figure 2.13 Top and side views of geometric structure of H atoms adsorbed graphene. [Reprinted with permission from ref[45]. Copyright 2011, Elsevier]

Ijas et al. investiagted the interaction of graphene with chlorine using DFT calculations.[46] Chlorine prefers to bind on graphene basal plane near the edges. In

addition, the ab initio thermodynamics calculation shows that high concentration of chlorine breaks the C-C bond in pristine graphene.

Denis et al. studied nitrene radicals adsorption on graphene using DFT calculations with LDA and PBE functionals.[47] The result showed that the perfect graphene had high reactivity with nitrene radicals. But it is difficult to open the band-gap of graphene with nitrene radical adsorption. Even one NH group per 32 carbons cannot open the band-gap of graphene.

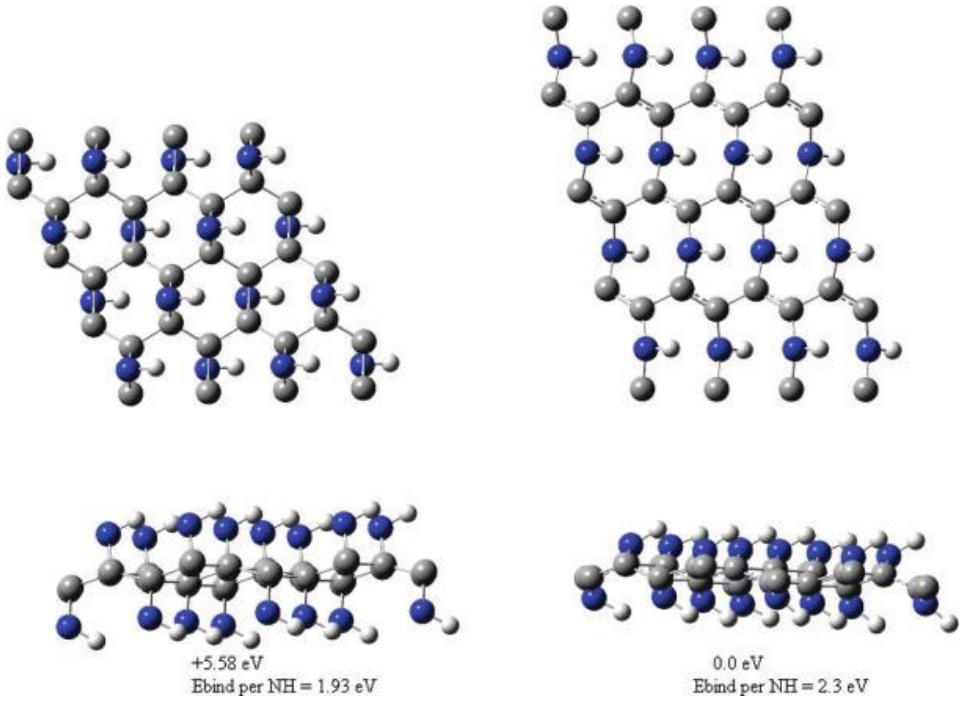

Figure 2.14 Top and side views of geometric structure of NH radicals adsorbed graphene. Left: C-C bonds unbroken, right: C-C bonds broken. [Reprinted with permission from Ref[47]. Copyright (2011) American Chemical Society.]

2.5.1.3 Interaction of graphene with Metals

The calculated adsorption energies of Ag, Pd and Au with graphene are 2.3, 19.7, and 4.2 kcal/mol, respectively[48] using the single and double electron excitations with perturbative evaluation of the contributions of triple excitations (CCSD(T)). It was obserbed that the nature of Ag, Pd and Au adsorption with graphene is different. Dispersion interactions dominate for the adsorption of Ag with graphene while the adsorption of Au involves charge transfer, dispersion interactions and relativistic effects. Pd adsorption can form covalent bond with carbon atoms of graphene.

2.5.2 Theoretical studies on oxidative unzipping of graphene

Oxidative unzipping of graphene can form GQDs and GNRs with different shapes and edges. Since, the electronic properties of GQDs and GNRs strongly depend on the shapes and edges configurations, thus it is neccessary to understand the oxidative cutting mechanism of graphene to control the shapes and edges of GQDs and GNRs. Numerous theoretical studies have been performed on oxidation of graphene. Je-Luen Li et al. observed the occurrence of line defect on partially oxidized graphite on the dark field optical microscope image.[49] The formation of epoxy groups on coronene ($C_{24}H_{12}$) and $C_{54}H_{18}$ was invesitaged using DFT calculations to understand the mechanism of formation of observed line defects.. The calculations show that the formation of epoxy chain along zigzag orientation on same side of coronene ($C_{24}H_{12}$) and $C_{54}H_{18}$ break the underlying C-C bonds.

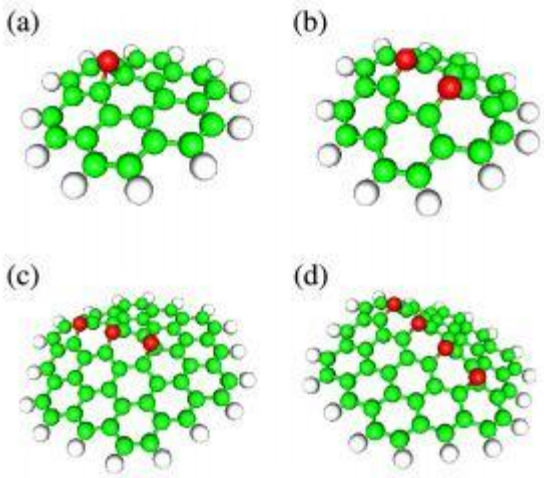

Figure 2.16 Epoxy groups adsorbed on graphene ($C_{24}H_{12}$ and $C_{54}H_{18}$). (a) One epoxy group on $C_{24}H_{12}$. (b) Two epoxy groups on $C_{24}H_{12}$. (c) Three epoxy groups on $C_{54}H_{18}$. (d) Four epoxy groups on $C_{54}H_{18}$.[Reprinted with permission from (Ref [49]). Copyright (2006) American Physical Society.]

However, Paci et al. showed that the occurrence of epoxy chain does not strongly affect the mechanical strength of graphene sheet using molecular dynamics (MD) simulations.[50] There is less than 17% weakening in the fracture stress due to epoxy chain defect as compared to a pristine sheet, which indicates that although epoxy chain breaks the underlying C-C bonds, it does not lead to the breakage of the graphene sheet itself.

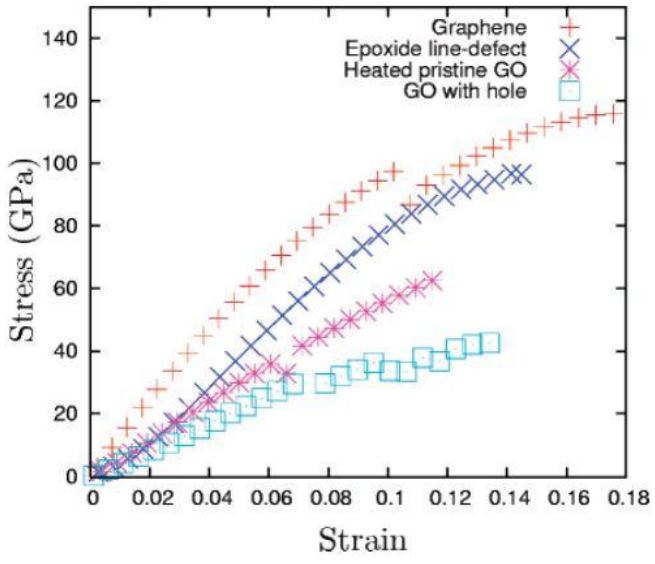

Figure 2.17 Stress versus strain figure of graphene, epoxide line-defect graphene, heated graphene and graphene oxide with holes. [Reprinted with permission from Ref[50]. Copyright (2007) American Chemical Society.]

Experimental study shows that there are carbonyl groups on graphene oxidation,[51] and solid state nuclear magnetic resonance (SSNMR) spectra show the carbonyl groups are spatially separated from the sp^2 carbon atoms, C-OH, and epoxide carbons.[52] These results indicate that the carbonyl groups on graphene oxide mainly appear at the graphene edge, closely related to the graphene cutting. Based on these findings, Zhen-Yn Li et al. further invesitaged the mechanism of oxidative cutting of graphene using DFT calculations.[53] They found that oxygen atoms can form epoxy pairs (***ep***) on both side of graphene sheet and these ***ep***s can transform into more stable carbonyl pairs (***cp***), and break the graphene sheet. Based on their calculations they have proposed a two steps mechanism - first: the formation of epoxy lines, second: the formation of epoxy pairs (***ep***) on both sides of graphene plane which is transformed into carbonyl pairs (***cp***).

Ma et al. studied the oxidation of graphene under applied external tensile strain using DFT.[54] The tensile strain breaks the high symmetry of graphene lattice and the epoxy groups prefer to align perpendicular to the strain direction. The applied strain significantly lowers the reaction energy barrier and enthalpy of ***ep***→***cp***. It was proposed that the applied tensile strain can control zigzag edge formation.

2.5.3 Theoretical study on Photoluminescence (PL) properties of GQDs

Schumacher studied the photophysics of GQDs using TDDFT calculations and found that in excited GQD the bright transition path is from S_0 to S_3 or S_4.[55] Zhao et al.

also showed that the maximum adsorption wavelength λ_{max} corresponding to S_0 to S_3 or S_4 transition energies[56] and the absorption wavelength red-shifted in prsesence of solvent. The functional groups present at the edge of GQDs also are attributed to the cause of red-shifting.

Jin et al. studied the band-gap of GQDs with amino groups using DFT calculations.[57] The GQD consisting of 13 aromatic rings with no amino group has a band-gap of 2.508 eV, which is highly agreed with the experimental data of the PL peak energy of GQD (2.480 eV). The gradual narrowing of band-gap is observed with more amino group attachment on GQDs due to electron donating nature of amino group.

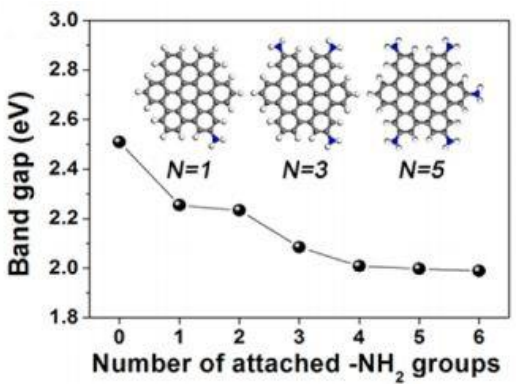

Figure 2.18 Band-gaps of GQDs versus number of attached amino groups. [Reprinted with permission from Ref[57]. Copyright (2013) American Chemical Society.]

Chapter 3

Theory and Computational Details

In this theoretical research, density functional theory (DFT) is used in all the calculations. The theory of DFT (including local density and generalized gradient approximations) is briefly discussed below. The computational models, calculations of

band structures and Bader charge analysis method are also briefly introduced in the following section.

The density functional theory (DFT) is a quantum mechanical modeling method used to investigate the geometric and electronic structure of many-body systems such as particular atoms and molecules. DFT method has its conceptual roots in the Thomas–Fermi model, but is originally derived from the Hohenberg–Kohn (HK) theorems[58], which state that the ground-state electron probability density ρ_0(x,y,z) uniquely determines both ground-state molecule energy, wave function, and other electronic properties of a molecule[59]. The ground-state electronic energy E_0 is a functional of ρ_0 represented as $E_0 = E_0(\rho_0)$. The HK theorem does not include how to calculate E_0 from ρ_0 or how to find ρ_0 without first finding the wave function[59]. Fortunately, with the help of Kohn-Sham (KS) method, one can get ρ_0 and E_0 practically. The electron density can be expressed by a linear combination of basic functions. The electron density obtained from Kohn-Sham orbitals, which are determinant formed from those basic functions, can be used to compute the ground-state electronic energy. In principle, KS theory allows one to solve the Schrodinger equation to obtain the exact ground-state energy. Unfortunately, the exact form of the exchange-correlation potential of KS theory is not known. Thus, the different approximations e.g., local density approximation (LDA), generalized gradient approximation (GGA) have been used.

3.1. Computational Details

All the calculations were performed mainly by density functional theory (DFT).[60] For periodic graphene systems, all the calculations were performed within generalized gradient approximation Perdew-Burke-Eznerhof (GGA-PBE)[61] as implemented in Vienna

ab initio simulation package (VASP)[62]. We used projector augmented wave method (PAW)[63] to describe the interaction between the atomic cores and electrons. The energy cutoff of 450 eV was used for all the calculations. We have used 2x2x1 Monkhorst-Pack k-point[64] for our studies on graphene. The molecular structures and bondings of graphene quantum dots (GQDs) were studied by DFT/B3LYP (Becke's three-parameter hybrid function[65] with the non-local correlation of Lee-Yang-Parr[66]) methods with 6-31g(d) basis set. The absorption and emission spectra of GQDs were studied by TDDFT/B3LYP method with 6-31g(d) basis set. All the calculations were carried out using Gaussian 09 suite of program[67].

3.2. Models

Periodic model of graphene was used to study the interaction between graphene and phenyl radical(s), oxygen atom(s) as shown in **Figure 3.1a**. To investigate the band-gap, absorption and emission of GQDs, the polyaromatic hydrocarbons are used as GQD models (see **Figure 3.1b**). The detailed descriptions of graphene models used for our studies were mentioned in the individual chapters.

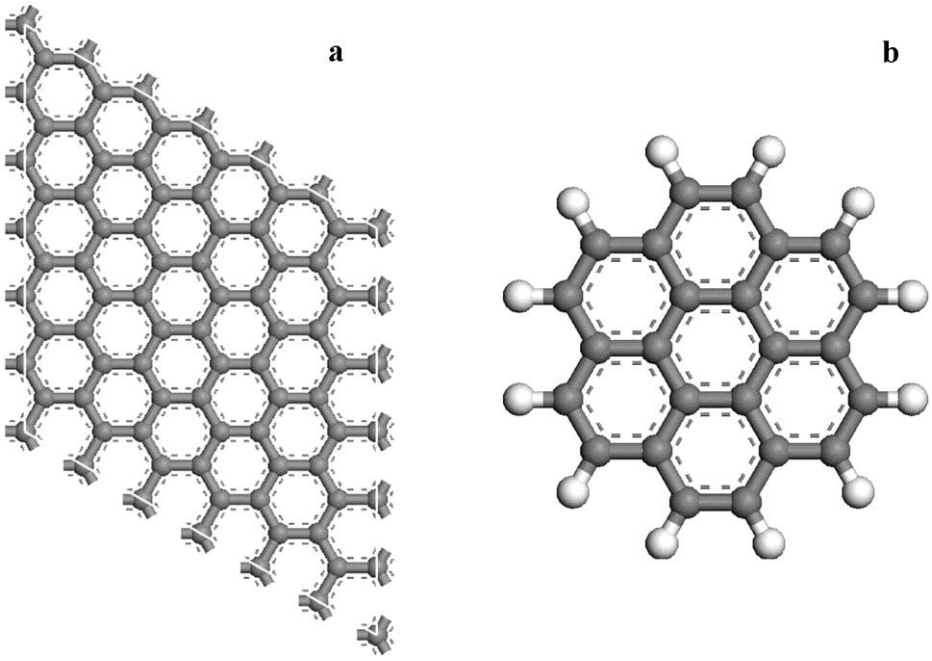

Figure 3.1. (a) Periodic model of graphene and. (b) polyaromatic hydrocarbons model of GQD.

3.3. Electronic Band Structures

Based on electronic conductivity, materials are classified as metal, semi-conductor and insulator. The energy band and band-gap are important concepts of semiconductor. In a solid, there are theoretically infinite numbers of bands. In the metal, the bands are partly empty and partly filled regardless of temperature. The almost fully occupied band is called valence band (bands below Fermi level) and almost unoccupied band is called conductance band (bands above the Fermi level). The valence band and conductance band are overlapped in a metal. Band-gap is the difference between valence band and conductance band energies. Insulators have larger band-gap than semi-conductors.

The band structure plot gives the energies of electronic orbitals for each point in the wave vector *k* called Brillouin zone (BZ) corresponding to the crystal lattice. The *k*-space

describes the bonding nature of orbitals, not a physical space. There are three dimensions (k_x, k_y, k_z) in a 3D crystal *k*-space. Γ represents the point where $k = 0$, *M* represents the point where $k = \pi/a$. $k = 0$ in some directions and $k = \pi/a$ in some other directions is designated as *X*, *Y*, *K* and *A* depending on the symmetry of the crystal.

The electronic band structure can be calculated by any methods yielding orbital energies. In recent years, with the developing of *ab intio* and DFT methods, the tendency to use these methods is incraesing. For band structure calculation, the plan wave basic functions are proposed because they reflect the infinite symmetry of the crystal. Unit cell vectors and crystallographic angles must provide to calculate the band structure. The band-gap can be simply got through the band structure.

3.4. Bader Charge Analysis

Richard Bader developed Quantum Theory of Atoms in Molecules (QTAIM) which can be used to divide atoms in molecules.[68] The QTAIM method uses zero flux surfaces, where the charge density is a minimum perpendicular to the surface, to definite the volumn of an atom. QTAIM can be used for atoms charge analysis, called Bader Charge Analysis.

Chapter 4

Theoretical study on the band-gap manipulation of graphene

Since the first discovery of graphene in 2004[3], a single atomic layer of graphite consisting of sp^2-hybridized carbon atoms, attracts a great deal of interest due to its unique properties, which can be widely applied in various fields such as field-effect transistors (FETs)[69], transparent conducting electrodes[70], optical modulators[71], solar cells[72], ultracapacitors[73], and bio-applications[74]. Graphene is widely accepted as a zero band-gap semi-metal. The major challenge for wider applications of graphene in electronic devices is to open its band-gap. However, there are limited reports on being successful in opening graphene's bandgap.[35b, 75]

Chemical surface modification is a possible way to open graphene's band-gap. Experimental observations showed that hydrogenation of graphene prefers to react on the single layer graphene rather than double layers, and the process can be controlled reversibly.[76] Hornekær et al. presented that atomic hydrogen preferentially stick on *ortho* and *para* sites on graphite using DFT method.[77] An *ortho-ortho* position hydrogen pairing (see below) on graphene was confirmed by first principles scanning tunneling microscopy (STM) simulations.[78] DFT calculations showed that hydrogen dimers chemisorbed on *ortho* and *para* positions are the most stable.[79] Atomistic simulations showed that when there are two or more hydrogen atoms chemisorbed on graphene sheet, the most stable configurations on monolayer graphene are hydrogen atoms adsorbed on *ortho-ortho* position on both sides of the graphene sheet, while *ortho-para* position combinations are less stable.[45] It has been showed theoretically that fully hydrogenated graphene sheet is a semiconductor with a band-gap larger than 3.5eV,[80] and 50% hydrogenated graphene sheet has a band-gap of ~ 0.43eV.[81] Wu *et al*. showed that graphene can be functionalized by chlorine using plasma reaction with much slower reaction kinetics indicating the controllable reaction.[82] A band-gap opening of chlorine functionalized graphene is observed by both ultraviolet visible (UV-vis) absorption spectroscopy[75c] and DFT calculations.[83] Sodium azide can be used to introduce nitrene group on graphene and to exfoliate graphene layers.[84] Theoretical calculations showed that high level of nitrene and nitrene derivative (perfluorophenylazide by cycloaddition reaction) functionalization is needed to open the band-gap.[47, 85] However, more nitrene radicals attachment on graphene damaged the graphene sheet by breaking the C-C bond of graphene.

Diazonium chemistry is a common and facile approach to functionalize the surface of graphene.[86] Bekyarova *et al*. reported that 4-nitrophenyl functionalized graphene is a semi-conductor.[87] Hossain *et al*. reported formation of covalent bond between 4-nitrophenyl group and graphene by STM study.[88] Covalent functionalization of graphene with 4-tert-butylphenyl groups (TBP) has been studied by Peizhe Tang *et al.* using first-principles calculations combined with the model Hamiltonian analysis.[89] Phenyl radical functionalized multiple-layer graphene has been reported.[90] However, there are limited reports on the adsorption of phenyl radicals with monolayer graphene sheet and their effects on electronic properties of graphene.

In this article, we report a systematic study of phenyl (Ph·) radical adsorption on monolayer graphene and their electronic properties using DFT calculations. First we investigate the adsorption of phenyl radical on graphene with different number of radicals to find the most favorable binding sites. Then, by analyzing the band structures of functionalized graphene we address the band-gap opening of monolayer graphene. We found that the even number of phenyl radical adsorptions on monolayer graphene open the graphene's band-gap when there is ortho-ortho or ortho-para pairings.

4.1. Computational methods

We use (6x6) graphene sheet for our current study. We generate the (6x6) graphene sheet from the graphite structure. All the calculations are performed within the frame work of DFT with the generalized gradient approximation (GGA) method

using Perdew-Burke-Eznerhof (PBE) functional[91] as implemented in Vienna ab initio simulation package (VASP).[92] To describe the interaction between the atomic cores and electrons the projector augmented wave method (PAW)[93] is used. For geometry optimization, a 2x2×1 Monkhorst-Pack *k*-point[94] mesh and an energy cut of 400 eV are used for all the calculations. The structure optimization is continued until the maximum forces acting on each atom become less than 0.01 eV $Å^{-1}$. The monolayer graphene is a 2D-structure. In our model the *x*- and *y*-axes are the periodic directions of graphene sheet. We apply vacuum in *z*-direction. We keep the distance ~ 1.0 nm between the two nearest supercells along *z*-axis to prevent the interactions between the neighboring atoms.

The binding energy of the 1st and nth phenyl radical on graphene is calculated using following equations –

$$E_{BE}(1^{st})=E_{graphene+Ph\bullet}-E_{graphene}-E_{Ph\bullet} \quad (1)$$

$$E_{BE}(nth)=E_{graphene+nPh\bullet}-E_{graphene+(n-1)Ph\bullet}-E_{Ph\bullet} \quad (2)$$

Where, E_{BE}(1st) and E_{BE}(nth) is the binding energy of 1st and nth Ph ·with graphene, $E_{graphene+\ Ph\ \cdot}$ is the total energy of Ph ·radical adsorbed graphene, $E_{graphene}$ is the total energy of pure graphene, $E_{graphene+\ n\ Ph\ \cdot}$ is the total energy of n number of Ph ·adsorbed graphene, $E_{graphene+\ (n-1)\ Ph\ \cdot}$ is the total energy of (n-1) number of Ph ·adsorbed graphene and $E_{Ph\ \cdot}$ is the total energy of Ph : The negative binding energy indicates favorable adsorption.

4.2. Results and Discussion

4.2.1. Pure Graphene.

We use (6x6) graphene sheet as shown in **Figure 4.2a** for our current study. The optimized lattice constant, a is 2.470 Å, agreed well with reported experimental lattice constant of graphene a = 2.454 Å at 300 ℃[95] and graphite a = 2.4589 Å at 297 ℃[96]. Lindsay and Broido calculated the lattice constant of graphene a = 2.460 Å with Brenner empirical optimization and a = 2.492 Å with Tersoff empirical optimization.[97] The calculated band-gap of (6x6) graphene sheet is zero in agreement with band structure of pure graphene reported by Zhou et al[98]. The calculated band structures of (3x3), (4x4), (5x5), (6x6), (7x7) and (8x8) graphene are shown in **Figure 4.1**. All these structures are zero band-gap semi-metal. The zero band-gap point of graphene (6x6) is at Γ point. We have calculated the band structure of graphene (6x6) along high symmetry K-K'-Γ-M-K paths (see **Figure A1** and **Table A1**, Appendix A) to make sure the Γ point is the lowest (0) band-gap point.

We choose 6x6 cell because the (3x3), (4x4) and (5x5) cells are small for our phenyl radicals adsorption especially when there are four radicals in consideration while graphene (7x7) and (8x8) are relatively large which are computationally more costly. Thus, the graphene model we have chosen here represents pure semi-metal graphene and is sufficient for our current study.

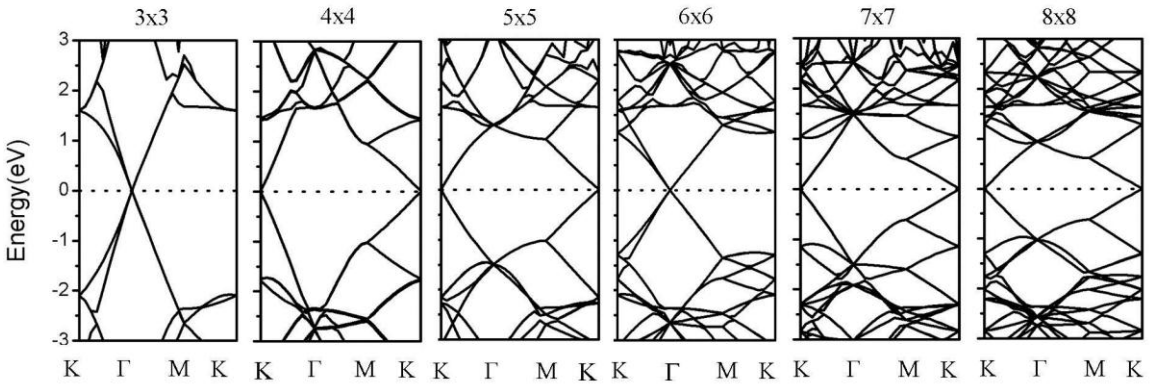

Figure 4.1 Band structures of grephene (3x3), (4x4), (5x5), (6x6), (7x7), (8x8) cell

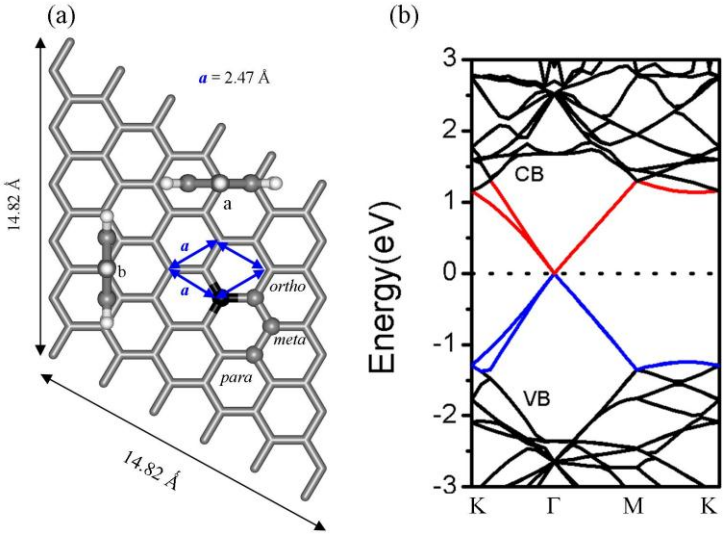

Figure 4.2 (a)Single phenyl radical adsorbed graphene with a. phenyl ring's plane parallel to one of the C-C bond on graphene; b. phenyl ring's plane perpendicular to that C-C bond on graphene. Grey spheres – C; black sphere – C attached with phenyl group; white sphere – H. (b)band structure of optimized (6x6) monolayer graphene sheet

4.2.2. Adsorption of Single Phenyl Radical on Graphene.

We start with adsorption of single phenyl radical on monolayer graphene. We consider two initial configurations for single Ph · radical adsorption on graphene: (a) the plane of the phenyl ring is parallel to one of the C-C bond on graphene and (b)

perpendicular to that C-C bond on graphene (see **Figure 4.2**). The Ph · radical interacts with graphene by forming C-C single bond with bond length of ~ 1.60 Å. The adsorption of Ph · radical introduces defect in pure graphene by changing the hybridization of the graphene's C atom attached with radical from sp^2 to sp^3.

The calculated binding energy of phenyl radical with parallel and perpendicular configuration is -0.23 eV and -0.22 eV, respectively (see Table 1). This indicates that the parallel configuration is of comparable stability. Jiang et al.[90] calculated the binding energy of single Ph ·radical with graphene sheet to be -0.25 eV using DFT-GGA method. Recent work of Tang et al.[89] showed the binding energy of 4-*tert*-butylphenyl with graphene is -0.29 eV using GGA-PBE method. Our results show that after single Ph · adsorbed on graphene, the magnetic moment becomes ~0.8 μ_B suggesting the presence of an unpaired electron. The reason is that adsorption of Ph· radical breaks one of π-bond of graphene and generates an unpaired electron. This motivate us to study the adsorption of two Ph ·on graphene.

Table 4.1 Calculated Binding Energy, Net Magnetic Moment and Band-gap of Phenyl Adsorbed Graphene

Radicals		nth E_{BE} (eV)	Band-gap (eV)	Net magnetic moment (μ_B)
one Ph ·radical	Parallel	-0.23	0.00	0.80
	Perpendicular	-0.22	0.00	0.80
Two Ph ·radicals	*ortho-s*	-1.05	0.05	0.00
	meta-s	-0.15	0.00	1.95
	para-s	-1.29	0.07	0.00
	ortho-d	-1.58	0.08	0.00
	meta-d	-0.12	0.00	1.96
	para-d	-0.97	0.06	0.00
Three Ph ·radicals	*ortho-s*	-0.72	0.00	0.88
	meta-s	-0.21	0.00	0.84
	para-s	-0.81	0.00	0.52
	ortho-d	-0.57	0.00	0.88
	meta-d	-0.18	0.00	0.87
	para-d	-0.48	0.00	0.49
Four Ph ·radicals	*1-s*	-0.77	0.09	0.00
	2-s	-1.14	0.06	0.00
	3-s	-0.09	0.06	0.00
	4-s	-1.01	0.05	0.00
	5-s	-0.90	0.09	0.00
	1-d	-1.50	0.09	0.00
	2-d	-1.21	0.06	0.00
	3-d	-0.93	0.06	0.00
	4-d	-1.38	0.07	0.00
	5-d	-1.16	0.09	0.00

[a] For definition see the text and Figure 4

4.2.3. Adsorption of Two Phenyl Radicals on Graphene.

We investigated the adsorption of two Ph• on graphene by attaching another Ph• to the ortho, meta and para site with respect to the initial adsorbed Ph• (see **Figure 4.2**). We also consider the adsorption of second radical in same (denoted as –s, i.e., *ortho-s, meta-s* and *para-s*) and different (denoted as *–d,* i.e., *ortho-d, meta-d* and *para-d*) sides of graphene plane (see **Figure 4.3**).

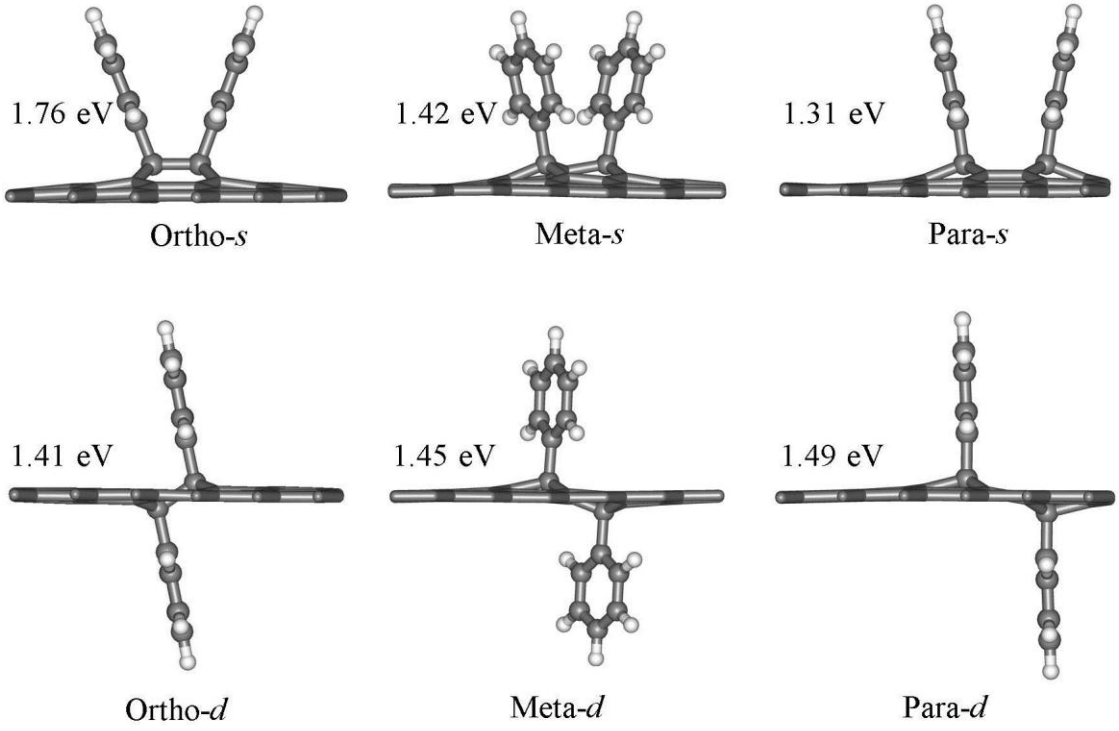

Figure 4.3 Optimized structure of two phenyl radical adsorbed graphene. The number is the corresponding calculated Buckling Energy of Second Phenyl Radical Adsorbed Graphene. Black sphere indicates C atom bonded to phenyl group, and pink sphere indicates the binding sites for second radical adsorption.

The binding energy of Ph · on *ortho-s*, *meta-s* and *para-s* position of pre-adsorbed Ph · graphene, is -1.05, -0.15 and -1.29 eV, respectively. The binding energy of second Ph · on graphene on *para*-s position calculated by Jiang et al.[90] is -1.27 eV. The binding at *meta* site is the least stable compared to *ortho* and *para* sites. The reason is that once the first radical is adsorbed, the generated unpaired electron is delocalized at *ortho* or *para* position due to the *mesomeric effect*.[30] Boukhvalov et al. first showed the mesomeric effect on hydrogen absorbed graphene.[99] The calculated local magnetic moments of single Ph · radical adsorbed graphene shows that localization of the unpaired electron is large at *ortho* and *para* sites as compared to *meta* site. When the second Ph · radical is

attached on *ortho* or *para* position it saturate the single Ph · adsorbed graphene by electron pairing and hence the calculated magnetic moment become zero for both *ortho-s* and *para-s*. However, the adsorption at *meta* position breaks another aromatic π-bond and generates one more unpaired electron, and the functionalized graphene remains as radical with two unpaired of electrons with calculated magnetic moment of ~1.95 μ_B. These are in agreement with the theoretical report by Ferro et al. for H adsorption on graphene with magnetic moment of about 2 μ_B.[100]

When the second Ph · is attached to the *ortho-d*, *meta-d* and *para-d* sites, (see **Figure 4.2**), the binding energy increases from -1.05 to -1.58 eV for *ortho-d* position, decreases from -0.15 to -0.12 eV for *meta-d* position and decreases from -1.29 to -0.97 eV for *para-d* position. Our results show large difference in binding energy for *ortho* and *para* positions with second radical adsorption on different side of graphene plane. This may be due to different factors e.g. steric repulsion between the two phenyl groups and structure buckling of graphene. We have calculated the steric repulsion energy between two phenyl groups adsorbed on same side of graphene plane. The calculated repulsive interaction energies of two phenyl groups at *ortho*, *meta* and *para* positions are ~0.53, ~0.34 and ~0.32 eV. Thus, the increase of binding energy of second Ph ·radical for *ortho* position and on different side of graphene plane, may be due to vanishing of the steric repulsion. However, in case of *meta* and *para* positions instead of increase, the binding energy decreases. This suggests that the steric repulsion is not the main factor which affects the binding energy of second Ph ·adsorptions. The difference in binding energy of two Ph · adsorption on different sides of graphene plane not only come from the steric repulsion but also from the structural changes of graphene near the adsorption sites,

which include buckling and dimerization of carbon atoms on graphene sheet.[101] Buckling is defined as the deformation of graphene plane due to radical adsorption. We have calculated the buckling energy (i.e., deformation energy) of graphene is 1.40 eV for single radical adsorption. The calculated buckling energy for second radical adsorption is 1.76 (1.41), 1.42 (1.45) and 1.31 (1.49) eV for *ortho*, *meta* and *para* position on the same (different) side (see **Figure 4.2**). The larger buckling energy on the same side of *ortho* position indicates that binding on the same side of *ortho* position is more difficult than different side, which explains the smaller binding energy on same side of *ortho* position. Moreover, on the *meta* and *para* positions, the buckling energy is larger on the different side compared to those on the same side, which lead to the smaller binding energy of the second radical adsorption on the different side. Thus, the buckling effect plays an important role to determine the binding energy of Ph · radical adsorption on same and different sides of graphene plane. In conclusion, our calculations show that the adsorption of two Ph ·on different side of graphene plane and at *ortho* position is more favorable as compared to *meta* and *para* positions.

4.2.4. Adsorption of Three and Four Phenyl Radicals on Graphene.

We use two Ph · adsorbed graphene with highest binding energy (i.e., *ortho-d* configuration) to investigate the adsorption of third Ph ·on graphene sheet. Since, the two sides of two Ph ·radicals adsorbed graphene sheet is symmetric, we use one of the phenyl group on graphene as reference to add the third Ph · radical. We consider the adsorption of third radical at *ortho*, *meta* and *para* positions (see **Figure 4.4**) and also on same and different sides of graphene plane. When the third radical is attached at *para* position and on same side of the reference phenyl group we observe the highest binding energy of -

0.81 eV (see **Figure 4.4** and **Table 4.1**). The binding energies vary from -0.18 to -0.72 eV for other configurations (see **Table 4.1**). All the three Ph ·adsorbed graphene systems have net magnetic moment varies from 0.49 to 0.88 μ_B (see **Table 4.1**). Similar to single Ph ·radical adsorption, these net magnetic moments suggest that the adsorption of third Ph· radical on graphene breaks an aromatic π-bond and generate an unpaired electron.

To investigate the adsorption of fourth Ph · radical on graphene we choose three radical adsorbed on graphene having highest binding energy. For fourth radical adsorption we consider 5 binding sites based on symmetry (see **Figure 4.4**, for ease of discussion we have denoted these binding sites by numerical) and adsorption at both sides of graphene plane i.e., total 10 configurations. Three radical adsorbed graphene we have selected has two phenyl groups at one side of graphene sheet and another one is at opposite side of graphene sheet. For ease of discussion the adsorption of fourth radical on graphene side containing two phenyl groups is denoted as same side and adsorption on graphene side containing one phenyl group is denoted as different side. As, the three radicals adsorbed graphene contains an unpaired of electron, this electron will be delocalized at *ortho* and *para* positions due to *mesomeric* effect (see **Figure 4.5**). Thus, for adsorption of fourth radical we only consider *ortho* and *para* sites. Adsorption of fourth Ph ·radical on graphene at binding sites 1, 2, 3, 4, 5 (see **Figure 4.4**) saturates the graphene by forming electron pairings which is shown by calculated net magnetic moment of zero (see Table 4.1).

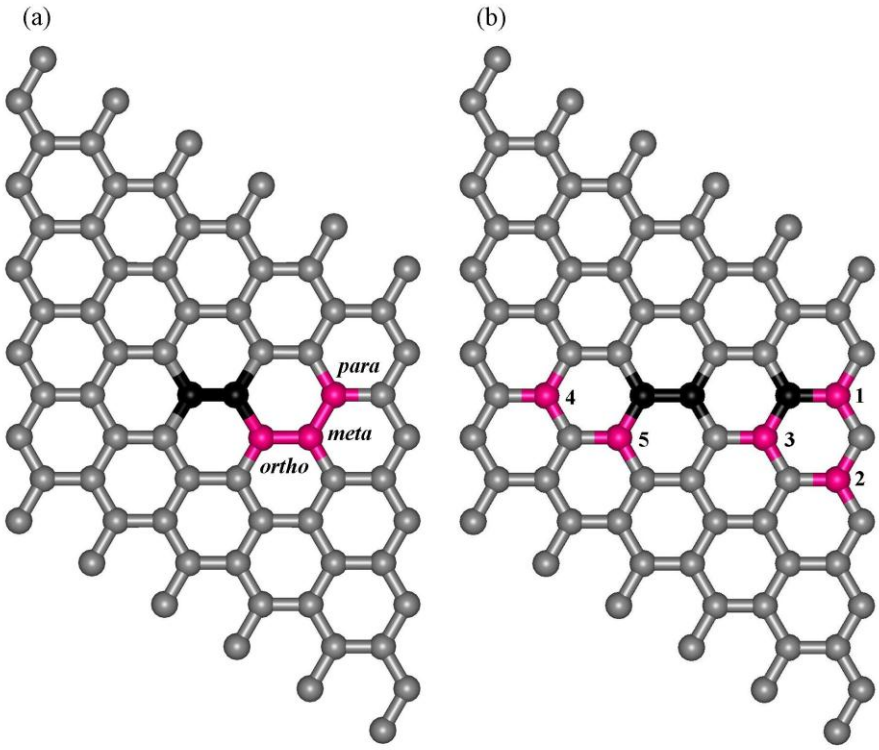

Figure 4.4 Binding sites for (a) third and (b) fourth radical adsorption on graphene. Black spheres indicate C atoms bonded to phenyl group, and pink spheres indicate the binding sites for next radical adsorptions

The calculated binding energy shows that when the fourth radical is adsorbed at binding sites 1, 2, 3, 4 and 5 at same side of graphene plane have comparable binding energy varies from -0.77 to -1.14 eV (see Table 4.1) expect for 3-s configuration, which have a very small binding energy of -0.09 eV due to the large steric repulsion. In addition the adsorption at binding site 1 at different side has highest binding energy of -1.50 eV. In addition, adsorption of fourth radical at same side has much lower binding energy as compared to different side. This indicates that the adsorption at same side is energetically not favorable due to large steric repulsion.

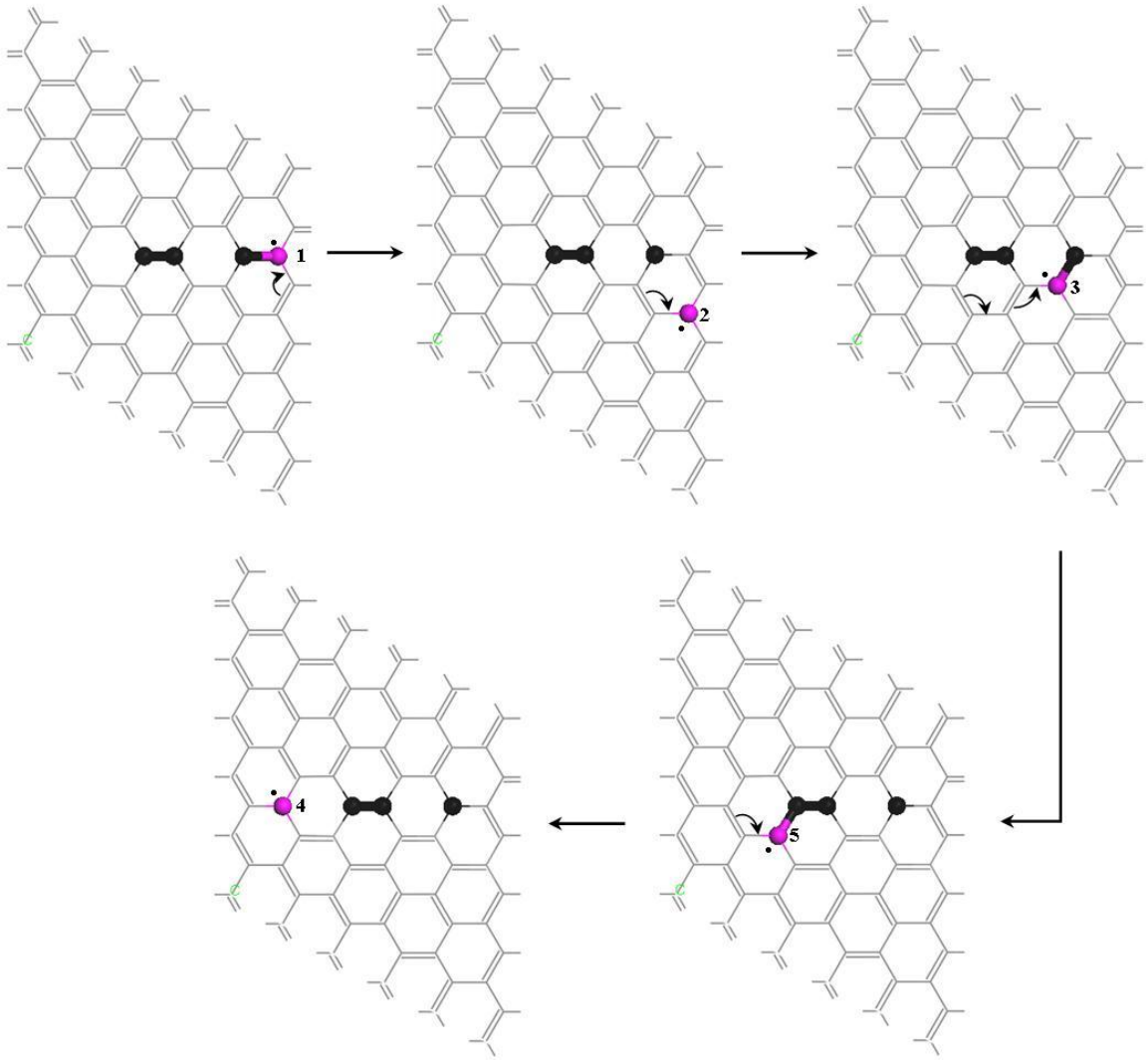

Figure 4.5 Possible delocalization sites of unpaired electron in three Ph radicals adsorbed graphene.

In summary, investigation of Ph ·adsorption on monolayer graphene shows that the adsorption of phenyl groups in pair-wise fashion is energetically more favorable than adsorption of odd number of Ph ·adsorption since odd number of Ph ·adsorption turns the graphene into radical by generating unpaired of electron. For pair-wise adsorption of Ph · radical on graphene, the ortho-ortho pairing at different side of graphene plane is more favorable for binding, than ortho-para pairing.

4.2.5. Electronic Properties of Modified Graphene.

We have calculated the band structures of pure and modified graphene sheet in two-dimensional Brillouin zone (BZ). The calculated band structures of pure and single Ph• radical adsorbed graphene are shown in **Figure 4.2** and **4.6**. The pure graphene has a band-gap of zero. The adsorption of single Ph ·radical on graphene push the valence band maximum (VBM) of graphene towards valence bands and similarly push the conduction band minimum (CBM) of graphene towards conduction bands and generates energy gap between VBM and CBM of graphene (see **Figure 4.6**). The reason is that the adsorption of Ph · radical formed C-C bond and breaks one of aromatic π-bond of graphene. Thus, changes the hybridization of C atom (attached with Ph ·) of graphene from sp^2 to sp^3 i.e., introduces defect to sp^2 hybridized graphene system. However, breaking of the aromatic π-bond of pure graphene generates an unpaired electron. This generated unpaired electron generates electronic band near the Fermi level as shown in red line (see **Figure 4.6**). The generated electronic band cut cross the Fermi level and turn the graphene to metallic. Our results suggest that the saturation of this unpaired electron will results in semiconducting graphene.

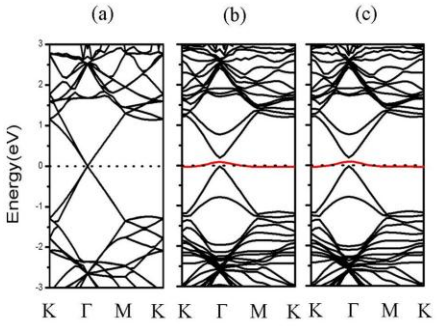

Figure 4.6 Band structures of (a) pure graphene and (b-c) single phenyl radical adsorbed graphene for different configurations

Here, we discuss the effect of second Ph · adsorption on electronic properties of graphene. The adsorption of second Ph · radical at *ortho* and *para* positions results in semiconducting graphene while the adsorption at *meta* position results in metallic graphene (see **Figure 4.7**). The reason is that upon adsorption of first radical on graphene the unpaired electron is delocalized at the *ortho* and *para* postions due to so-called *mesomeric effect*[100]. Thus, the adsorption of second Ph · on graphene at *ortho* and *para* positions saturates the graphene system by electron pairing and results in semiconducting graphene. However, adsorption of second Ph · on graphene at *meta* position breaks another aromatic π-bond and generates one more unpaired electron. Thus, the graphene with second Ph · adsorbed at *meta* position has two unpaired electrons with triplet spin configuration which is supported by net magnetic moment of ~1.95 and 1.96 μ_B. These two unpaired electrons generate two electronic bands near Fermi level. The generated electronic bands cut cross the Fermi level and results in metallic graphene (see **Figure 4.6**). However, the adsorption of second Ph · on graphene at *ortho-s* (*ortho-d*) and *para-s* (*para-d*) open a band-gap of 0.05 eV (0.08 eV) and 0.07 eV (0.06eV), respectively. Moreover, the adsorption of second Ph · on graphene at *ortho* position at different side of graphene plane has highest binding energy and highest band-gap (0.08 eV). Adsorption of third radical on graphene makes graphene metallic. As discussed above, the adsorption of third Ph · radical will break another aromatic π-bond and will generate an unpaired electron which is supported by calculated net magnetic moments (see Table 4.1). This unpaired electron will generate electronic band and cut cross the Fermi level and results in metallic graphene (see **Figure 4.9**).

Adsorption of fourth radical on graphene at ortho and para sites leads to semiconducting graphene with band-gap varies from 0.05 eV to 0.09 eV. (see **Figure 4.8** and **Table 4.1**). As discussed above the unpaired electron of three radicals adsorbed graphene can be delocalized to ortho and para binding sites thus, the adsorption at these binding sites will saturates the graphene system by electron pairing and resulted in semiconducting graphene at the site 1 and 5 on either same side or different site, both on the ortho positions to the already adsorbed carbon sites, the band-gaps are all 0.09 eV, which is a litter larger than the largest band-gap of two radicals adsorbed graphene, 0.08eV. While at the rest sites, the band-gaps are a little smaller, from 0.05 eV to 0.07 eV.

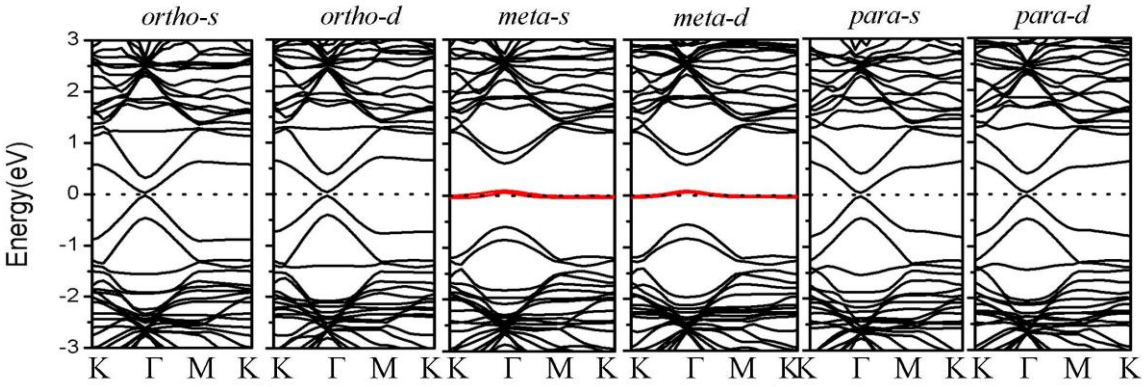

Figure 4.7 Band structures of two phenyl radicals adsorbed graphene

In summary, adsorption of odd number of Ph · leads to metallic graphene by generation of unpaired electron. This leads to electronic band near Fermi level and crossing the Fermi level. Adsorption of even number of Ph · leads to semiconducting graphene for *ortho-ortho* and *ortho-para* pairings. Our, current study shows that *ortho-ortho* pairing of Ph · radicals are energetically more favorable and leads to semiconducting graphene.

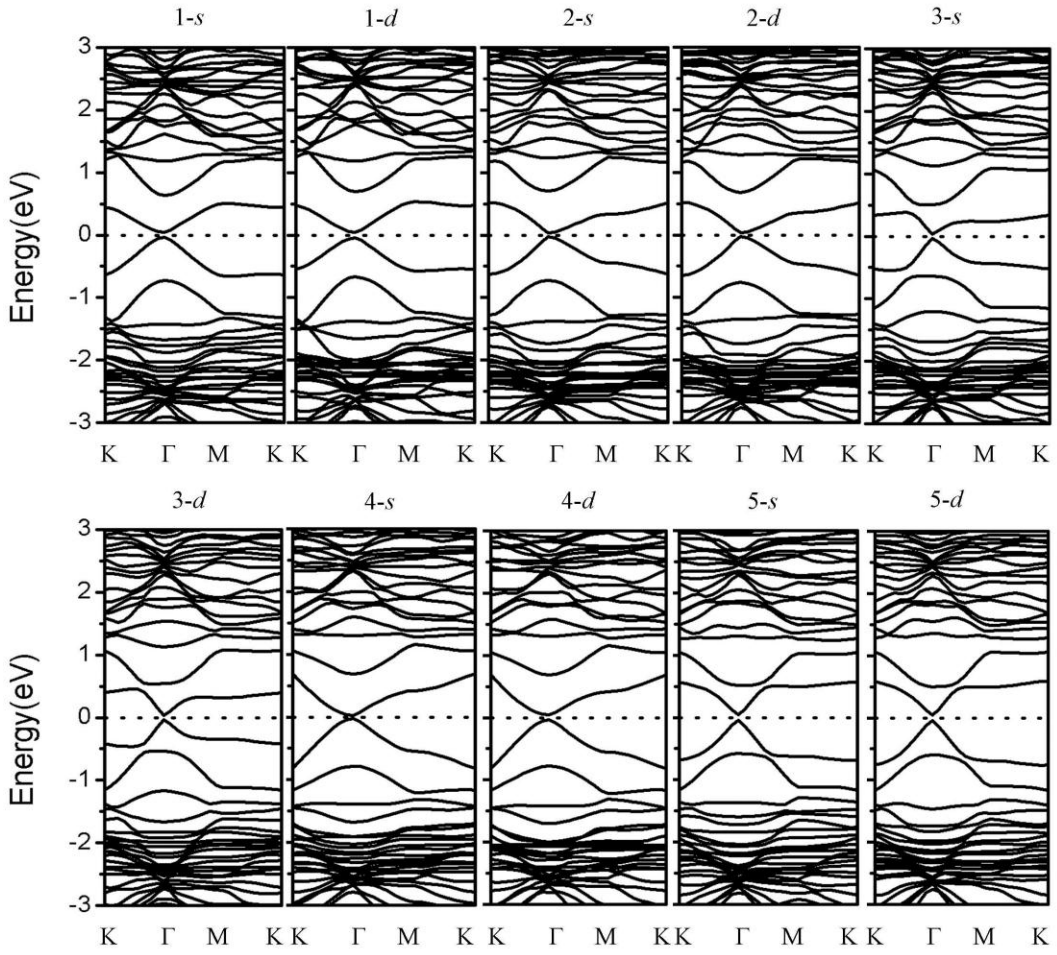

Figure 4.8 Band structures of four phenyl radicals adsorbed graphene.

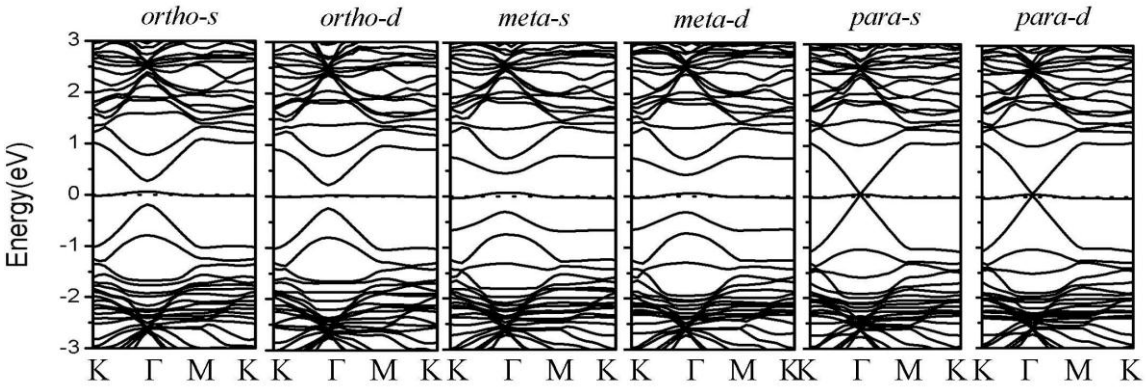

Figure 4.9 Band structures of three phenyl radicals adsorbed grapheme

4.3. Conclusion

We have used DFT calculations to investigate the adsorption of phenyl radicals on monolayer graphene sheet and effects of phenyl radical adsorption on electronic band-gap of graphene. We find that adsorption of single radical on graphene breaks one of the aromatic π-bond of graphene and generate unpaired electron. The unpaired electron generates electronic band which cuts cross the Fermi level and leads to metallic graphene. Binding of second radical with graphene is more favorable at ortho position as compared to para and meta positions. Binding at ortho or para positions saturate the graphene by electron pairing with unpaired electron generated by single radical adsorption and obtain semiconducting graphene with band-gap varying from 0.05 to 0.08 eV. However, adsorption at meta position breaks another aromatic π-bond of graphene and leads to metallic graphene. We find that adsorption of third radical on graphene leads to metallic graphene similarly to single radical adsorption. For adsorption offourth radical on graphene, the ortho-ortho pairing is more favorable for binding, than ortho-para pairing similar as two radical adsorbed graphene. The ortho-ortho and ortho-para pairings lead to semiconducting graphene. We reveal here that (a) the adsorption of phenyl radicals on graphene occurs in pair-wise fashion, (b) the ortho-ortho pairing at different side of graphene plane has stronger effects on band-gap opening as compared to ortho-para pairing, and (c) the adsorption of more of phenyl radicals on graphene by ortho-ortho or ortho-para pairings, in general, increases the band-gap of graphene. Thus in conclusion our study shows promise of band-gap manipulation of monolayer graphene by phenyl radical adsorption.

Chapter 5

Theoretical study on graphene edge controlling by oxidation cutting

Graphene-based materials e.g., graphene nanoribbons (GNRs) and graphene quantum dots (GQDs), have attracted great attention of researchers after experimental

report of graphene sheet by Novoselov et al. in 2004.[3] GNRs have potential applications in field effect transistors[102], gas- and bio- sensors[20, 103] and memory cells[104]. On the other hand GQDs have great potential in various applications such as bio-imaging and display[30, 105], sensing[106,107], energy storage[108] and photovoltaics[109]. It has been reported that GNRs with dominantly armchair edges have larger band gap as compared to similar sized GNRs with dominantly zigzag edges.[28] The origin of band gap in GNRs with armchair edges is attributed to both quantum confinement and crucial edge effect. However, the appearance of band gap in GNRs with zigzag edges is attributed to the staggered sub-lattice potential on hexagonal lattice due to edge magnetization.[110] Recent, theoretical calculations[29] from our group revealed that GQDs with armchair edges have different electronic and optical properties compared to similar sized GQDs with zigzag edges. It is evident that the edges of GNRs and GQDs control their electronic and optical properties. Therefore, it is essential to develop synthetic tools to control the edges of GNRs and GQDs to tailor for their applications.

The synthetic methods used for the production of GNRs and GQDs includes electron-beam lithography and plasma etching[37, 111], sonochemical and electrochemical etching[38, 112], metal catalyzed cutting[39], and reduction of exfoliated graphene oxide (hydrothermal method)[12, 40] and oxidation unzipping[41, 113]. However, no methods have been reported to be able to selectively produce GNRs and GQDs with either zigzag or armchair edge. Therefore, it is meaningful to understand the cutting mechanism of graphene to control the edges of GNRs and GQDs. Numerous studies have been performed to explore the mechanism of oxidative unzipping of graphene both experimentally[49, 51] and theoretically[49, 105a, 109a, 114]. Li et al.[49] reported the occurrence of

line defects on partially oxidized highly oriented pyrolytic graphite (HOPG) by examining the dark field optical microscope image. The strain generated by the cooperative alignment of epoxy groups is attributed to be the cause of cracking on graphite oxide (GO) using density-functional theory (DFT) calculations[49]. The formation of epoxy chain along zigzag orientation on same side of graphene sheet breaks the C-C bonds which are demonstrated by DFT calculations. This led to conclusion that the breaking of C-C bonds by formation of epoxy chain is responsible for the cutting of graphene sheet. In contrast, molecular dynamics simulations reported that breaking of underlying C-C bonds does not lead to cutting of the graphene sheet.[50] A two-steps mechanism of oxidative cutting of graphene sheet was proposed using DFT calculations by Li et al.[53] – (a) oxygen (O) atoms form epoxy pairs on both sides of graphene sheet and (b) then transformed to more stable carbonyl pairs which results in the breaking of graphene sheet. DFT calculations[54] also predicted that the oxidative cutting of graphene can form GNRs with large and controllable aspect ratios by applying external tensile strain.

Alignments of epoxy chain on same side of graphene sheet along the zigzag orientation are considered (see **Figure 5.1**) in most of the theoretical calculations. In present study, we have performed systematic DFT calculations for the adsorption of O atoms to form epoxy groups on both sides of graphene planes. Our study reveals that the formation of epoxy chains along armchair orientation (see **Figure 5.1**) is energetically most favorable considering oxidation on both sides. The formation of zigzag epoxy chain becomes more favorable when external strain is applied on graphene sheet.

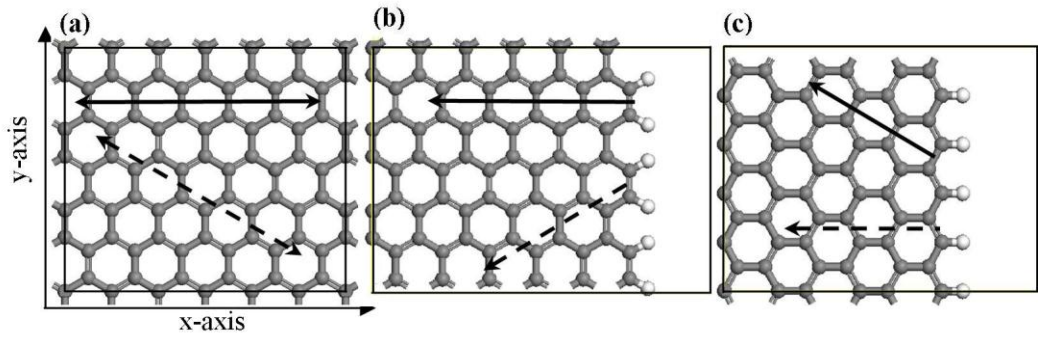

Figure 5.1 The structural model of (a) 2D graphene; and 1D graphene with (b) armchair and (c) zigzag edges. The edge of graphene is terminated with H. Grey sphere – C atom, white sphere – H atom, solid arrow - zigzag epoxy chain and dotted arrow - armchair epoxy chain.

5.1. Computational methods

All the calculations are performed in the frame work of density functional theory (DFT) within the generalized gradient approximation (GGA) method using Perdew-Burke-Eznerhof (PBE) functional (GGA-PBE)[91] as implemented in Vienna ab initio simulation package (VASP).[92] The projector augmented wave method (PAW)[93] is used to describe the interaction between the atomic cores and electrons. A 2×2×1 Monkhorst-Pack *k*-point[94] mesh and an energy cut of 450 eV are used for all calculations. The structure optimization is continued until the maximum forces acting on each atom become less than 0.01 eV $Å^{-1}$.

5.2. Results and Discussion

5.2.1. Oxidation cutting on graphene center

The oxidation of graphene is often done by treating graphene with oxidizing agents (e.g. solution of $KMnO_4$ in H_2SO_4). The generated oxygen leads to oxidation of graphene. Due to large size of graphene sheet, the oxidation process can initiate either from edge or middle of the graphene sheet. To model the oxidation at the middle part of graphene we have considered 2D periodic (x and y-directions) model of graphene (6x6) as shown in **Figure 5.1a**. To study the oxidation at both armchair (**Figure 5.1b**) and zigzag (**Figure 5.1c**) edges of graphene, we used a 1D periodic (y-direction) models. The armchair and zigzag edges of graphene are passivated with H atoms (**Figure 5.1b-c**) for edge-models. Adsorption of O atoms with graphene is used to model graphene oxidation. For the adsorption of O atom at middle part of graphene, only possible adsorption site is the carbon atoms at basal plane. The calculated binding energy of O atom on graphene is -2.41 eV in agreement to the reported value of -2.4 eV[49] on coronene molecule by Li et al.[49] They have studied the epoxy chain formation on the same side of coronene because one side of graphene sheet is usually accessible to oxidation due to experimental conditions e.g., usually one side of graphene is accessible for oxidation in graphite[41, 115]. This is likely the reason that the subsequent theoretical studies focused on same side oxidation of graphene.[54, 110] However, Schniepp et al. reported that it is possible to obtain epoxy functional groups on both sides of graphene by treating graphite in an oxidizing solution.[116] Here, we use the adsorption of O atoms on both sides of graphene sheet as the model for the formation of epoxy groups on both sides of graphene sheet[53] as reported by Schniepp et. al[116]. We also consider the binding sites near to the pre-adsorbed O atom for

subsequent O atoms adsorption (see **Figure B1-B3,** Appendix B) as the adsorption of O atom on oxidized graphene prefers carbon atoms with nearby oxygen[49].

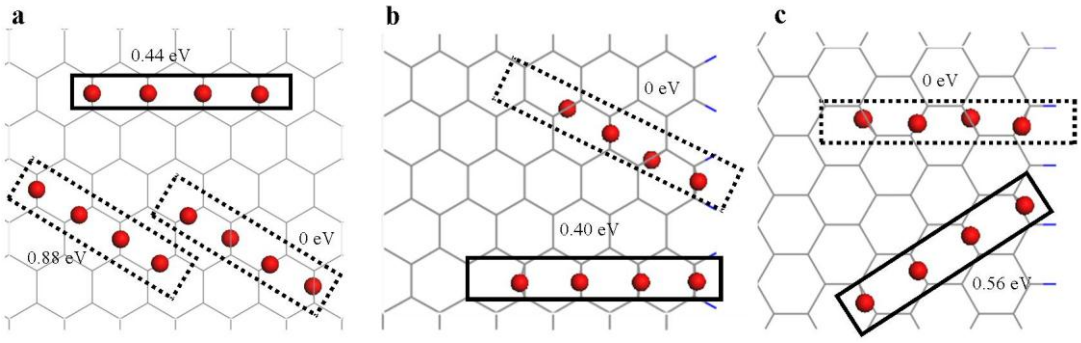

Figure. 5.2 Epoxy chain formation along armchair and zigzag orientation at (a) middle and (b-c) edge part of graphene. The value in eV is the relative energy. Grey stick – C atom and blue stick – H atom.

To study the formation of second epoxy group on graphene, we have considered five binding sites (**Figure B2**, Appendix B). Our calculations show that the formation of second epoxy group along armchair orientation but on opposite side of the pre-adsorbed O atom is energetically most favorable (**Figure B2d**, Appendix B). Our result is consistent with the previously reported works[117]. The reason is that the calculated buckling energy (deformation energy) for this configuration is less than other considered configurations (**Figure B2**, Appendix B). Lower buckling energy means less energy is needed to distort the graphene plane. Bader charge analysis of oxidized graphene shows more negative charge on O atoms bound to same side of graphene sheet (**Figure B2**, Appendix B). This indicates that the oxidized graphene with O atoms bound to same side of graphene sheet will be less stable due to charge repulsion between neighboring O atoms. In contrast, the O atoms are separated by graphene layer in oxidized graphene

with O atoms bound to opposite sides of graphene sheet. It is evident that there will be less charge repulsion between O atoms which makes this configuration more stable. We have also studied the third O atom adsorption based on the most favorable adsorption sites for the second O atom adsorption. The calculated highest binding energy for third O atom adsorption is -3.18eV and preferred armchair orientation (**Figure B3i**, Appendix B). The calculated relative energy of graphene with epoxy chair (four epoxy groups are considered here) along armchair (both sides), armchair (same side) and zigzag (same side) orientations is 0.00, 0.44, and 0.88 eV, respectively. This suggests that the formation of epoxy chain is energetically most preferred along the armchair orientation but on different sides of graphene sheet (**Figure 5.2a**). We also observe that the formation of two epoxy groups on the same side of graphene sheet prefers armchair orientation as compared to zigzag one (**Figure B2c**, Appendix B). However, the formation of armchair epoxy chain on the same side of graphene sheet is energetically less favorable as compared to the zigzag orientation (**Figure 5.2a**).

In addition, we have investigated the oxidative cutting of graphene via formation of carbonyl pair for armchair epoxy chain (**Figure 5.3**) based on the mechanism proposed by Li et al[53]. The formation of epoxy pair breaks the C-C bond and forms a four-member ring (**Figure 5.3b**) which is under high strain. The epoxy pair is converted to carbonyl pair to stabilize the oxidized graphene by releasing the high ring strain. The binding energy of O atom to form an epoxy pair along armchair (**Figure 5.3a-b**) and zigzag orientations (**Figure B4a-b**, Appendix B) is -2.75 and -3.32 eV, respectively. This suggests that the graphene with epoxy pair along armchair orientation is energetically less stable than zigzag orientation. This is the reason that the conversion of armchair epoxy

pair to carbonyl pair is much easier than zigzag epoxy pair (see **Figure 5.3** and **B4c**, Appendix B). Our theoretical calculations show that experimental design which allows the oxidation of graphene to happen at both sides of graphene sheet can generate GNRs and GQDs with dominantly armchair edges. However, to achieve oxidation at both sides of graphene experimentally one should use free graphene sheet. The both sides oxidation of single layer graphene has already been demonstrated experimentally by Liu et al[118].

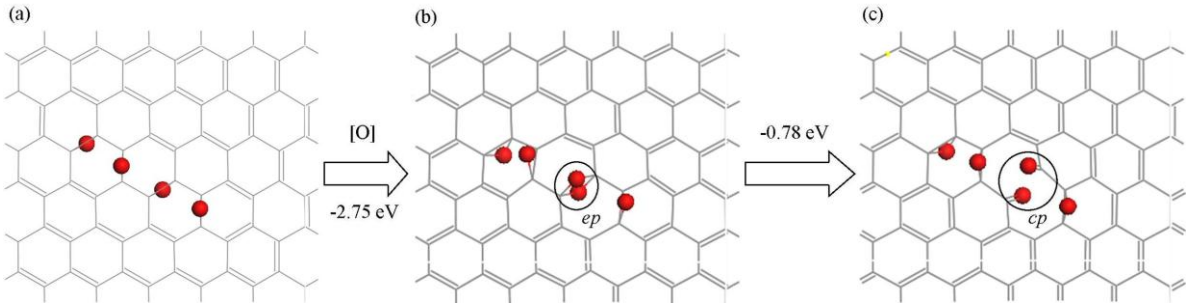

Figure 5.3 Structure of graphene with (a) armchair epoxy chain, (b) epoxy pair, **ep** and (c) carbonyl pair, **cp**.

Ma et al. in 2014 have proposed a potential experimental route to apply external tensile strain to graphene sheet and showed that external tensile strain on graphene makes the formation of epoxy chain energetically more favorable depending on the direction of applied strain.[54] The applied strain breaks the symmetry of graphene and allows epoxy chain to form in a particular orientation. To investigate the effect of external strain on epoxy chain formation on graphene sheet we have applied both compressive and tensile strains. The applied strain is calculated according to the expression $(L-L_0)/L_0$, where L is the lattice constant of strained graphene along the strain direction, and L_0 is the equilibrium lattice constant of relaxed graphene along the strain direction. By convention, the tensile strain is positive and compressive strain is negative. We have applied strain in

four directions with θ = 0, 30, 60 and 90° as shown in **Figure 5.4** (θ is the angle between epoxy chain and strain direction). The formation of epoxy chain on graphene sheet becomes more favorable when applying both tensile and compressive strains (**Figure 5.5**). This can be explained by the elongation or contraction of C-C bonds oriented along applied strain directions. The formation of armchair epoxy chain becomes more favorable (indicated by more negative binding energy) when the compressive strain is applied at θ = 30 ° direction as compared to three other directions. In contrast, the formation of zigzag epoxy chain becomes more favorable when the strain is applied at θ = 90° as compared to other directions. This is because the application of compressive strain will contract the C-C bonds (along the applied strain directions) and thus will increase the C-C repulsion. To overcome this C-C repulsion the plane of graphene will be more susceptible to deform. Thus, less buckling energy is required to deform the graphene plane when the O atom is adsorbed on strained graphene and makes the formation of epoxy chain more favorable than on unstrained graphene. Our calculations reveal that when compressive strain is applied along armchair direction of graphene sheet, the formation of epoxy chain is preferential along zigzag orientation. However, the formation of epoxy chain is observed along armchair orientation (θ = 30°) when compressive strain is applied along zigzag direction of graphene sheet. In addition, formation of zigzag epoxy chain under compressive strain is energetically most favorable as compared to armchair epoxy chain. We conclude here that by engineering the strain on graphene the orientation of epoxy chain formation can be controlled i.e., the edges of GNRs and GQDs. Since single-walled carbon nanotubes (SWNTs) can be seen as graphene sheet applied with higher strain,

Guo et al. also found the similar result using oxidation cutting on SWNTs to get zigzag edges.[119]

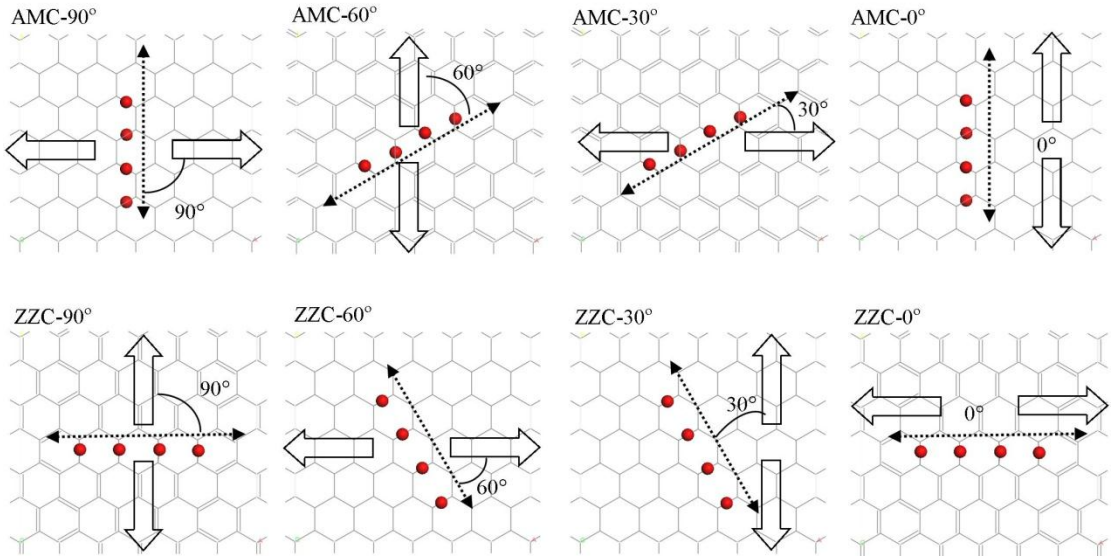

Figure. 5.4 Applied strain direction and epoxy chain formation direction.

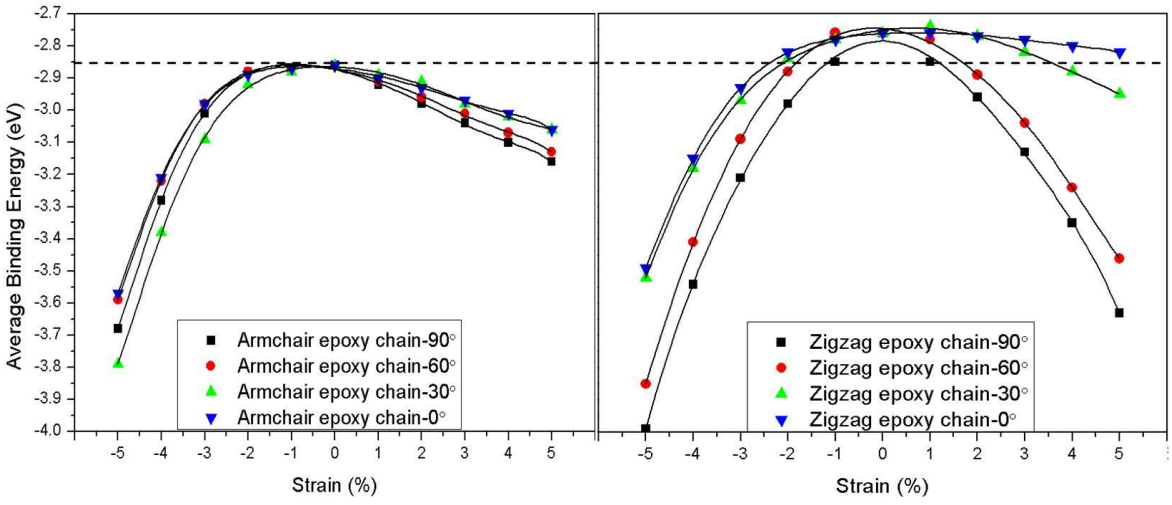

Figure. 5.5 Average binding energy of O atoms adsorption on graphene as a function of applied compressive and tensile strain.

5.2.2. Oxidation cutting on graphene edge

We now consider the oxidation of graphene sheet at graphene edge considering both armchair (**Figure 5.1b**) and zigzag (**Figure 5.1c**) types. Binding energy of O atom at zigzag and armchair edge is -3.19 and -3.61 eV, respectively, which is much greater than binding at middle part of graphene sheet (-2.41 eV). For subsequent oxidation we have considered both edge and basal plane near the graphene edge for O atoms adsorption (**Figure 5.6**). We observe that the epoxy pair formation at edge is more favorable than middle part of graphene sheet (**Figure 5.6**). Similar to the oxidation at middle part of graphene the formed epoxy pair is converted to carbonyl pair as shown in **Figure 5.6**. We conclude that the oxidation of graphene sheet at edge is most favorable, when the edges of graphene are fully oxidized then the oxidation proceeds at the basal planes near edges. Similar to middle part of graphene, epoxy chair formation near graphene edge along armchair orientation is energetically more favorable (**Figure 5.2b-c**) as compared to zigzag orientation irrespective of graphene edge type (graphene with armchair or zigzag edge). The formation of zigzag epoxy chain become most favorable when compressive strain is applied along armchair direction of graphene sheet (**Figure B6**, Appendix B). We reveal here that whether the oxidation of graphene sheet initiated at middle or edge of graphene, the formation of epoxy chain along armchair orientation is most preferable. Moreover, formation of zigzag epoxy chain becomes energetically most favorable when compressive strain is applied along the armchair direction of graphene sheet.

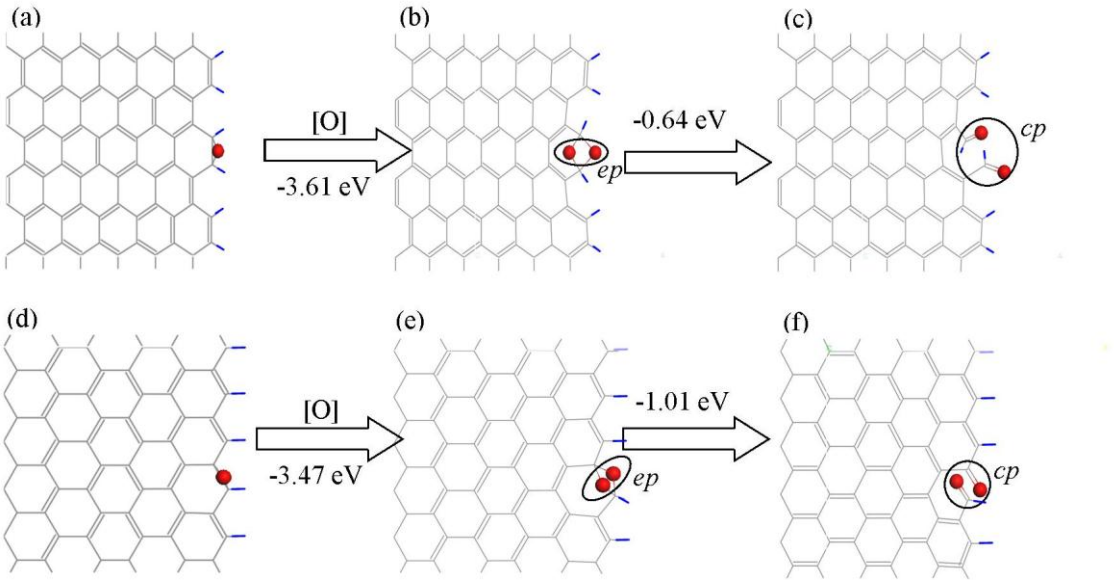

Figure. 5.6 Structure of armchair graphene edge with (a) epoxy group, (b) epoxy pair, ep and (c) carbonyl pair, cp; zigzag graphene edge with (a) epoxy group, (b) epoxy pair, ep and (c) carbonyl pair, cp

Both oxidation of substrate bound graphene and free graphene sheet have been demonstrated experimentally. In our present study we have modelled the oxidation of graphene sheet on same and both sides of graphene sheet. The results obtained from the oxidation on same side of graphene can be used to understand the oxidation mechanism of substrate bound graphene while the oxidation on both sides of graphene can be used for the oxidation of free graphene sheet. We reveal that the oxidation on same side of strained graphene is energetically favorable than both sides and preferred to form epoxy chain along zigzag orientations. Our study shows that zigzag edges can be controlled by oxidizing substrate bound graphene under application of strain while the armchair edges can be controlled by oxidizing free graphene sheets.

5.3. Conclusion

In summary, we have performed systematic study of graphene oxidation using DFT calculations. The oxidation at graphene edge is energetically more favorable as compared to middle part of graphene. Irrespective of binding sites on graphene, adsorption of O atoms leads to formation of armchair epoxy chain considering oxidation at both sides of graphene, which can be used to understand the oxidation cutting of graphene on substrate free condition. However, zigzag epoxy chain is formed when oxidation is considered on same side of graphene sheet. In addition, application of strain on graphene increases the binding affinity of O atoms with graphene. The orientation of epoxy chain formation on graphene changes from armchair to zigzag under applied compressive strain along armchair orientation of graphene sheet. Our calculations reveal that by manipulating the experimental conditions and strain on graphene, the edges of GNRs and GQDs can be engineered.

Chapter 6

Theoretical study on photoluminescence properties of GQDs

Graphene is a single-atom-thin two-dimensional sheet consisting of hexagonally-packed carbon atoms (or a giant polycyclic aromatic molecule from chemist's point of

view). It has been recently discovered that, when graphene shrinks to zero-dimension (nanoscale lateral dimensions), it fluoresces.[120] These so-called graphene quantum dots (GQDs) have quickly received much attention due to their unique structural and optoelectronic properties, and their great potentials in various applications such as bio-imaging[26] and display, photovoltaics,[121] energy storage,[122] and sensing.[27] Particularly, these glowing carbon nano-crystals can serve as new guiding lights for cell biologists. As Chen et al. have shown recently, GQDs can be employed as the universal fluorescent tags to specifically label the molecular targets and enable real-time imaging of their trafficking dynamics in live cells.[26e] GQDs are expected to outperform the current fluorescent reporters (fluorescent proteins, organic dyes, and semiconductor quantum dots) in many applications because of the unique combination of several key merits including tunable photoluminescence (PL) properties, excellent photo-stability, bio-compatibility, molecular size, and ease to be chemically paired with any biomolecule without compromising its functions.

The widespread use of GQDs, however, is currently hindered by the lack of controllable synthesis methods and the poor understanding of their tunable photoluminescence (PL) properties. Contradictory hypotheses sometimes arise from inconsistent experimental observations because of the large heterogeneity of GQDs synthesized by the current methods and the fact that the PL properties of GQDs are intriguingly determined by a number of parameters. Using density functional theory (DFT) and time-dependent density functional theory (TDDFT), we herein provide systematic theoretical investigations to show that the emission of GQDs can be widely

tuned from deep ultraviolet to near infrared by its size, edge configuration, shape, functional groups, defects, and heterogeneous hybridization of carbon network.

Pristine graphene is known as a zero band-gap material with infinite exciton Bohr radius due to the linear energy dispersion of the charge carriers.[123] Therefore, quantum confinement arises in a graphene sheet with finite size and becomes prominent in GQDs. Hence, band-gap opening (and related PL emission) of GQD should be highly size-dependent, i.e., the larger its diameter the longer wavelength it emits. Such expected size-dependent emission, however, has not been unambiguously demonstrated experimentally. The synthesized GQDs (ranging from 1.5 to 60 nm) can emit different PL colors (including deep UV, blue, green, yellow and red) without obvious size dependence[120a]. The large GQDs (~60 nm) synthesized by pyrolysis of hexa-*peri*-hexabenzocoronene (HBC) molecules emit blue fluorescence.[124] However, the small GQDs (1.5 – 5 nm) hydrothermally cropped from graphene oxide (GO) sheets are green fluorescent.[125] With similar size (2 – 3 nm), the GQDs oxidatively exfoliated from carbon black are green[26e] while the GQDs electrochemically cut from defect-free CVD-grown graphene are blue.[27b] These observed discrepancies are because of the large and uncontrolled heterogeneity of GQDs synthesized by the current approaches and the fact that the optical properties of GQDs sensitively depend on a number of parameters (e.g., size, chemical moieties, and defects). Theoretical modeling and calculations allow us to specifically investigate the influences of any particular parameter (computational methods are described in Appendix C).

6.1. Computational methods

All the calculations are carried out using Gaussian 09 suite of program.[67] The ground-state geometries of GQDs were firstly optimized by DFT[126] B3LYP (Becke's three-parameter hybrid function[65] with the non-local correlation of Lee-Yang-Parr[66]) method with the Pople 6-31G(d) basis set (B3LYP/6-31G(d)). The dangling carbon bonds are passivated by hydrogen atoms. The absorption spectra of GQDs were calculated using TDDFT method (at the B3LYP/6-31G(d) level) based on optimized ground-state geometries. The first excited state was optimized using TDDFT method to calculate the emission energy (wavelength) which is the energy difference between the ground and the first excited state.

6.2. Results and Discussion

6.2.1. Size-dependent photoluminescence properties of GQDs

To reveal the size-dependent PL of GQD, we calculated the emission wavelength of pristine zigzag-edged GQDs with different diameters (**Figure C1**, Appendix C). As shown in **Figure** 6.1, these GQDs (G1- G6) fluoresce from deep UV to near infrared while varying the size from 0.46 to 2.31 nm. Specifically, the smallest GQD (benzene) emits at 235.2 nm while 2.31 nm GQD emits at 999.5 nm. The observed linear and steep size-dependence indicates that by varying the diameter of GQD from 0.89 to 1.80 nm its emission covers the entire visible light spectrum (400 - 770 nm). The calculated emission wavelengths in vacuum (235.2, 399.5, 492.3 nm) of G1-G3 (defect- and functionality-free small sp^2-carbon clusters known as benzene, coronene, ovalene) correlates well with the experimental measurements (~278 nm in water,[127] ~427 nm in dimethyl

sulphoxide,[128] ~484 nm in tetrabutylammonium sulfonate salt,[129] respectively). The red-shift of emission wavelength with increasing size is due to decrease of band-gap resulting from π-electron delocalization (Table C1, Appendix C). Similar size-dependent emission has also been observed in various spherical semi-conductor QDs [130]. But it is much more prominent in GQDs due to their small size.

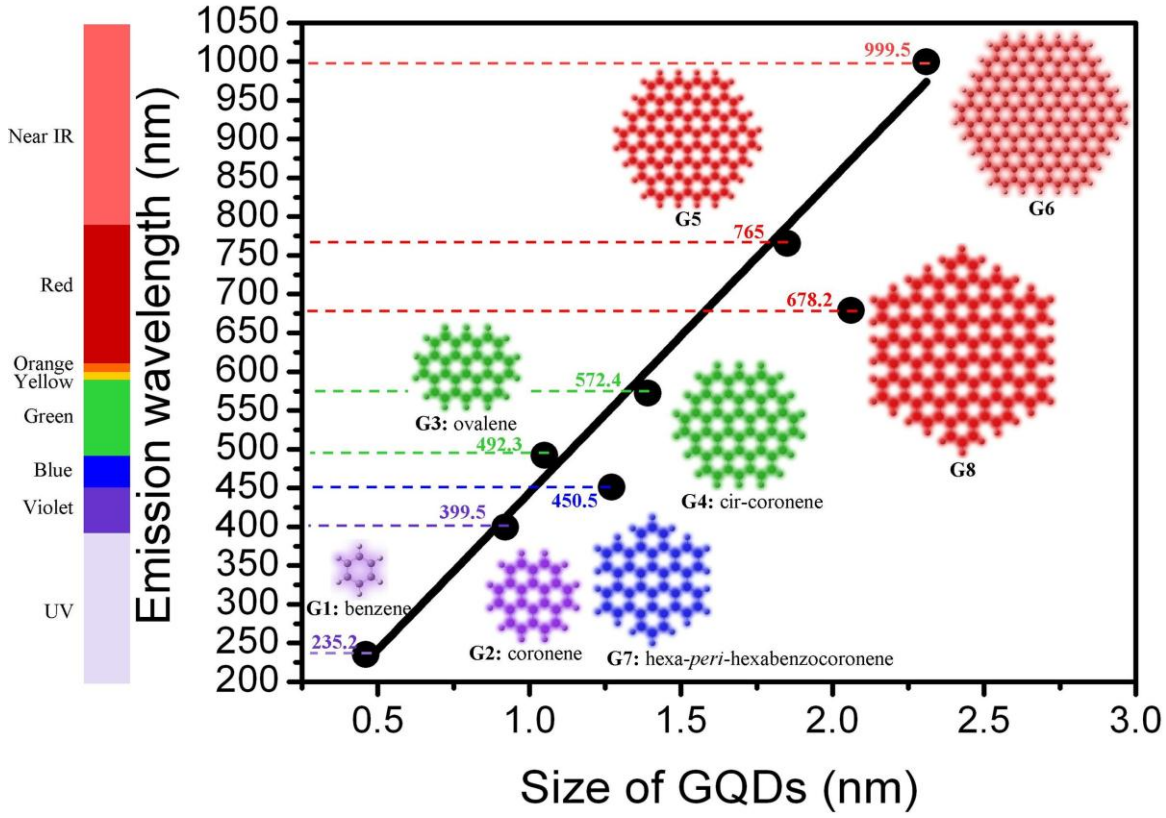

Figure 6.1 Calculated emission wavelength (nm) using TDDFT method in vacuum as a function of the diameter of GQDs. The solid line is the linear fitting of zigzag-edged GQDs (G1 – G6). The indicated diameter is the average of the horizontal and vertical dimensions.

6.2.2. Edge-dependent photoluminescence properties of GQDs

Graphene can have either zigzag or armchair edges which exhibit distinct quantum confinement properties. It has been shown that graphene nanoribbons (GNRs) with dominant zigzag edges have a smaller band-gap (0.14 eV) as compared to similarly-sized GNRs with dominant armchair edges (0.38 eV),[131] because of localized states on zigzag edges.[132] Consistently, we observe that the localized states in zigzag-edged GQD are pushed to the edge sites while similarly-sized armchair-edged GQD has localized states scattered in the center (**Figure C2**, Appendix C). Distinct to armchair-edged counterparts, the localized states at zigzag edge sites lower the energy of conduction band and thus reduce the band-gap. Thus, it is expected that the armchair edge would widen the band-gap of GQD and consequently blue-shift the emission. Indeed, our calculations show that 1.27 nm and 2.06 nm armchair-edged GQDs (G7 and G8 in **Figure 6.1**) emit at 450.5 and 678.2 nm while the predicted emission wavelengths of their zigzag-edged counterparts are ~551 and ~872 nm, respectively.

As we have shown, the pristine GQD of ~2 nm in size is red-fluorescent. But most GQDs of similar size synthesized by top-down exfoliation of larger-sized carbon materials are green or blue,[26e, 27b, 125] presumably because of the disruption of the crystalline sp^2-hybridized carbon network of graphene caused by the exfoliation processes. Using a bottom-up strategy, a pristine armchair-edged GQD (consisting of 132 conjugated carbon atoms, approximately arranged in rectangle shape) has been synthesized by conjugating benzene derivatives (**Figure 6.2a**, G9).[133] Such GQD (a polycyclic aromatic hydrocarbon) emits red fluorescence (670 nm) in toluene,[134] which is close to our calculated emission wavelength of 667.4 nm in vacuum and calculation by

Zhao et al[135]. The adsorption spectrum of this GQD peaks at ~535 nm attributed to the transition from ground-state S_0 to excited singlet state S_3 ($S_0 \rightarrow S_3$).[134] Consistently, our calculations also predict the $S_0 \rightarrow S_3$ transition at 542.96 nm. Another pristine armchair-edged GQD (**Figure 6.2b**, G10: 168 carbons approximately arranged in triangle shape) synthesized by a bottom-up method shows the absorption maximum at ~591 nm[136]. Our calculated absorption peak in vacuum (594.6 nm) is in good agreement with the experimental observation and the values calculated by Zhao et al[135] and Schumacher.[137] We predict that this GQD emits red fluorescence at 747.0 nm which is consistent with the calculated emission wavelength of 748.60 nm in toluene by Zhao et al.[135]

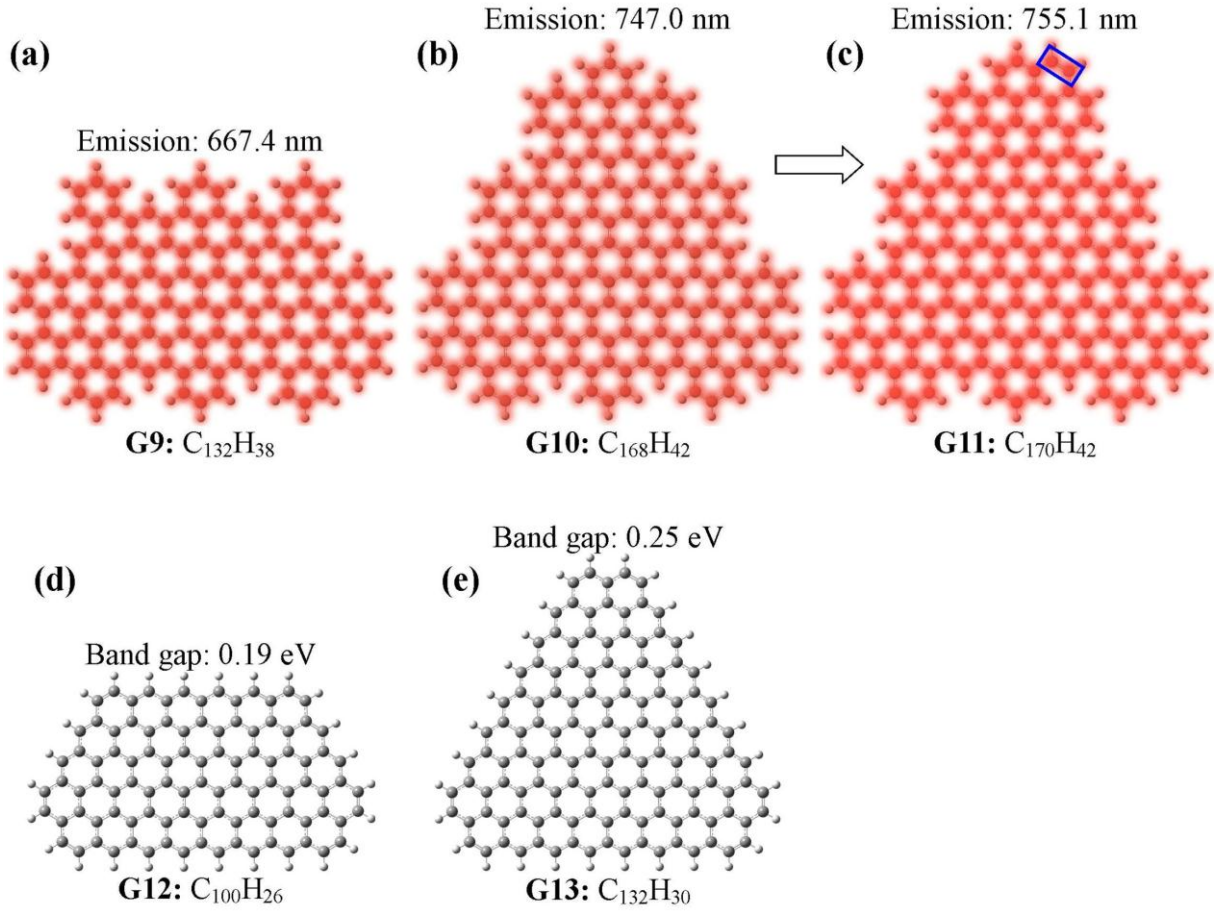

Figure 6.2 The structure of pristine (a) armchair-edged GQD ($C_{132}H_{38}$), (b) armchair-edged GQD ($C_{168}H_{42}$), (c) armchair-edged GQD ($C_{170}H_{42}$), formed by inserting two additional carbons (marked by blue rectangle) on $C_{168}H_{42}$ GQD, (d) zigzag-edged GQD ($C_{100}H_{256}$) and (e) zigzag-edged GQD ($C_{132}H_{30}$).

It is experimentally found that inserting two additional carbon atoms to create 6 zigzag edge sites on G10 (**Figure 6.2c**, G11) red-shifts the absorption peak[133] from ~591 to ~604 nm which perfectly matches with our calculated value of 603.86 nm. We attribute this red-shift to band-gap reduction of 0.06 eV. We also predict that G11 (**Figure 6.2c**) emits red fluorescence at 755.1 nm which agrees with the calculation by Zhao et al.[135] Furthermore, we find that transforming G9 and G10 to zigzag-edged by removing some carbon atoms at the edges (G12, G13 in **Figure 6.2d** and **e**) renders them non-fluorescent because of large reduction of band-gap (from 2.34 to 0.19 eV, 2.14 to 0.25 eV, respectively). Clearly, optoelectronic properties of GQDs are highly sensitive to the edge configurations. Moreover, hexagonal zigzag-edged GQDs (G5 with 96 carbons and G6 with 150 carbons) exhibit much larger band-gap as compared with similarly-sized and also zigzag-edged G12 (100 carbons arranged in rectangle shape) and G13 (132 carbons and triangle shape). Evidently, in addition to size and edge configuration, shape also plays an important role in determining the optoelectronic properties of GQDs.

6.2.3. Functional-groups-dependeet photoluminescence properties of GQDs

The synthesized GQDs often bear functional groups (e.g., oxygenated groups resulting from the oxidative exfoliation processes). We show here that oxidation of GQDs

by –OH or –COOH functional groups red-shifts the emission peaks due to band-gap reduction, in a coverage dependent manner (**Figure 6.3a**). Attaching –OH groups to the edge carbon atoms (varying from 0 - 100% coverage) continuously tunes G4 from green (572.4 nm) to red (732.3 nm). Edged -COOH groups also red-shift the fluorescence emission (**Figure 6.3a**). Compared to the edge functionalization, -OH groups conjugated on the basal plane of GQD cause more drastic red-shift because of disruption of graphitic carbon lattice. Specifically, two -OH groups on the basal plane of G4 makes it to emit red fluorescence at 746.1 nm. The predicted red-shift of oxidized GQDs is in line with experimental observations. For example, the GQDs (2-7 nm) exfoliated by acid oxidation emit greenish yellow-luminescence (~500 nm) and they become blue-luminescence (~450 nm) after reduction by $NaBH_4$.[138] GQDs synthesized by top-down methods usually bear defects. Our calculations show that creating single or double vacancy defects on green G4 largely red-shifts the emission peak to 1787.3 or 1217.0 nm, respectively (**Figure 6.3b** and **c**). It indicates the strong influence of vacancy defects.

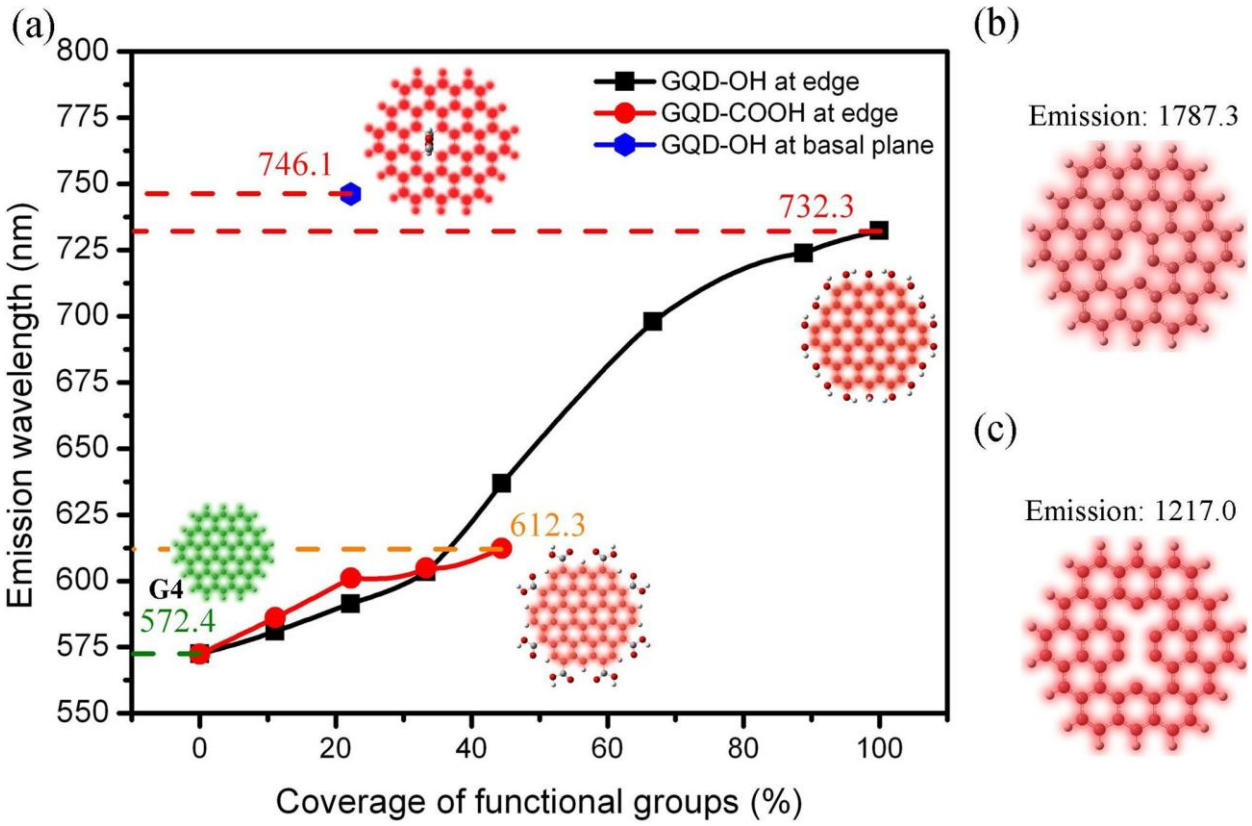

Figure 6.3 (a) Emission wavelength of oxidized GQD (G4) as a function of the coverage of –OH and –COOH groups. (b) and (c) are G4 with single or double vacancy defect, respectively.

Heteroatom doping is another way to alter the optoelectronic properties of graphene materials.[139] For example, it has been shown by Li et al that nitrogen-doping (with pyridinic and pyrrolic N atoms; N/C atomic ratio of ca. 4.3%) causes blue-shift of GQD emission.[140,121a]. To understand this phenomenon, we investigate the effects of three different N-doping configurations (graphitic, pyridinic, and pyrrolic). Graphitic N-doping (at edge or center) on the green G4 GQD drastically lowers the band-gap, thus rendering it non-fluorescent (**Figure 6.4a**). In contrast, graphitic N-doping in large graphene sheet opens band-gap near Dirac point by suppressing the density of state.[139,141] On the other hand, pyridinic N-doping on GQD causes slight blue-shift in a concentration dependent

manner (i.e., 12.5 at% N-doping shifts the G4 emission from 572.4 to 550.3 nm) (**Figure 6.4b**). Pyrrolic N-doping usually forms at the edged five-membered rings of GQD. To simulate its effect, we modify G4 GQD by attaching six cyclopentadiene at the edges. The resultant N-free GQD emits red fluorescence at 624.4 nm (**Figure 6.4c**). It is observed that introduction of pyrrolic N atoms at the edges significantly blue-shifts the emission in a concentration dependent manner. Specifically, 9.09 at% pyrrolic N-doping transforms the red GQD to green (emission at 575.5 nm). Our calculations suggest that the blue-shift observed by Li et al is mainly due to pyrrolic N-doping.

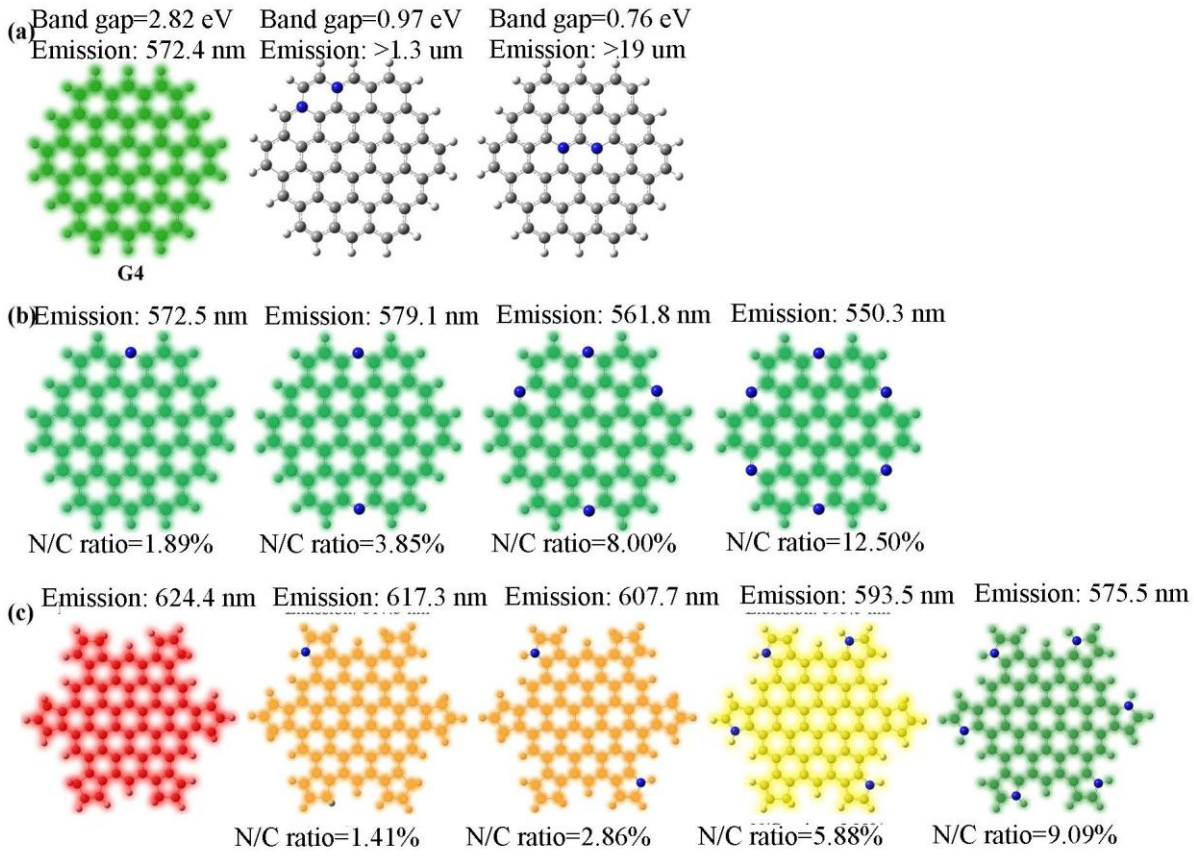

Figure 6.4 N-doped GQDs with (a) graphitic, (b) pyridine-like and (c) pyrrolic nitrogen. Blue spheres represent N atoms

6.3. Conclusion

In summary, we for the first time have systematically studied the mechanisms underlying the tunable PL properties of GQDs using DFT and TDDFT calculations. It is revealed that the emission of zigzag-edged pristine GQDs can cover the entire visible light spectrum by varying the diameter from 0.89 to 1.80 nm. Armchair edge and pyrrolic N-doping blue-shift the GQD PL emission whereas chemical functionalities and defects cause red-shift. As shown, GQDs can be tailored to emit a wide range of wavelengths.

Chapter 7

Summary

To achieve Moore's law, new semiconducting materials such as graphene and related materials attracted interests of many researchers. Graphene and related materials are proposed for various applications e.g., sensors, transparent electrodes and battery,

field emission (FE) displays, field effect transistors (FETs). However, intrinsic graphene is a zero band-gap semi-metal. To use graphene in semiconducting industry, its band-gap should be opened. GQDs and GNRs are commonly used graphene related materials. The edge shapes of GQDs and GNRs affect their electronic and optical properties. Thus, controlling the edges of GNRs and GQDs is important for their wider applications. GQDs can be employed as the universal fluorescent tags to specifically label the molecular targets and enable real-time imaging of their trafficking dynamics in live cells. Better understanding of PL properties of GQDs can widen the applications of GQDs. In this thesis using density functional theory (DFT) calculations, we investigated the structure and electronic properties of phenyl radical adsorbed graphene to investigate the graphene band-gap opening. We also investigated the structure and banding energies of epoxy group adsorbed graphene to obtain the fundamental understanding about the graphene oxidation cutting mechanism. Using DFT and TDDFT calculations, we systematically studied the mechanisms underlying the tunable photoluminescence (PL) properties of GQDs.In Chapter 4, we have used DFT calculations to investigate the adsorption of phenyl radicals on monolayer graphene sheet and effects of phenyl radical adsorption on electronic band-gap of graphene. We find that adsorption of single radical on graphene breaks one of the aromatic π-bond of graphene and generate unpaired electron. The generated unpaired electron generates electronic band which cut cross the Fermi level and leads to metallic graphene. Binding of second radical with graphene is more favorable at ortho position as compared to para and meta positions. Binding at ortho or para positions saturate the graphene by electron pairing with unpaired electron generated by single radical adsorption and obtain semiconducting graphene with band-gap varying from 0.05

to 0.08 eV. However, adsorption at meta position breaks another aromatic π-bond of graphene and leads to metallic graphene. We find that adsorption of third radical on graphene leads to metallic graphene similarly to single radical adsorption. For adsorption of fourth radical on graphene, the ortho-ortho pairing is more favorable for binding, than ortho-para pairing similar as two radicals adsorbed graphene. The ortho-ortho and ortho-para pairings lead to semiconducting graphene. We reveal that (a) the adsorption of phenyl radicals on graphene occurs in pair-wise fashion, (b) the ortho-ortho pairing at different side of graphene plane has stronger effects on band-gap opening as compared to ortho-para pairing, and (c) the adsorption of more of phenyl radicals on graphene by ortho-ortho or ortho-para pairings, in general, increases the band-gap of graphene. Thus in conclusion our study shows promise of band-gap manipulation of monolayer graphene by phenyl radical adsorption.

In Chapter 5, we have performed systematic study of graphene oxidation using DFT calculations. The oxidation at graphene edge is energetically more favorable as compared to middle part of graphene. Irrespective of binding sites on graphene, adsorption of O atoms leads to formation of armchair epoxy chain considering oxidation at both sides of graphene. However, zigzag epoxy chain is formed when oxidation is considered on same side of graphene sheet. In addition, application of strain on graphene increases the binding affinity of O atoms with graphene. The orientation of epoxy chain formation on graphene changes from armchair to zigzag under applied compressive strain along armchair orientation of graphene sheet. Our calculations reveal that by manipulating the experimental conditions and strain on graphene, the edges of GNRs and GQDs can be engineered.

In Chapter 6, we for the first time have systematically studied the mechanisms underlying the tunable PL properties of GQDs using DFT and TDDFT calculations. We reveal that the emission of zigzag-edged pristine GQDs can cover the entire visible light spectrum by varying the diameter from 0.89 to 1.80 nm. We show that the armchair edge and pyrrolic N-doping blue-shift the GQD PL emission whereas chemical functionalities and defects cause red-shift. As shown, GQDs can be tailored to emit a wide range of wavelengths.

In conclusion, we achieved the following objectives set out at the beginning of this thesis –

(a) We demonsrated the band-gap opening of graphene by phenyl radicals adsorption

(b) We proposed a method to engineer the edges of GNRs and GQDs by controlling experimental conditions and strain on graphene.

(c) We revealed the photoluminescence (PL) mechanism of GQDs and contributed to understand the effect of size, edge configuration, shape, attached chemical functionalities, heteroatom doping and defects on photoluminescence (PL) properties of GQDs.

Appendix A

Supplementary materials for theoretical study on band-gap manipulation of graphene

Table A1. Calculated energy gap (in eV) at K, K', Γ, M point of graphene (6x6) and two phenyl radical adsorbed graphene.

	Energy gap (eV)				
	Graphene (6x6)	ortho-s	ortho-d	para-s	para-d
K	2.46	1.46	1.39	1.46	1.44
K'	2.46	1.46	1.39	1.46	1.44

Γ	0.00	0.05	0.08	0.07	0.06
M	2.64	1.54	1.47	1.23	1.22

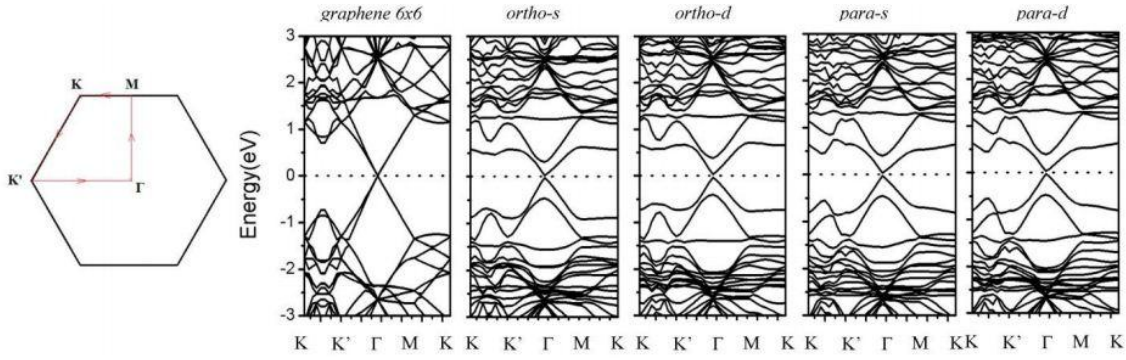

Figure A1. Band structures of graphene (6x6) and two phenyl radical adsorbed graphene along high symmetry K-K'-Γ-M-K paths

Appendix B

Supplementary materials for theoretical study on graphene edge controlling by oxidation cutting

Binding energy of first and nth O atom adsorption is calculated according to equations 1 and 2, respectively. The average binding energy of O atoms with pure graphene is calculated according to equation 3. The average binding energy of O atoms on strained graphene is also calculated according to equation 3; the only difference is that the total energy of pure graphene ($E_{graphene}$) and graphene-oxygen complexes ($E_{graphene + (n) oxygen}$) is calculated including strains (-5% to +5% with a increment of 1).

$$E_{BE}(1^{st}) = E_{graphene+oxygen} - E_{graphene} - E_{oxygen} \quad (1)$$

$$E_{BE}(n^{st}) = E_{graphene + (n) oxygen} - E_{graphene + (n-1) oxygen} - E_{oxygen} \quad (2)$$

$$E_{BE}(average) = [E_{graphene + (n) oxygen} - E_{graphene} - n^* E_{oxygen}]/n \quad (3)$$

Where, E_{BE} is the binding energy, $E_{graphene + (n) oxygen}$ is the total energy of graphene adsorbed with n O atoms, $E_{graphene}$ is the total energy of graphene, E_{oxygen} is the total energy of O atom.

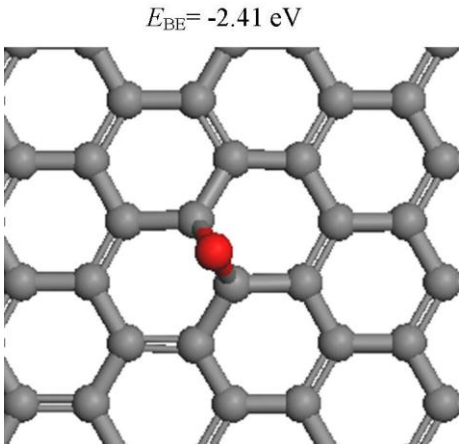

Figure B1. Structure and binding energy (E_{BE}) of of oxidized graphene with one epoxy group.

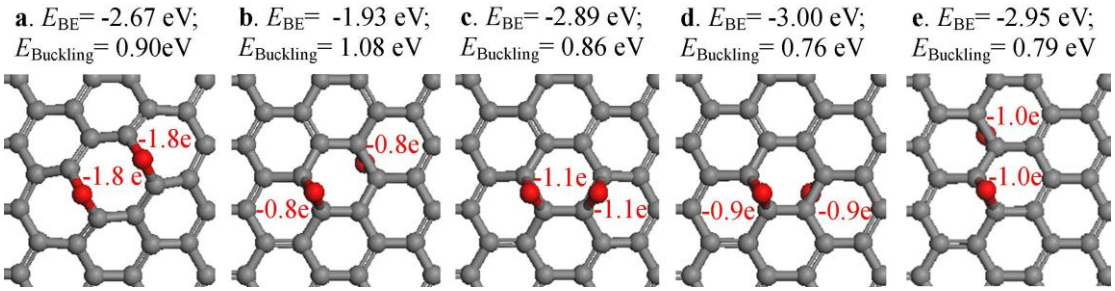

Figure B2. Structure, binding energies (E_{BE}) and buckling energies ($E_{Buckling}$) of oxidized graphene with two epoxy groups. The red color text indicates the charge on O atom.

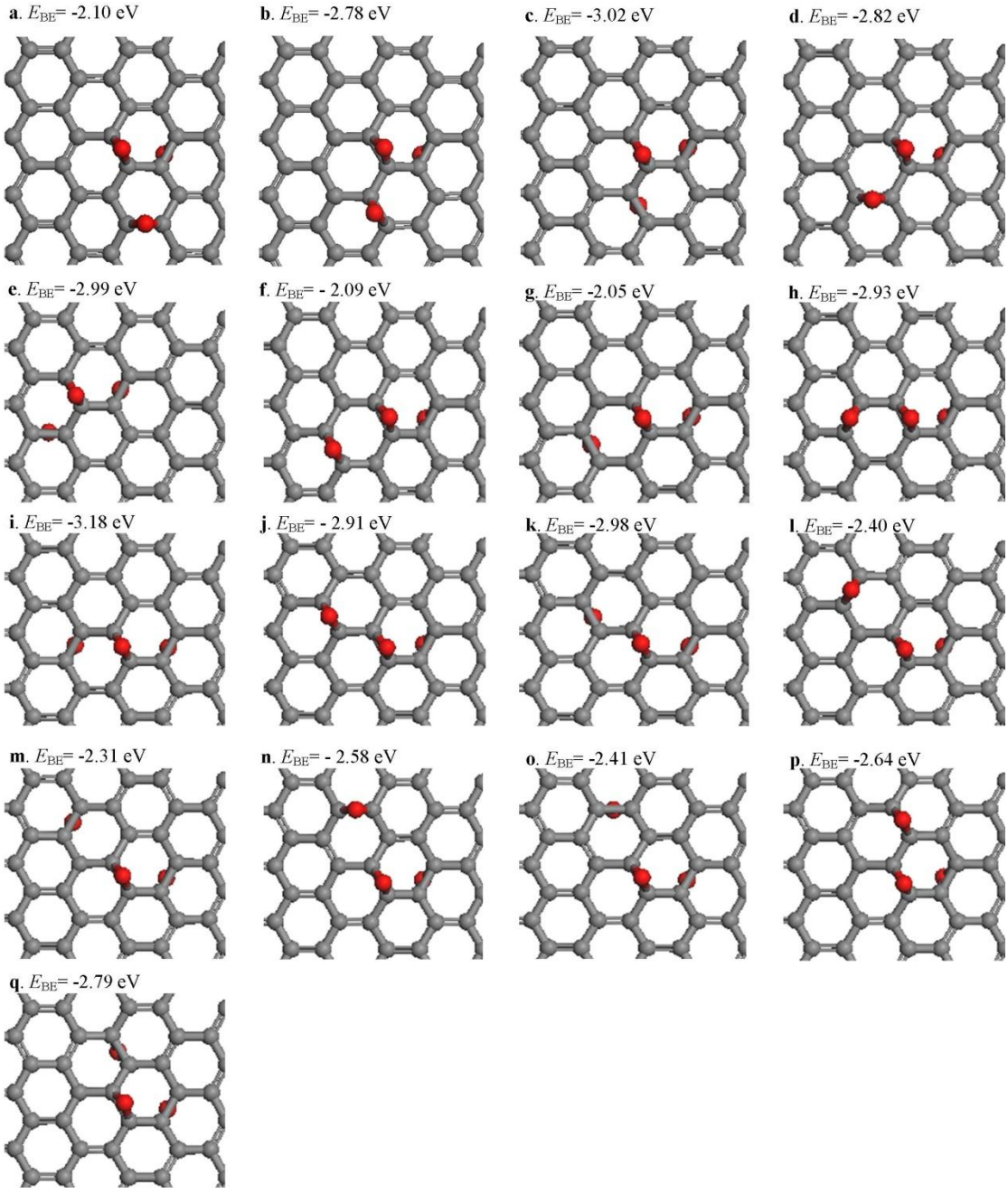

Figure B3. Structure and binding energies (E_{BE}) of oxidized graphene with three epoxy groups.

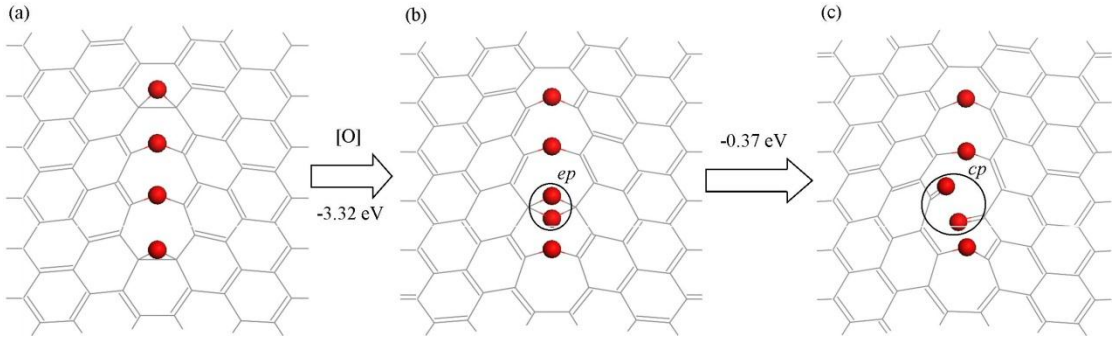

Figure B4. Structure of oxidized graphene with (a) zigzag epoxy chain, (b) epoxy pair, ep and (c) carbonyl pair, cp.

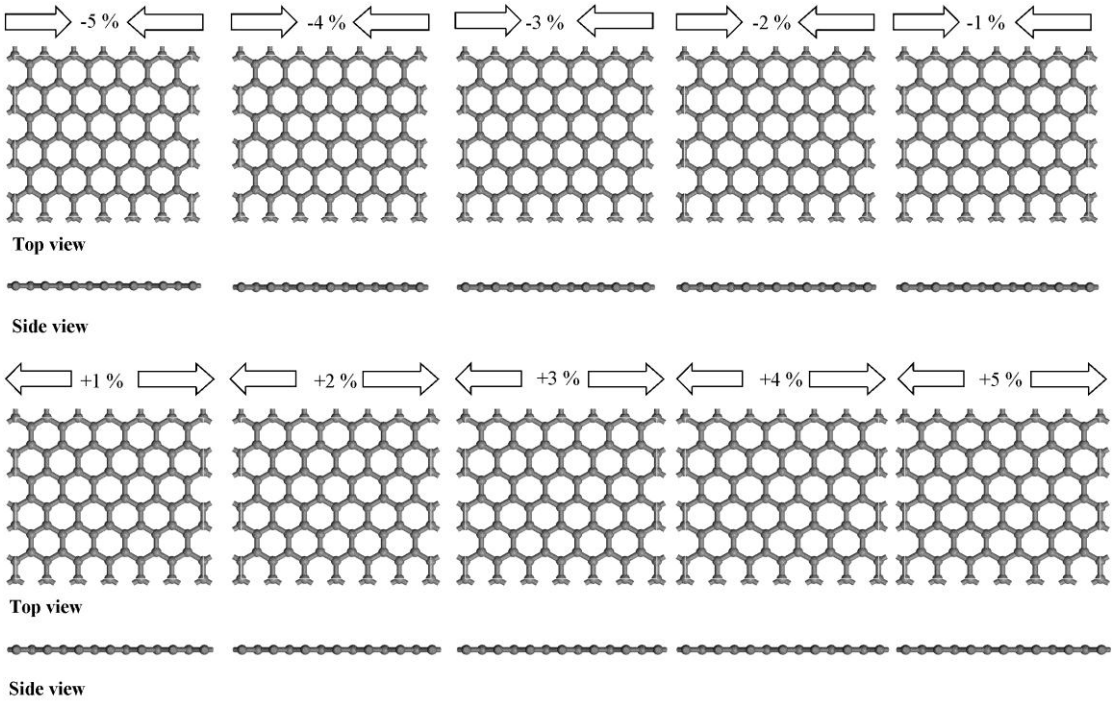

Fig. B5. Top view and side view of structure of graphene with strain (from -5% to +5%).

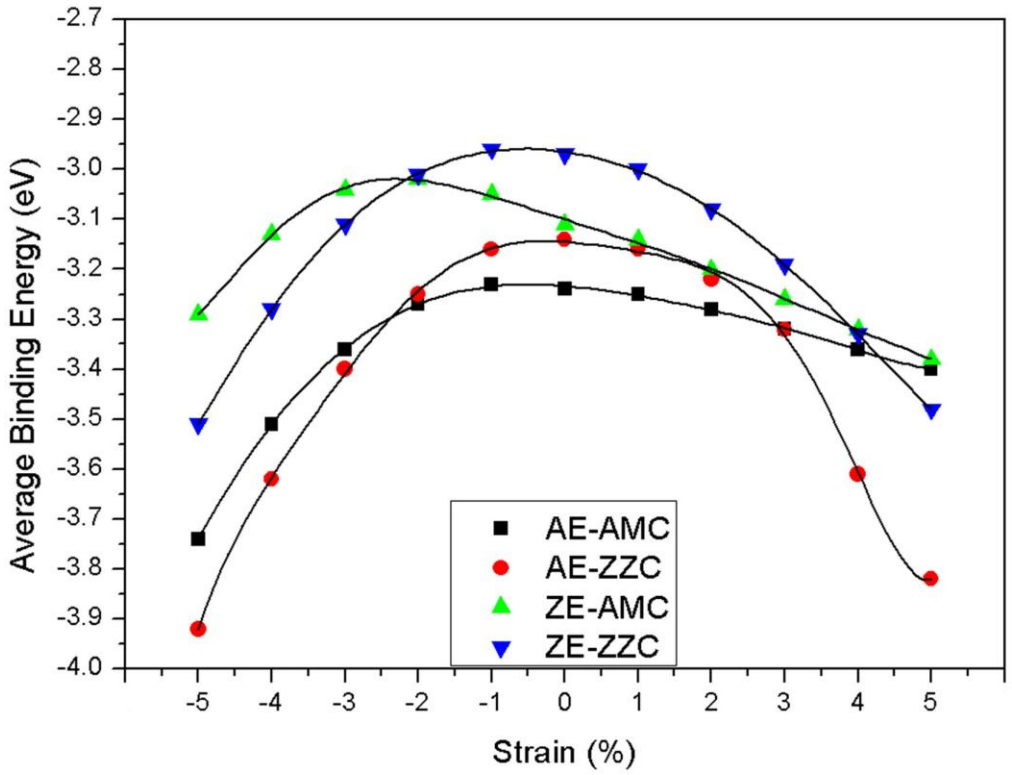

Figure B6. Average binding energy of O atoms adsorption on graphene edge as a function of applied compressive and tensile strain. AE, ZE, AMC and ZZC indicate armchair, edge zigzag edge, armchair epoxy chain and zigzag epoxy chain, respectively.

Appendix C

Supplementary materials for theoretical study of photoluminescence properties of GQDs

Table C1. Calculated Ground-state Band-gap (Egap), Emission Energy, and Emission Wavelength of GQDs

GQDs		E_{gap} (eV)[a]	$E_{emission}$ (eV)	Wavelength (nm)	Color
G1: Benzene	0.46 nm	6.81	5.27	235.2	DUV
G2: Coronene	0.92 nm	4.04	3.10	399.5	Violet
G3:Ovalene	1.05 nm	2.93	2.52	492.0	Green
G4: Cir-coronene	1.39 nm	2.82	2.17	572.4	Green
G5	1.85 nm	2.12	1.62	765.2	Red
G6	2.31 nm	1.64	1.24	999.5	Near IR
G7: HBC	1.27 nm	3.59	2.75	450.5	Blue
G8	2.06 nm	2.37	1.83	678.2	Red

a.band gap means HOMO-LUMO gap here.

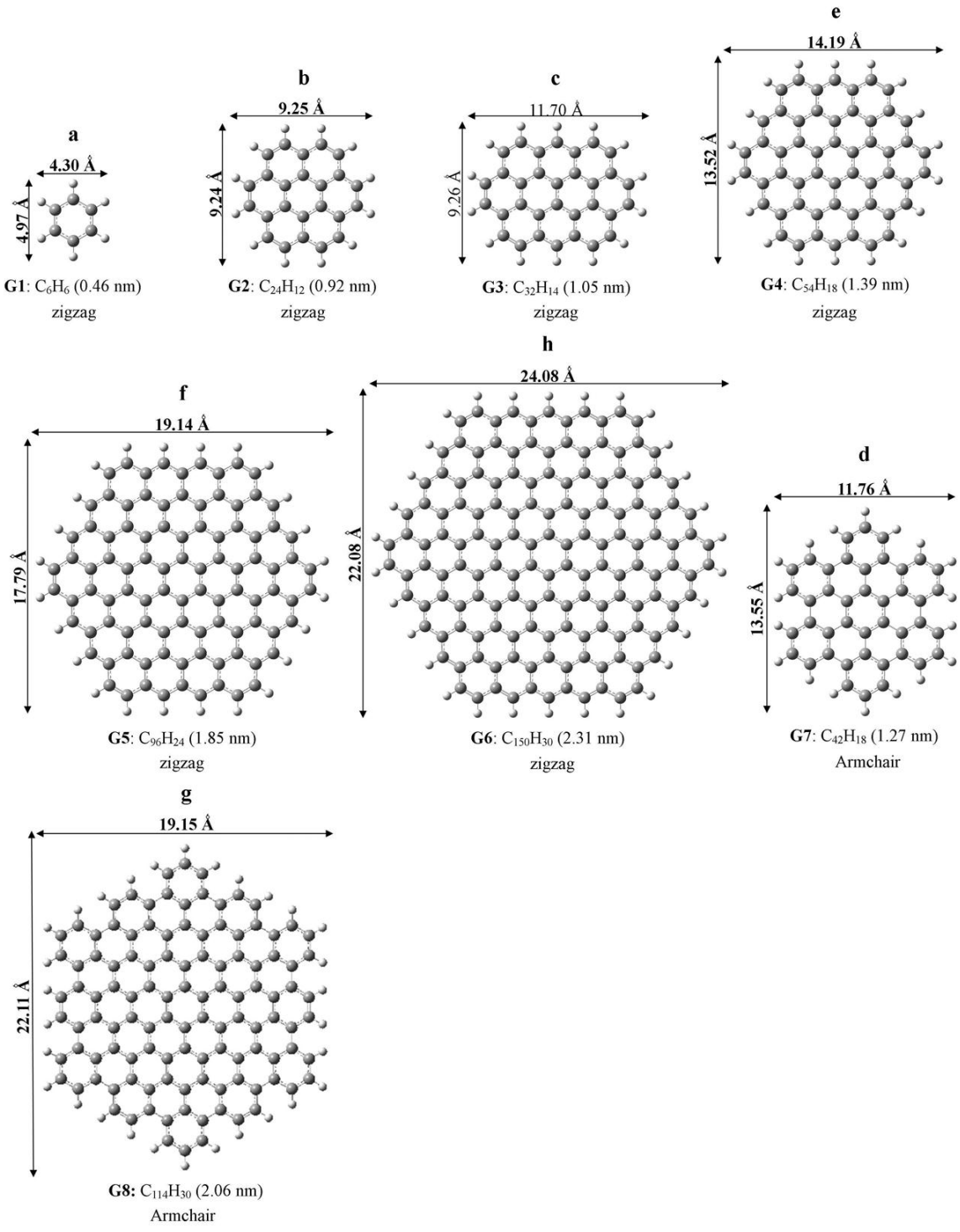

Figure C1. Structure of hexagonal GQDs with zigzag edge (G1-G6) and armchair edge (G7-G8).

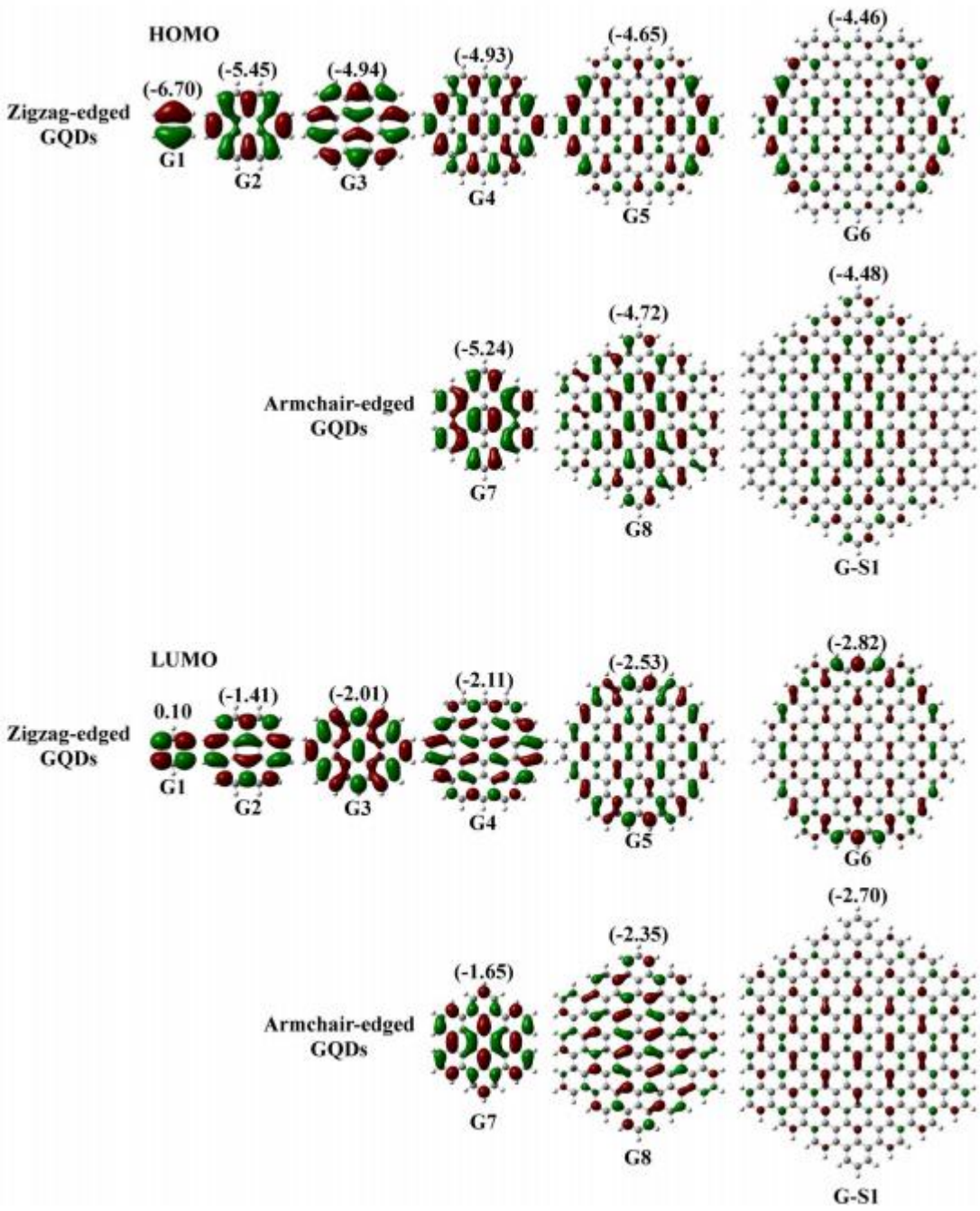

Figure C2. Molecular orbitals for HOMO and LUMO of zigzag and armchair-edged GQDs.Molecular orbitals are concentrated on edge sites in zigzag-edged GQDs but scattered in the center in armchair-edge GQDs. G-S1 is 2.87 nm armchair-edged GQD. Values in the parentheses are orbital energies in eV

List of Publications

Journal Publications

(1) **Lin Huang**, Mahasin Alam Sk, Peng Chen, Kok Hwa Lim. Controlling armchair and zigzag edges in oxidative cutting of graphene. 2015, submitted.

(2) Mahasin Alam Sk, Arundithi Ananthanarayanan, **Lin Huang**, Kok Hwa Lim and Peng Chen. Revealing the tunable photoluminescence properties of graphene quantum dots. Journal of Materials Chemistry C, **2014**, *2*, 6954-6960

(3) **Lin Huang**, Mahasin Alam Sk, Peng Chen and Kok Hwa Lim. Band-Gap Manipulations of Monolayer Graphene by Phenyl Radical Adsorptions: A Density Functional Theory Study. ChemPhysChem, **2014**, *15*, 2610-2617

(4) Mahasin Alam Sk, Man-Fai Ng, **Lin Huang** and Kok Hwa Lim. Modulating the electronic properties of germanium nanowires via applied strain and surface passivation. Physical Chemistry Chemical Physics, **2013**,*15*, 5927-5935

Reference

1. **Geim, A. K.; Novoselov, K. S., The rise of graphene. *Nat. Mater.* 2007, *6* (3), 183-191.**
2. **Alpha, T. N. D.; Johann, C.; Tim, N. P.; Carsten, B.; Thomas, M., Structure of epitaxial graphene on Ir(111). *New J. Phys.* 2008, *10* (4), 043033.**
3. **Novoselov, K. S.; Geim, A. K.; Morozov, S. V.; Jiang, D.; Zhang, Y.; Dubonos, S. V.; Grigorieva, I. V.; Firsov, A. A., Electric field effect in atomically thin carbon films. *Science* 2004, *306* (5696), 666-669.**
4. **Stankovich, S.; Dikin, D. A.; Dommett, G. H. B.; Kohlhaas, K. M.; Zimney, E. J.; Stach, E. A.; Piner, R. D.; Nguyen, S. T.; Ruoff, R. S., Graphene-based composite materials. *Nature* 2006, *442* (7100), 282-286.**
5. **(a) Li, X.; Cai, W.; An, J.; Kim, S.; Nah, J.; Yang, D.; Piner, R.; Velamakanni, A.; Jung, I.; Tutuc, E.; Banerjee, S. K.; Colombo, L.; Ruoff, R. S., Large-Area Synthesis of High-Quality and Uniform Graphene Films on Copper Foils. *Science* 2009, *324* (5932), 1312-1314; (b) Malesevic, A.; Vitchev, R.; Schouteden, K.; Volodin, A.; Zhang, L.; Van Tendeloo, G.; Vanhulsel, A.; Van Haesendonck, C., Synthesis of few-layer graphene via microwave plasma-enhanced chemical vapour deposition. *Nanotechnology* 2008, *19* (30); (c) Dervishi, E.; Li, Z.; Watanabe, F.; Biswas, A.; Xu, Y.; Biris, A. R.; Saini, V.; Biris, A. S., Large-scale graphene production by RF-cCVD method. *Chemical Communications* 2009, (27), 4061-4063; (d) Reina, A.; Jia, X.; Ho, J.; Nezich,**

D.; Son, H.; Bulovic, V.; Dresselhaus, M. S.; Kong, J., Large Area, Few-Layer Graphene Films on Arbitrary Substrates by Chemical Vapor Deposition. *Nano Lett.* 2008, *9* (1), 30-35; (e) Sutter, P. W.; Flege, J.-I.; Sutter, E. A., Epitaxial graphene on ruthenium. *Nat Mater* 2008, *7* (5), 406-411; (f) Srivastava, A.; Galande, C.; Ci, L.; Song, L.; Rai, C.; Jariwala, D.; Kelly, K. F.; Ajayan, P. M., Novel Liquid Precursor-Based Facile Synthesis of Large-Area Continuous, Single, and Few-Layer Graphene Films. *Chem. Mat.* 2010, *22* (11), 3457-3461.

6. **Wu, Z.-S.; Ren, W.; Gao, L.; Zhao, J.; Chen, Z.; Liu, B.; Tang, D.; Yu, B.; Jiang, C.; Cheng, H.-M., Synthesis of Graphene Sheets with High Electrical Conductivity and Good Thermal Stability by Hydrogen Arc Discharge Exfoliation. *ACS Nano* 2009, *3* (2), 411-417.**

7. **(a) Shivaraman, S.; Barton, R. A.; Yu, X.; Alden, J.; Herman, L.; Chandrashekhar, M. V. S.; Park, J.; McEuen, P. L.; Parpia, J. M.; Craighead, H. G.; Spencer, M. G., Free-Standing Epitaxial Graphene. *Nano Lett.* 2009, *9* (9), 3100-3105; (b) Aristov, V. Y.; Urbanik, G.; Kummer, K.; Vyalikh, D. V.; Molodtsova, O. V.; Preobrajenski, A. B.; Zakharov, A. A.; Hess, C.; Hänke, T.; Büchner, B.; Vobornik, I.; Fujii, J.; Panaccione, G.; Ossipyan, Y. A.; Knupfer, M., Graphene Synthesis on Cubic SiC/Si Wafers. Perspectives for Mass Production of Graphene-Based Electronic Devices. *Nano Lett.* 2010, *10* (3), 992-995; (c) Emtsev, K. V.; Bostwick, A.; Horn, K.; Jobst, J.; Kellogg, G. L.; Ley, L.; McChesney, J. L.; Ohta, T.; Reshanov, S. A.; Rohrl, J.; Rotenberg, E.; Schmid, A. K.; Waldmann, D.; Weber, H. B.; Seyller, T.,**

Towards wafer-size graphene layers by atmospheric pressure graphitization of silicon carbide. ***Nat Mater*** **2009,** ***8*** **(3), 203-207.**

8. Li, D.; Muller, M. B.; Gilje, S.; Kaner, R. B.; Wallace, G. G., Processable aqueous dispersions of graphene nanosheets. ***Nat Nano*** **2008,** ***3*** **(2), 101-105.**

9. Dato, A.; Radmilovic, V.; Lee, Z.; Phillips, J.; Frenklach, M., Substrate-Free Gas-Phase Synthesis of Graphene Sheets. ***Nano Lett.*** **2008,** ***8*** **(7), 2012-2016.**

10. Lotya, M.; Hernandez, Y.; King, P. J.; Smith, R. J.; Nicolosi, V.; Karlsson, L. S.; Blighe, F. M.; De, S.; Wang, Z.; McGovern, I. T.; Duesberg, G. S.; Coleman, J. N., Liquid Phase Production of Graphene by Exfoliation of Graphite in Surfactant/Water Solutions. ***Journal of the American Chemical Society*** **2009,** ***131*** **(10), 3611-3620.**

11. Shao, Y.; Wang, J.; Engelhard, M.; Wang, C.; Lin, Y., Facile and controllable electrochemical reduction of graphene oxide and its applications. ***J. Mater. Chem.*** **2010,** ***20*** **(4), 743-748.**

12. Li, X.; Wang, X.; Zhang, L.; Lee, S.; Dai, H., Chemically Derived, Ultrasmooth Graphene Nanoribbon Semiconductors. ***Science*** **2008,** ***319*** **(5867), 1229-1232.**

13. Wei, D.; Liu, Y.; Zhang, H.; Huang, L.; Wu, B.; Chen, J.; Yu, G., Scalable Synthesis of Few-Layer Graphene Ribbons with Controlled Morphologies by a Template Method and Their Applications in Nanoelectromechanical Switches. ***Journal of the American Chemical Society*** **2009,** ***131*** **(31), 11147-11154.**

14. **Simpson, C. D.; Brand, J. D.; Berresheim, A. J.; Przybilla, L.; Rader, H. J.; Mullen, K., Synthesis of a giant 222 carbon graphite sheet. *Chemistry-a European Journal* 2002, *8* (6), 1424-1429.**

15. **Lee, C.; Wei, X.; Kysar, J. W.; Hone, J., Measurement of the Elastic Properties and Intrinsic Strength of Monolayer Graphene. *Science* 2008, *321* (5887), 385-388.**

16. **Morozov, S. V.; Novoselov, K. S.; Katsnelson, M. I.; Schedin, F.; Elias, D. C.; Jaszczak, J. A.; Geim, A. K., Giant intrinsic carrier mobilities in graphene and its bilayer. *Phys. Rev. Lett.* 2008, *100* (1).**

17. **Bolotin, K. I.; Sikes, K. J.; Jiang, Z.; Klima, M.; Fudenberg, G.; Hone, J.; Kim, P.; Stormer, H. L., Ultrahigh electron mobility in suspended graphene. *Solid State Communications* 2008, *146* (9–10), 351-355.**

18. **(a) Wallace, P. R., THE BAND THEORY OF GRAPHITE. *Physical Review* 1947, *71* (9), 622-634; (b) Semenoff, G. W., CONDENSED-MATTER SIMULATION OF A 3-DIMENSIONAL ANOMALY. *Phys. Rev. Lett.* 1984, *53* (26), 2449-2452.**

19. **Charlier, J. C.; Eklund, P. C.; Zhu, J.; Ferrari, A. C., Electron and phonon properties of graphene: Their relationship with carbon nanotubes. In *Carbon Nanotubes: Advanced Topics in the Synthesis, Structure, Properties and Applications*, Jorio, A.; Dresselhaus, G.; Dresselhaus, M. S., Eds. Springer-Verlag Berlin: Berlin, 2008; Vol. 111, pp 673-709.**

20. Schedin, F.; Geim, A. K.; Morozov, S. V.; Hill, E. W.; Blake, P.; Katsnelson, M. I.; Novoselov, K. S., Detection of individual gas molecules adsorbed on graphene. *Nat Mater* 2007, *6* (9), 652-655.

21. Yu, B.; Sun, X. H.; Calebotta, G. A.; Dholakia, G. R.; Meyyappan, M., One-dimensional Germanium Nanowires for Future Electronics. *J Clust Sci* 2006, *17* (4), 579-597.

22. (a) Shan, C.; Yang, H.; Song, J.; Han, D.; Ivaska, A.; Niu, L., Direct Electrochemistry of Glucose Oxidase and Biosensing for Glucose Based on Graphene. *Analytical Chemistry* 2009, *81* (6), 2378-2382; (b) Alwarappan, S.; Erdem, A.; Liu, C.; Li, C.-Z., Probing the Electrochemical Properties of Graphene Nanosheets for Biosensing Applications. *The Journal of Physical Chemistry C* 2009, *113* (20), 8853-8857.

23. (a) Wang, X.; Zhi, L.; Müllen, K., Transparent, Conductive Graphene Electrodes for Dye-Sensitized Solar Cells. *Nano Lett.* 2008, *8* (1), 323-327; (b) Hong, W.; Xu, Y.; Lu, G.; Li, C.; Shi, G., Transparent graphene/PEDOT–PSS composite films as counter electrodes of dye-sensitized solar cells. *Electrochemistry Communications* 2008, *10* (10), 1555-1558.

24. (a) Eda, G.; Emrah Unalan, H.; Rupesinghe, N.; Amaratunga, G. A. J.; Chhowalla, M., Field emission from graphene based composite thin films. *Applied Physics Letters* 2008, *93* (23), 233502; (b) Wu, Z.-S.; Pei, S.; Ren, W.; Tang, D.; Gao, L.; Liu, B.; Li, F.; Liu, C.; Cheng, H.-M., Field Emission of Single-Layer Graphene Films Prepared by Electrophoretic Deposition. *Adv. Mater.* 2009, *21* (17), 1756-1760.

25. **Kim, K. S.; Zhao, Y.; Jang, H.; Lee, S. Y.; Kim, J. M.; Kim, K. S.; Ahn, J.-H.; Kim, P.; Choi, J.-Y.; Hong, B. H., Large-scale pattern growth of graphene films for stretchable transparent electrodes.** ***Nature*** **2009,** ***457*** **(7230), 706-710.**

26. **(a) Dong, Y.; Chen, C.; Zheng, X.; Gao, L.; Cui, Z.; Yang, H.; Guo, C.; Chi, Y.; Li, C. M., One-step and high yield simultaneous preparation of single- and multi-layer graphene quantum dots from CX-72 carbon black.** ***J. Mater. Chem.*** **2012,** ***22,*** **8764-8766; (b) Zhang, L.; Xing, Y.; He, N.; Zhang, Y.; Lu, Z.; Zhang, J.; Zhang, Z., Preparation of graphene quantum dots for bioimaging application.** ***J. Nanosci. Nanotechnol.*** **2012,** ***12,*** **2924-2928; (c) Liu, Q.; Guo, B.; Rao, Z.; Zhang, B.; Gong, J. R., Strong two-photon-induced fluorescence from photostable, biocompatible nitrogen-doped graphene quantum dots for cellular and deep-tissue imaging.** ***Nano letters*** **2013,** ***13*** **(6), 2436-2441; (d) Xie, W. J.; Fu, Y. Y.; Ma, H.; Zhang, M.; Fan, L. Z., Preparation of Fluorescent Graphene Quantum Dots as Biological Imaging Marker for Cells.** ***Acta Chimica Sinica*** **2012,** ***70*** **(20), 2169-2172; (e) Zheng, X. T.; Than, A.; Ananthanaraya, A.; Kim, D.-H.; Chen, P., Graphene quantum dots as universal fluorophores and their use in revealing regulated trafficking of insulin receptors in adipocytes.** ***ACS Nano*** **2013,** ***7,*** **6278-6286; (f) Xie, M. M.; Su, Y. J.; Lu, X. N.; Zhang, Y. Z.; Yang, Z.; Zhang, Y. F., Blue and green photoluminescence graphene quantum dots synthesized from carbon fibers.** ***Mater Lett*** **2013,** ***93,*** **161-164; (g) Abdullah-Al-Nahain; Lee, J. E.; In, I.; Lee, H.; Lee, K. D.; Jeong, J. H.; Park, S. Y., Target Delivery and Cell Imaging Using Hyaluronic Acid-Functionalized Graphene Quantum Dots.** ***Mol.***

Pharmaceut. **2013,** ***10*** **(10), 3736-3744; (h) Wu, X.; Tian, F.; Wang, W. X.; Chen, J.; Wu, M.; Zhao, J. X., Fabrication of highly fluorescent graphene quantum dots using L-glutamic acid for in vitro/in vivo imaging and sensing.** ***J Mater Chem C*** **2013,** ***1*** **(31), 4676-4684.**

27. (a) Sun, H.; Wu, L.; Wei, W.; Qu, X., Recent advances in graphene quantum dots for sensing. ***Mater. Today*** **2013,** ***16*** **(11), 433-442; (b) Ananthanarayanan, A.; Wang, X.; Routh, P.; Sana, B.; Lim, S.; Kim, D.-H.; Lim, K.-H.; Li, J.; Chen, P., Facile Synthesis of Graphene Quantum Dots from 3D Graphene and their Application for Fe3+ Sensing.** ***Adv. Funct. Mater.*** **2014,** ***24,*** **3021-3026.**

28. Ritter, K. A.; Lyding, J. W., The influence of edge structure on the electronic properties of graphene quantum dots and nanoribbons. ***Nat Mater*** **2009,** ***8*** **(3), 235-242.**

29. Sk, M. A.; Ananthanarayanan, A.; Huang, L.; Lim, K. H.; Chen, P., Revealing the tunable photoluminescence properties of graphene quantum dots. ***Journal of Materials Chemistry C*** **2014,** ***2*** **(34), 6954-6960.**

30. Zheng, X. T.; Than, A.; Ananthanaraya, A.; Kim, D.-H.; Chen, P., Graphene Quantum Dots as Universal Fluorophores and Their Use in Revealing Regulated Trafficking of Insulin Receptors in Adipocytes. ***ACS Nano*** **2013,** ***7*** **(7), 6278-6286.**

31. Subrahmanyam, K. S.; Panchakarla, L. S.; Govindaraj, A.; Rao, C. N. R., Simple Method of Preparing Graphene Flakes by an Arc-Discharge Method. ***The Journal of Physical Chemistry C*** **2009,** ***113*** **(11), 4257-4259.**

32. Tung, V. C.; Allen, M. J.; Yang, Y.; Kaner, R. B., High-throughput solution processing of large-scale graphene. *Nat Nano* 2009, *4* (1), 25-29.

33. Gui, G.; Li, J.; Zhong, J., Band structure engineering of graphene by strain: First-principles calculations. *Phys. Rev. B* 2008, *78* (7), 075435.

34. Castro, E. V.; Novoselov, K. S.; Morozov, S. V.; Peres, N. M. R.; dos Santos, J. M. B. L.; Nilsson, J.; Guinea, F.; Geim, A. K.; Neto, A. H. C., Biased Bilayer Graphene: Semiconductor with a Gap Tunable by the Electric Field Effect. *Phys. Rev. Lett.* 2007, *99* (21), 216802.

35. (a) Varykhalov, A.; Scholz, M. R.; Kim, T. K.; Rader, O., Effect of noble-metal contacts on doping and band gap of graphene. *Phys. Rev. B* 2010, *82* (12), 121101; (b) Balog, R.; Jorgensen, B.; Nilsson, L.; Andersen, M.; Rienks, E.; Bianchi, M.; Fanetti, M.; Laegsgaard, E.; Baraldi, A.; Lizzit, S.; Sljivancanin, Z.; Besenbacher, F.; Hammer, B.; Pedersen, T. G.; Hofmann, P.; Hornekaer, L., Bandgap opening in graphene induced by patterned hydrogen adsorption. *Nat Mater* 2010, *9* (4), 315-319.

36. (a) Chernozatonskiĭ, L. A.; Sorokin, P. B.; Belova, E. É.; Brüning, J.; Fedorov, A. S., Superlattices consisting of "lines" of adsorbed hydrogen atom pairs on graphene. *Jetp Lett.* 2007, *85* (1), 77-81; (b) Duplock, E. J.; Scheffler, M.; Lindan, P. J. D., Hallmark of Perfect Graphene. *Phys. Rev. Lett.* 2004, *92* (22), 225502.

37. (a) Chen, Z.; Lin, Y.-M.; Rooks, M. J.; Avouris, P., Graphene nano-ribbon electronics. *Physica E: Low-dimensional Systems and Nanostructures* 2007, *40* (2), 228-232; (b) Han, M. Y.; Özyilmaz, B.; Zhang, Y.; Kim, P., Energy Band-

Gap Engineering of Graphene Nanoribbons. *Phys. Rev. Lett.* 2007, *98* (20), 206805; (c) Stampfer, C.; Güttinger, J.; Molitor, F.; Graf, D.; Ihn, T.; Ensslin, K., Tunable Coulomb blockade in nanostructured graphene. *Applied Physics Letters* 2008, *92* (1), 012102.

38. Wu, Z.-S.; Ren, W.; Gao, L.; Liu, B.; Zhao, J.; Cheng, H.-M., Efficient synthesis of graphene nanoribbons sonochemically cut from graphene sheets. *Nano Res.* 2010, *3* (1), 16-22.

39. (a) Ci, L.; Xu, Z.; Wang, L.; Gao, W.; Ding, F.; Kelly, K.; Yakobson, B.; Ajayan, P., Controlled nanocutting of graphene. *Nano Res.* 2008, *1* (2), 116-122; (b) Datta, S. S.; Strachan, D. R.; Khamis, S. M.; Johnson, A. T. C., Crystallographic Etching of Few-Layer Graphene. *Nano Lett.* 2008, *8* (7), 1912-1915.

40. Pan, D.; Zhang, J.; Li, Z.; Wu, M., Hydrothermal Route for Cutting Graphene Sheets into Blue-Luminescent Graphene Quantum Dots. *Adv. Mater.* 2010, *22* (6), 734-738.

41. Fujii, S.; Enoki, T., Cutting of Oxidized Graphene into Nanosized Pieces. *Journal of the American Chemical Society* 2010, *132* (29), 10034-10041.

42. Thierfelder, C.; Witte, M.; Blankenburg, S.; Rauls, E.; Schmidt, W. G., Methane adsorption on graphene from first principles including dispersion interaction. *Surf. Sci.* 2011, *605* (7-8), 746-749.

43. Abe, S.; Watari, F.; Tachikawa, H., Interaction of Ethylene Carbonate and Graphene Chip: Density Functional Theory Study. *Jpn. J. Appl. Phys.* 2012, *51* (1).

44. Liu, H.; Lee, J. Y., Electric Field Effects on the Adsorption of CO on a Graphene Nanodot and the Healing Mechanism of a Vacancy in a Graphene Nanodot. *J. Phys. Chem. C* 2012, *116* (4), 3034-3041.

45. Dzhurakhalov, A. A.; Peeters, F. M., Structure and energetics of hydrogen chemisorbed on a single graphene layer to produce graphane. *Carbon* 2011, *49* (10), 3258-3266.

46. Ijas, M.; Havu, P.; Harju, A., Fracturing graphene by chlorination: A theoretical viewpoint. *Phys. Rev. B* 2012, *85* (3).

47. Denis, P. A.; Iribarne, F., Monolayer and Bilayer Graphene Functionalized with Nitrene Radicals. *J. Phys. Chem. C* 2011, *115* (1), 195-203.

48. Granatier, J.; Lazar, P.; Otyepka, M.; Hobza, P., The Nature of the Binding of Au, Ag, and Pd to Benzene, Coronene, and Graphene: From Benchmark CCSD(T) Calculations to Plane-Wave DFT Calculations. *J. Chem. Theory Comput.* 2011, *7* (11), 3743-3755.

49. Li, J.-L.; Kudin, K. N.; McAllister, M. J.; Prud'homme, R. K.; Aksay, I. A.; Car, R., Oxygen-Driven Unzipping of Graphitic Materials. *Phys. Rev. Lett.* 2006, *96* (17), 176101.

50. Paci, J. T.; Belytschko, T.; Schatz, G. C., Computational Studies of the Structure, Behavior upon Heating, and Mechanical Properties of Graphite Oxide. *The Journal of Physical Chemistry C* 2007, *111* (49), 18099-18111.

51. Szabó, T.; Berkesi, O.; Forgó, P.; Josepovits, K.; Sanakis, Y.; Petridis, D.; Dékány, I., Evolution of Surface Functional Groups in a Series of Progressively Oxidized Graphite Oxides. *Chem. Mat.* 2006, *18* (11), 2740-2749.

52. Cai, W.; Piner, R. D.; Stadermann, F. J.; Park, S.; Shaibat, M. A.; Ishii, Y.; Yang, D.; Velamakanni, A.; An, S. J.; Stoller, M.; An, J.; Chen, D.; Ruoff, R. S., Synthesis and Solid-State NMR Structural Characterization of 13C-Labeled Graphite Oxide. *Science* 2008, *321* (5897), 1815-1817.

53. Li, Z.; Zhang, W.; Luo, Y.; Yang, J.; Hou, J. G., How Graphene Is Cut upon Oxidation? *Journal of the American Chemical Society* 2009, *131* (18), 6320-6321.

54. Ma, L.; Wang, J.; Ding, F., Strain-Induced Orientation-Selective Cutting of Graphene into Graphene Nanoribbons on Oxidation. *Angewandte Chemie International Edition* 2012, *51* (5), 1161-1164.

55. Schumacher, S., Photophysics of graphene quantum dots: Insights from electronic structure calculations. *Phys. Rev. B* 2011, *83* (8), 081417.

56. Zhao, M.; Yang, F.; Xue, Y.; Xiao, D.; Guo, Y., A Time-Dependent DFT Study of the Absorption and Fluorescence Properties of Graphene Quantum Dots. *ChemPhysChem* 2014, *15* (5), 950-957.

57. Jin, S. H.; Kim, D. H.; Jun, G. H.; Hong, S. H.; Jeon, S., Tuning the Photoluminescence of Graphene Quantum Dots through the Charge Transfer Effect of Functional Groups. *ACS Nano* 2013, *7* (2), 1239-1245.

58. DC, Y., *Computational Chemistry: A Partical Guide for Applying Techniques to Real-World Problems.* John Wiley & Sons, Inc: New York, 2001.

59. IN, L., *Quantum Chemistry*. 4th ed.; Prentice Hall: New Jersey, 2000.

60. (a) Hohenberg, P.; Kohn, W., Inhomogeneous Electron Gas. *Physical Review* 1964, *136* (3B), B864-B871; (b) Kohn, W.; Sham, L. J., Self-Consistent

Equations Including Exchange and Correlation Effects. *Physical Review* 1965, *140* (4A), A1133-A1138.

61. Perdew, J. P.; Burke, K.; Ernzerhof, M., Generalized Gradient Approximation Made Simple. *Phys. Rev. Lett.* 1996, *77* (18), 3865-3868.

62. (a) Kresse, G.; Furthmüller, J., Efficient iterative schemes for \textit{ab initio} total-energy calculations using a plane-wave basis set. *Phys. Rev. B* 1996, *54* (16), 11169-11186; (b) Kresse, G.; Furthmüller, J., Efficiency of ab-initio total energy calculations for metals and semiconductors using a plane-wave basis set. *Computational Materials Science* 1996, *6* (1), 15-50; (c) Kresse, G.; Hafner, J., \textit{Ab initio} molecular dynamics for open-shell transition metals. *Phys. Rev. B* 1993, *48* (17), 13115-13118.

63. (a) Blöchl, P. E., Projector augmented-wave method. *Phys. Rev. B* 1994, *50* (24), 17953-17979; (b) Kresse, G.; Joubert, D., From ultrasoft pseudopotentials to the projector augmented-wave method. *Phys. Rev. B* 1999, *59* (3), 1758-1775.

64. Monkhorst, H. J.; Pack, J. D., Special points for Brillouin-zone integrations. *Phys. Rev. B* 1976, *13* (12), 5188-5192.

65. Becke, A. D., Density‐functional thermochemistry. III. The role of exact exchange. *The Journal of Chemical Physics* 1993, *98* (7), 5648-5652.

66. Lee, C.; Yang, W.; Parr, R. G., Development of the Colle-Salvetti correlation-energy formula into a functional of the electron density. *Phys. Rev. B* 1988, *37* (2), 785-789.

67. Frisch, M. J.; Trucks, G. W.; Schlegel, H. B.; Scuseria, G. E.; Robb, M. A.; Cheeseman, J. R.; Scalmani, G.; Barone, V.; Mennucci, B.; Petersson, G. A.;

Nakatsuji, H.; Caricato, M.; Li, X.; Hratchian, H. P.; Izmaylov, A. F.; Bloino, J.; Zheng, G.; Sonnenberg, J. L.; Hada, M.; Ehara, M.; Toyota, K.; Fukuda, R.; Hasegawa, J.; Ishida, M.; Nakajima, T.; Honda, Y.; Kitao, O.; Nakai, H.; Vreven, T.; Montgomery Jr., J. A.; Peralta, J. E.; Ogliaro, F.; Bearpark, M. J.; Heyd, J.; Brothers, E. N.; Kudin, K. N.; Staroverov, V. N.; Kobayashi, R.; Normand, J.; Raghavachari, K.; Rendell, A. P.; Burant, J. C.; Iyengar, S. S.; Tomasi, J.; Cossi, M.; Rega, N.; Millam, N. J.; Klene, M.; Knox, J. E.; Cross, J. B.; Bakken, V.; Adamo, C.; Jaramillo, J.; Gomperts, R.; Stratmann, R. E.; Yazyev, O.; Austin, A. J.; Cammi, R.; Pomelli, C.; Ochterski, J. W.; Martin, R. L.; Morokuma, K.; Zakrzewski, V. G.; Voth, G. A.; Salvador, P.; Dannenberg, J. J.; Dapprich, S.; Daniels, A. D.; Farkas, Ö.; Foresman, J. B.; Ortiz, J. V.; Cioslowski, J.; Fox, D. J. *Gaussian 09*, Gaussian, Inc.: Wallingford, CT, USA, 2009.

68. Biegler-könig, F. W.; Bader, R. F. W.; Tang, T.-H., Calculation of the average properties of atoms in molecules. II. *Journal of Computational Chemistry* 1982, *3* (3), 317-328.

69. Lin, Y. M.; Dimitrakopoulos, C.; Jenkins, K. A.; Farmer, D. B.; Chiu, H. Y.; Grill, A.; Avouris, P., 100-GHz Transistors from Wafer-Scale Epitaxial Graphene. *Science* 2010, *327* (5966), 662-662.

70. Wang, X.; Zhi, L. J.; Mullen, K., Transparent, conductive graphene electrodes for dye-sensitized solar cells. *Nano Lett.* 2008, *8* (1), 323-327.

71. Liu, M.; Yin, X. B.; Ulin-Avila, E.; Geng, B. S.; Zentgraf, T.; Ju, L.; Wang, F.; Zhang, X., A graphene-based broadband optical modulator. *Nature* 2011, *474* (7349), 64-67.

72. De Arco, L. G.; Zhang, Y.; Schlenker, C. W.; Ryu, K.; Thompson, M. E.; Zhou, C. W., Continuous, Highly Flexible, and Transparent Graphene Films by Chemical Vapor Deposition for Organic Photovoltaics. *ACS Nano* 2010, *4* (5), 2865-2873.

73. Stoller, M. D.; Park, S. J.; Zhu, Y. W.; An, J. H.; Ruoff, R. S., Graphene-Based Ultracapacitors. *Nano Lett.* 2008, *8* (10), 3498-3502.

74. (a) Mohanty, N.; Berry, V., Graphene-Based Single-Bacterium Resolution Biodevice and DNA Transistor: Interfacing Graphene Derivatives with Nanoscale and Microscale Biocomponents. *Nano Lett.* 2008, *8* (12), 4469-4476; (b) Hu, W. B.; Peng, C.; Luo, W. J.; Lv, M.; Li, X. M.; Li, D.; Huang, Q.; Fan, C. H., Graphene-Based Antibacterial Paper. *ACS Nano* 2010, *4* (7), 4317-4323.

75. (a) Zhou, S. Y.; Gweon, G. H.; Fedorov, A. V.; First, P. N.; De Heer, W. A.; Lee, D. H.; Guinea, F.; Neto, A. H. C.; Lanzara, A., Substrate-induced bandgap opening in epitaxial graphene. *Nat Mater* 2007, *6* (10), 770-775; (b) Englert, J. M.; Dotzer, C.; Yang, G. A.; Schmid, M.; Papp, C.; Gottfried, J. M.; Steinruck, H. P.; Spiecker, E.; Hauke, F.; Hirsch, A., Covalent bulk functionalization of graphene. *Nat Chem* 2011, *3* (4), 279-286; (c) Li, B.; Zhou, L.; Wu, D.; Peng, H. L.; Yan, K.; Zhou, Y.; Liu, Z. F., Photochemical Chlorination of Graphene. *ACS Nano* 2011, *5* (7), 5957-5961.

76. (a) Ryu, S.; Han, M. Y.; Maultzsch, J.; Heinz, T. F.; Kim, P.; Steigerwald, M. L.; Brus, L. E., Reversible Basal Plane Hydrogenation of Graphene. *Nano Lett.* 2008, *8* (12), 4597-4602; (b) Elias, D. C.; Nair, R. R.; Mohiuddin, T. M. G.; Morozov, S. V.; Blake, P.; Halsall, M. P.; Ferrari, A. C.; Boukhvalov, D. W.; Katsnelson, M. I.; Geim, A. K.; Novoselov, K. S., Control of Graphene's Properties by Reversible Hydrogenation: Evidence for Graphane. *Science* 2009, *323* (5914), 610-613.

77. (a) Hornekær, L.; Rauls, E.; Xu, W.; Šljivančanin, Ž.; Otero, R.; Stensgaard, I.; Lægsgaard, E.; Hammer, B.; Besenbacher, F., Clustering of Chemisorbed H(D) Atoms on the Graphite (0001) Surface due to Preferential Sticking. *Phys. Rev. Lett.* 2006, *97* (18), 186102; (b) Hornekær, L.; Šljivančanin, Ž.; Xu, W.; Otero, R.; Rauls, E.; Stensgaard, I.; Lægsgaard, E.; Hammer, B.; Besenbacher, F., Metastable Structures and Recombination Pathways for Atomic Hydrogen on the Graphite (0001) Surface. *Phys. Rev. Lett.* 2006, *96* (15), 156104.

78. Khazaei, M.; Bahramy, M. S.; Ranjbar, A.; Mizuseki, H.; Kawazoe, Y., Geometrical indications of adsorbed hydrogen atoms on graphite producing star and ellipsoidal like features in scanning tunneling microscopy images: Ab initio study. *Carbon* 2009, *47* (14), 3306-3312.

79. Ferro, Y.; Teillet-Billy, D.; Rougeau, N.; Sidis, V.; Morisset, S.; Allouche, A., Stability and magnetism of hydrogen dimers on graphene. *Phys. Rev. B* 2008, *78* (8).

80. Sofo, J. O.; Chaudhari, A. S.; Barber, G. D., Graphane: A two-dimensional hydrocarbon. *Phys. Rev. B* 2007, *75* (15), 153401.

81. Zhou, J.; Wu, M. M.; Zhou, X.; Sun, Q., Tuning electronic and magnetic properties of graphene by surface modification. *Appl. Phys. Lett.* 2009, *95* (10).

82. Wu, J.; Xie, L. M.; Li, Y. G.; Wang, H. L.; Ouyang, Y. J.; Guo, J.; Dai, H. J., Controlled Chlorine Plasma Reaction for Noninvasive Graphene Doping. *J. Am. Chem. Soc.* 2011, *133* (49), 19668-19671.

83. Sahin, H.; Ciraci, S., Chlorine Adsorption on Graphene: Chlorographene. *J. Phys. Chem. C* 2012, *116* (45), 24075-24083.

84. Salvio, R.; Krabbenborg, S.; Naber, W. J. M.; Velders, A. H.; Reinhoudt, D. N.; van der Wiel, W. G., The Formation of Large-Area Conducting Graphene-Like Platelets. *Chem. Eur. J.* 2009, *15* (33), 8235-8240.

85. Suggs, K.; Reuven, D.; Wang, X. Q., Electronic Properties of Cycloaddition-Functionalized Graphene. *J. Phys. Chem. C* 2011, *115* (8), 3313-3317.

86. (a) Lomeda, J. R.; Doyle, C. D.; Kosynkin, D. V.; Hwang, W.-F.; Tour, J. M., Diazonium Functionalization of Surfactant-Wrapped Chemically Converted Graphene Sheets. *Journal of the American Chemical Society* 2008, *130* (48), 16201-16206; (b) Sun, Z.; Pint, C. L.; Marcano, D. C.; Zhang, C.; Yao, J.; Ruan, G.; Yan, Z.; Zhu, Y.; Hauge, R. H.; Tour, J. M., Towards hybrid superlattices in graphene. *Nat Commun* 2011, *2*, 559; (c) Huang, P.; Jing, L.; Zhu, H.; Gao, X., Diazonium Functionalized Graphene: Microstructure, Electric, and Magnetic Properties. *Accounts Chem. Res.* 2012, *46* (1), 43-52; (d) Paulus, G. L. C.; Wang, Q. H.; Strano, M. S., Covalent Electron Transfer Chemistry of Graphene with Diazonium Salts. *Accounts Chem. Res.* 2012, *46* (1), 160-170.

87. **Bekyarova, E.; Itkis, M. E.; Ramesh, P.; Berger, C.; Sprinkle, M.; de Heer, W. A.; Haddon, R. C., Chemical Modification of Epitaxial Graphene: Spontaneous Grafting of Aryl Groups. *J. Am. Chem. Soc.* 2009, *131* (4), 1336-1337.**

88. **Hossain, M. Z.; Walsh, M. A.; Hersam, M. C., Scanning Tunneling Microscopy, Spectroscopy, and Nanolithography of Epitaxial Graphene Chemically Modified with Aryl Moieties. *J. Am. Chem. Soc.* 2010, *132* (43), 15399-15403.**

89. **Tang, P.; Chen, P.; Wu, J.; Kang, F.; Li, J.; Rubio, A.; Duan, W., Metallicity retained by covalent functionalization of graphene with phenyl groups. *Nanoscale* 2013, *5* (16), 7537-7543.**

90. **Jiang, D.-e.; Sumpter, B. G.; Dai, S., How Do Aryl Groups Attach to a Graphene Sheet? *J.Phys.Chem.B* 2006, *110* (47), 23628-23632.**

91. **Perdew, J. P.; Burke, K.; Ernzerhof, M., Generalized Gradient Approximation Made Simple. *Phys. Rev. Lett.* 1996, *77*, 3865-3868.**

92. **(a) Kresse, G.; Hafner, J., Ab initio molecular dynamics for open-shell transition metals. *Phys. Rev. B* 1993, *48*, 13115-13118; (b) Kresse, G.; Furthmuller, J., Efficient iterative schemes for ab initio total-energy calculations using a plane-wave basis set. *Phys. Rev. B* 1996, *54*, 11169-11186; (c) Kresse, G.; Furthmüller, J., Efficiency of ab initio total-energy calculations for metals and semiconductors using a plane-wave basis set. *J. Comp. Mat. Sci.* 1996, *6*, 15-50.**

93. **(a) Blochl, P. E., Projector augmented-wave method. *Phys. Rev. B* 1994, *50*, 17953; (b) Kresse, G.; Joubert, D., From ultrasoft pseudopotentials to the projector augmented-wave method. *Phy. Rev. B* 1999, *59*, 1758-1775.**

94. **Monkhorst, H. J.; Pack, J. D., Special points for Brillouin-zone integrations. *Phy. Rev. B* 1976, *13*, 5188-5192.**

95. **Hattab, H.; N'Diaye, A. T.; Wall, D.; Klein, C.; Jnawali, G.; Coraux, J.; Busse, C.; Gastel, R. v.; Poelsema, B.; Michely, T.; Heringdorf, F.-J. M. z.; Hoegen, M. H.-v., Interplay of Wrinkles, Strain, and Lattice Parameter in Graphene on Iridium. *Nano Lett.* 2012, *12*, 678-682.**

96. **Baskin, Y.; Meyer, L., Lattice Constants of Graphite at Low Temperatures. *Phys. Rev.* 1955, *100* (19), 544-544.**

97. **Lindsay, L.; Broido, D. A., Optimized Tersoff and Brenner empirical potential parameters for lattice dynamics and phonon thermal transport in carbon nanotubes and graphene. *Phys. Rev. B* 2010, *81* (20), 205441.**

98. **Zhou, W. W.; Zhou, J. J.; Shen, J. Q.; Ouyang, C. Y.; Shi, S. Q., First-principles study of high-capacity hydrogen storage on graphene with Li atoms. *J.Phys.Chem.Solids* 2012, *73* (2), 245-251.**

99. **Boukhvalov, D. W.; Katsnelson, M. I.; Lichtenstein, A. I., Hydrogen on graphene: Electronic structure, total energy, structural distortions and magnetism from first-principles calculations. *Phys. Rev. B* 2008, *77* (3), 035427.**

100. **Ferro, Y.; Teillet-Billy; Rougeau, N.; Sidis, V.; Morisset, S.; Allouche, A., Stability and magnetism of hydrogen dimers on graphene. *Phys. Rev. B* 2008, *78*, 085417.**

101. Shkrebtii, A. I.; Heritage, E.; McNelles, P.; Cabellos, J. L.; Mendoza, B. S., Graphene and graphane functionalization with hydrogen: electronic and optical signatures. *Phy. Stat. Sol. (c)* 2012, *9* (6), 1378-1383.

102. Wang, X.; Ouyang, Y.; Li, X.; Wang, H.; Guo, J.; Dai, H., Room-Temperature All-Semiconducting Sub-10-nm Graphene Nanoribbon Field-Effect Transistors. *Phys. Rev. Lett.* 2008, *100* (20), 206803.

103. Dong, X.; Long, Q.; Wang, J.; Chan-Park, M. B.; Huang, Y.; Huang, W.; Chen, P., A graphene nanoribbon network and its biosensing application. *Nanoscale* 2011, *3* (12), 5156-5160.

104. Stützel, E. U.; Burghard, M.; Kern, K.; Traversi, F.; Nichele, F.; Sordan, R., A Graphene Nanoribbon Memory Cell. *Small* 2010, *6* (24), 2822-2825.

105. (a) Dong, Y.; Chen, C.; Zheng, X.; Gao, L.; Cui, Z.; Yang, H.; Guo, C.; Chi, Y.; Li, C. M., One-step and high yield simultaneous preparation of single- and multi-layer graphene quantum dots from CX-72 carbon black. *J. Mater. Chem.* 2012, *22* (18), 8764-8766; (b) Liu, Q.; Guo, B.; Rao, Z.; Zhang, B.; Gong, J. R., Strong Two-Photon-Induced Fluorescence from Photostable, Biocompatible Nitrogen-Doped Graphene Quantum Dots for Cellular and Deep-Tissue Imaging. *Nano Lett.* 2013, *13* (6), 2436-2441; (c) Wu, X.; Tian, F.; Wang, W.; Chen, J.; Wu, M.; Zhao, J. X., Fabrication of highly fluorescent graphene quantum dots using l-glutamic acid for in vitro/in vivo imaging and sensing. *Journal of Materials Chemistry C* 2013, *1* (31), 4676-4684.

106. Sun, H.; Wu, L.; Wei, W.; Qu, X., Recent advances in graphene quantum dots for sensing. *Materials Today* 2013, *16* (11), 433-442.

107. Ananthanarayanan, A.; Wang, X.; Routh, P.; Sana, B.; Lim, S.; Kim, D.-H.; Lim, K.-H.; Li, J.; Chen, P., Facile Synthesis of Graphene Quantum Dots from 3D Graphene and their Application for Fe3+ Sensing. ***Advanced Functional Materials*** **2014,** ***24*** **(20), 3021-3026.**

108. Liu, W.-W.; Feng, Y.-Q.; Yan, X.-B.; Chen, J.-T.; Xue, Q.-J., Superior Micro-Supercapacitors Based on Graphene Quantum Dots. ***Advanced Functional Materials*** **2013,** ***23*** **(33), 4111-4122.**

109. (a) Li, Y.; Hu, Y.; Zhao, Y.; Shi, G.; Deng, L.; Hou, Y.; Qu, L., An Electrochemical Avenue to Green-Luminescent Graphene Quantum Dots as Potential Electron-Acceptors for Photovoltaics. ***Adv. Mater.*** **2011,** ***23*** **(6), 776-780; (b) Gupta, V.; Chaudhary, N.; Srivastava, R.; Sharma, G. D.; Bhardwaj, R.; Chand, S., Luminscent Graphene Quantum Dots for Organic Photovoltaic Devices.** ***Journal of the American Chemical Society*** **2011,** ***133*** **(26), 9960-9963.**

110. Son, Y.-W.; Cohen, M. L.; Louie, S. G., Energy Gaps in Graphene Nanoribbons. ***Phys. Rev. Lett.*** **2006,** ***97*** **(21), 216803.**

111. (a) Yang, R.; Zhang, L.; Wang, Y.; Shi, Z.; Shi, D.; Gao, H.; Wang, E.; Zhang, G., An Anisotropic Etching Effect in the Graphene Basal Plane. ***Adv. Mater.*** **2010,** ***22*** **(36), 4014-4019; (b) Krauss, B.; Nemes-Incze, P.; Skakalova, V.; Biro, L. P.; Klitzing, K. v.; Smet, J. H., Raman Scattering at Pure Graphene Zigzag Edges.** ***Nano Lett.*** **2010,** ***10*** **(11), 4544-4548.**

112. Guo, Y.; Guo, W., Favorable Zigzag Configuration at Etched Graphene Edges. ***The Journal of Physical Chemistry C*** **2011,** ***115*** **(42), 20546-20549.**

113. Gao, X.; Wang, L.; Ohtsuka, Y.; Jiang, D.-e.; Zhao, Y.; Nagase, S.; Chen, Z., Oxidation Unzipping of Stable Nanographenes into Joint Spin-Rich Fragments. *Journal of the American Chemical Society* 2009, *131* (28), 9663-9669.

114. Sun, T.; Fabris, S., Mechanisms for Oxidative Unzipping and Cutting of Graphene. *Nano Lett.* 2011, *12* (1), 17-21.

115. McAllister, M. J.; Li, J.-L.; Adamson, D. H.; Schniepp, H. C.; Abdala, A. A.; Liu, J.; Herrera-Alonso, M.; Milius, D. L.; Car, R.; Prud'homme, R. K.; Aksay, I. A., Single Sheet Functionalized Graphene by Oxidation and Thermal Expansion of Graphite. *Chem. Mat.* 2007, *19* (18), 4396-4404.

116. Schniepp, H. C.; Li, J.-L.; McAllister, M. J.; Sai, H.; Herrera-Alonso, M.; Adamson, D. H.; Prud'homme, R. K.; Car, R.; Saville, D. A.; Aksay, I. A., Functionalized Single Graphene Sheets Derived from Splitting Graphite Oxide. *The Journal of Physical Chemistry B* 2006, *110* (17), 8535-8539.

117. (a) Wang, L.; Sun, Y. Y.; Lee, K.; West, D.; Chen, Z. F.; Zhao, J. J.; Zhang, S. B., Stability of graphene oxide phases from first-principles calculations. *Phys. Rev. B* 2010, *82*, 161406(R); (b) Lu, N.; Yin, D.; Li, Z.; Yang, J., Structure of Graphene Oxide: Thermodynamics versus Kinetics. *J. Phys. Chem. C* 2011, *115*, 11991-11995; (c) Yan, J.-A.; Chou, M. Y., Oxidation functional groups on graphene: Structural and electronic properties. *Phys. Rev. B* 2010, *82*, 125403.

118. Liu, L.; Ryu, S.; Tomasik, M. R.; Stolyarova, E.; Jung, N.; Hybertsen, M. S.; Steigerwald, M. L.; Brus, L. E.; Flynn, G. W., Graphene Oxidation:

Thickness-Dependent Etching and Strong Chemical Doping. *Nano Lett.* 2008, *8* (7), 1965-1970.

119. Guo, Y.; Jiang, L.; Guo, W., Opening carbon nanotubes into zigzag graphene nanoribbons by energy-optimum oxidation. *Phys. Rev. B* 2010, *82* (11), 115440.

120. (a) Li, L.; Wu, G.; Yang, G.; Peng, J.; Zhao, J.; Zhu, J.-J., Focusing on luminescent graphene quantum dots: current status and future perspectives. *Nanoscale* 2013, *5*, 4015-4039; (b) Lin, L.; Rong, M.; Luo, F.; Chen, D.; Wanga, Y.; Chen, X., Luminescent graphene quantum dots as new fluorescent materials for environmental and biological applications. *Trends Anal. Chem.* 2014, *54*, 83-102.

121. (a) Li, Y.; Hu, Y.; Zhao, Y.; Shi, G.; Deng, L.; Hou, Y.; Qu, L., An Electrochemical Avenue to Green-Luminescent Graphene Quantum Dots as Potential Electron-Acceptors for Photovoltaics. *Adv. Mater.* 2011, *23*, 776-780; (b) Gupta, V.; Chaudhary, N.; Srivastava, R.; Sharma, G. D.; Bhardwaj, R.; Chand, S., Luminscent Graphene Quantum Dots for Organic Photovoltaic Devices. *J Am Chem Soc* 2011, *133*, 9960-9963.

122. Liu, W.-W.; Feng, Y.-Q.; Yan, X.-B.; Chen, J.-T.; Xue, Q.-J., Superior Micro-Supercapacitors Based on Graphene Quantum Dots. *Adv. Funct. Mater.* 2013, *23* (33), 4111-4122.

123. Geim, A. K.; Nonoselov, K. S., The rise of graphene. *Nat. Mater.* 2007, *6*, 183-191.

124. Liu, R.; Wu, D.; Feng, X.; Mullen, K., Bottom-Up Fabrication of Photoluminescent Graphene Quantum Dots with Uniform Morphology. *J. Am. Chem. Soc.* 2011, *133*, 15221-15223.

125. Pan, D.; Guo, L.; Zhang, J.; Xi, C.; Xue, Q.; Huang, H.; Li, J.; Zhang, Z.; Yu, W.; Chen, Z.; Li, Z.; Wu, M., Cutting sp^2 clusters in graphene sheets into colloidal graphene quantum dots with strong green fluorescence. *J. Mater. Chem.* 2012, *22*, 3314-3318.

126. (a) Koch, W. H., M. C., *A Chemist's Guide to Density Functional Theory.* Wiley-VCH: 2000; (b) Parr, R. G. Y., W., *Density-Functional Theory of Atoms and Molecules.* Oxford University Press: 1989.

127. Schwarz, F. P.; Wasik, S. P., Fluorescence Measurements of Benzene, Naphthalene, Anthracene, Pyrene, Fluoranthene, and Benzo[e]pyrene in Water. *Anal. Chem.* 1976, *48*, 524-528.

128. Waris, R.; Rembert, M. A.; Sellers, D. M.; William E. Acree, J.; Kenneth W. Street, J., Polycyclic Aromatic Hydrocarbon Solute Probes Part II.* Effect of Solvent Polarity on the Fluorescence Emission Fine Structures of Coronene Derivatives. *Analyst* 1989, *114*, 195-199.

129. Tucker, S. A.; William E. Acree, J.; Kenneth W. Street, J.; Fetzer, J. C., Polycyclic Aromatic Hydrocarbon Solute Probes. Part III: Fluorescence Emission Spectra of Pyrene, Ovalene, Benzo[ghi]perylene, and Coronene Dissolved in Liquid Tetrabutylammonium Sulfonate Salts. *Appl. Spectrosc.* 1989, *43*, 162-164.

130. **(a) Zhang, L.; Yin, L.; Wang, C.; lun, N.; Qi, Y.; Xiang, D., Origin of Visible Photoluminescence of ZnO Quantum Dots: Defect-Dependent and Size-Dependent. *J. Phys. Chem. C* 2010, *114*, 9651-9658; (b) Cheng, H.-M.; Lin, K.-F.; Hsu, H.-C.; Hsieh, W.-F., Size dependence of photoluminescence and resonant Raman scattering from ZnO quantum dots. *Appl. Phys. Lett.* 2006, *88*, 261909; (c) Bailey, R. E.; Nie, S., Alloyed Semiconductor Quantum Dots: Tuning the Optical Properties without Changing the Particle Size. *J. Am. Chem. Soc.* 2003, *125*, 7100-7106; (d) Efros, A. L.; Rosen, M.; Kuno, M.; Nirmal, M.; Norris, D. J.; Bawendi, M., Band-edge exciton in quantum dots of semiconductors with a degenerate valence band: Dark and bright exciton states. *Phys. Rev. B* 1996, *54*, 4843-4856; (e) Pedrueza, E.; Segura, A.; Abargues, R.; Bailach, J. B.; Chervin, J. C.; Mart´ınez-Pastor, J. P., The effect of quantum size confinement on the optical properties of PbSe nanocrystals as a function of temperature and hydrostatic pressure. *Nanotech* 2013, *24*, 205701.**

131. **Ritter, K. A.; Lyding, J., The influence of edge structure on the electronic properties of graphene quantum dots and nanoribbons. *Nat. Mater.* 2009, *8*, 235-242.**

132. **Nakada, K.; Fujita, M.; Dresselhaus, G.; Dresselhaus, M. S., Edge state in graphene ribbons: Nanometer size effect and edge shape dependence. *Phys. Rev. B* 1996, *54*, 17954-17961.**

133. **Yan, X.; Cui, X.; Li, L.-s., Synthesis of Large, Stable Colloidal Graphene Quantum Dots with Tunable Size. *J. Am. Chem. Soc.* 2010, *132*, 5944-5945.**

134. Mueller, M. L.; Yan, X.; McGuire, J. A.; Li, L.-s., Triplet States and Electronic Relaxation in Photoexcited Graphene Quantum Dots. *Nano Lett.* 2010, *10*, 2679-2682.

135. Zhao, M.; Yang, F.; Xue, Y.; Xiao, D.; Guo, Y., A Time-Dependent DFT Study of the Absorption and Fluorescence Properties of Graphene Quantum Dots. *ChemPhysChem* 2014, *15*, 950-957.

136. Yan, X.; Cui, X.; Li, B.; Li, L.-s., Large, Solution-Processable Graphene Quantum Dots as Light Absorbers for Photovoltaics. *Nano Lett.* 2010, *10*, 1869-1873.

137. Schumacher, S., Photophysics of graphene quantum dots: Insights from electronic structure calculations. *Phys. Rev. B* 2011, *83*, 081417.

138. Li, L.-L.; Ji, J.; Fei, R.; Wang, C.-Z.; Lu, Q.; Zhang, J.-R.; Jiang, L.-P.; Zhu, J.-J., A facile microwave avenue to electrochemiluminescent two-color graphene quantum dots. *Adv. Funct. Mater.* 2012, *22*, 2971-2979.

139. Wang, X.; Sun, G.; Routh, P.; Kim, D.-H.; Huang, W.; Chen, P., Heteroatom-doped graphene materials: syntheses, properties and applications. *Chem. Soc. Rev.* 2014, DOI: 10.1039/C4CS00141A.

140. Li, Y.; Zhao, Y.; Cheng, H.; Hu, Y.; Shi, G.; Dai, L.; Qu, L., Nitrogen-Doped Graphene Quantum Dots with Oxygen-Rich Functional Groups. *J. Am. Chem.Soc.* 2012, *134*, 15-18.

141. Usachov, D.; Vilkov, O.; Gruneis, A.; Haberer, D.; Fedorov, A.; Adamchuk, V. K.; Preobrajenski, A. B.; Dudin, P.; Barinov, A.; Oehzelt, M.; Laubschat, C.;

Vyalikh, D. V., Nitrogen-Doped Graphene: Efficient Growth, Structure, and Electronic Properties. *Nano Lett.* 2011, *11*, 5401-5407.